LONDON metropolitan university

Novel Metamaterial Frequency Discriminating Devices for Next Generation Wireless Communication Systems

Kafil Uddin Ahmed
BEng (Hons), MIET

A thesis submitted in partial fulfilment
of the requirements of London Metropolitan University
for the degree of Doctor of Philosophy

Centre for Communications Technology
Faculty of Life Sciences and Computing

March 2013

THE FOLLOWING HAVE NOT BEEN COPIED ON INSTRUCTION FROM THE UNIVERSITY

Publications after p123

ABSTRACT

In this research, novel metamaterial structures based on microstrip integrated circuit technology have been investigated for filter application in the next generation of microwave wireless communication systems. A number of novel microstrip planar filter structures have been developed that are able to meet the stringent requirements for high-performance systems and subsystems, such as sharp-cutoff frequency response, low passband insertion-loss and high return-loss, high out-of-band rejection, compact size, low cost and ease of integration. The filters are approximately 70% smaller than their conventional counterparts. Analysis and mathematical modeling of these microstrip devices involved the use of transmission-line theory and EM simulation tools which were based on the method of moments and finite element analyses. Measured results were used to validate the predicted behavior and performance of these devices. In fact there was good agreement with the theory and simulation modeling.

A Composite right/left-handed (CRLH) metamaterial unit-cell whose ground-plane is defected with a rectangular dielectric slot was used to develop a single and multi-pole bandpass filters. The unit-cell comprises of serial inter-digital capacitors whose junction is connected to a short-circuited inductive stub. By defecting the ground-plane of the unit-cell's structure with a dielectric slot, which is located immediately below the unit-cell, enables substantial tuning of the filter's centre frequency in the order of 26.5%. This was achieved with minimal effect on the unit-cell's insertion- and return-loss performance as well as its selectivity. The filters were fabricated on conventional dielectric substrate and their performance measured to verify the design methodology. The proposed technique eases the trade-off constraints that plague conventional filter designs and makes possible the realization of challenging filter specifications constituted from CRLH unit-cells using distributed transmission-lines.

A novel multilayer technique is presented that enables (i) the control of the filter's bandwidth, (ii) significantly improves its passband selectivity, and (iii) enhances its out-of-band rejection without affecting the filter's overall dimensions. The technique involves

implementation of identical filter structures on both sides of the dielectric substrate that are interconnected through vias. The filter circuit is laid on top of another identical substrate with a ground-plane. This structure results in a device that exhibits a sharp selectivity that is substantially smaller than traditional filter constructions. The sharpness of the filter is due to the upper and lower transmission zeros present on either side of the filter's passband being shifted closer together which causes reduction in its bandwidth. This effect is opposite to that encountered in conventional multilayer filter structures. It is shown the filter's bandwidth can be controlled while maintaining a good passband insertion- and return-loss performance, i.e. <1.2 dB and >10 dB, respectively. Furthermore, the proposed filter is relatively easy to fabricate using conventional technology.

A diplexer was developed based on the proposed multilayer technique and was shown to yield a high out-of-band rejection and high isolation between the two very closely spaced channels. Normally isolators are used to provide isolation between channels in order to prevent inter-channel interference. The technique is relatively simple to realize and cost effective to manufacture. Design methodology and experimental results are presented that show good correlation between the measured and simulation results. This diplexer should find application in multiband wireless communication systems.

A triplexer design is also presented whose multiband performance was created using CRLH unit-cell structures. The three passband channels of the triplexer have a common input splitter and transmission-line matching network is used to ensure high isolation between the channels is maintained in order to prevent undesired interaction between the channels which would otherwise adversely affect the triplexer's passband response. This was achieved using stepped impedance lines (SIL). No isolators were necessary using the proposed technique. It is also shown that by curving the SIL can provide enhancement in the triplexer's loss performance, bandwidth, and suppression of high order spurii. The design analysis and performance of the triplexer was verified via fabrication and measurement.

A novel compact microstrip wideband bandpass filter was presented for wideband application that possesses good insertion- and return-loss, sharp frequency selectivity and high out-of-band rejection. The proposed filter comprises of two inter-digital capacitors with four inductive stubs. It employs a T-shaped open stub that is inserted between the symmetrical unit-cell structures.

Finally, a novel high performance ultra-wideband (UWB) bandpass filter design is presented that meets the UWB specifications of FCC. The proposed UWB filter is based on a CRLH structure consisting of an asymmetric unit-cell with a short circuited inductive stub that exhibits stopband rejection level greater than 25 dB at the lower and upper band edges whilst maintaining an insertion-loss of less than 0.5 dB across its passband. In addition, a simple and effective technique is proposed to create and control sharp rejection notch bands within the filter's passband in order to provide interference immunity from undesired radio signals, such as wireless local area networks (WLAN) that co-exist within the UWB spectrum.

The planar filters that have been developed in this research work are intended for wireless communication systems. Compared to existing microstrip filters they exhibit superior performance in terms of low passband insertion-loss, sharp passband response and high out-of-band selectivity. In addition, the filters are small in size and relatively cheap to fabricate. The commercial benefit of these devices is very significant in terms of reduction in power consumption by such systems employing it as well as increase in channel capacity. The low power consumption by such systems translates to increase in their reliability and life.

Table of Contents

List of Figures

Chapter 1

Chapter 2

Chapter 3

Chapter 4

Chapter 5

List of Tables

List of Acronyms

ADS	Advance design system
BWM	Backward wave medium
CRLH	Composite right/left-handed
DNG	Double negative
DNM	Double negative medium
DPS	Double positive
EBG	Electromagnetic bandgap
EM	Electromagnetic
ENG	Epsilon negative
FEM	Finite element method
FF	Fixed frequency
FCC	Federal Communications Committee
GP	Ground plane
IDC	Inter-digital capacitor
LH	Left-handed
LHM	Left-handed medium
MoM	Method of moments
MTM	Metamaterial
MNG	Mu negative
NIM	Negative index medium
NPV	Negative phase velocity
NRI	Negative refractive index
PBC	Periodic boundary condition
PCB	Printed circuit board
PIM	Positive index medium
PEC	Perfect electric conductor

PMC	Perfect magnetic conductor
PRI	Positive refractive index
RH	Right-handed
RHM	Right-handed medium
SRR	Split-ring resonator
TEM	Transverse electromagnetic
TL	Transmission-line
TW	Thin wire
TM	Transverse magnetic
UWB	Ultra-wideband
WG	Waveguide
WB	Wideband

ACKNOWLEDGEMENTS

Foremost, I would like to express my sincere gratitude to my supervisor Professor Bal S. Virdee for the continuous support of my PhD study and research, for his patience, motivation, enthusiasm, and immense knowledge. His extraordinary guidance and assistance helped me immensely throughout my research time at the University. I could not have imagined having a better supervisor and mentor for my PhD study!

Thanks to Mr Peter Pettit and Mr Suhail Bashir for fabricating the circuits in this research project.

Thanks to my family, in particular my parents and my wife for their warm encouragement as well as the generous financial support throughout my study.

Thanks to Dr Peter Song from Quintel Technology Ltd for offering a short project to investigate the feasibility of metamaterial diplexers. The results of this work are included in this thesis. Although there was no financial incentive for this however the work provided me with a good understanding on filter applications for real systems.

Thanks to all my friends here in England and abroad for their continuous support and encouragement.

AUTHOR'S DECLARATION

I declare that all the material contained in this thesis is my own work.

List of Publications

Journal Papers:

1. "Fine control of filter performance based on composite right/left-handed metamaterial technology," International Journal of RF and Microwave Computer-Adided Engineering, Wiley, DOI: 10.1002/mmce.20710, 2013.
2. "Compact ultra wideband filter with based on CRLH transmission line unit cell," IEEE Transaction of MTT, Vol. 61, Issue. 2, pp. 782-788, 2013

Conference Papers:

1. "Miniaturized tuneable passive microwave devices based on transmission line metamaterials," IET passive component Seminar, Glasgow, UK DOI: 10.1049/ic.2011.0201, 2011.
2. "Compact quasi-elliptic bandpass filter," Asia Pacific Microwave Conference, Australia, pp. 121-123. 2011.
3. "Triplexer based on composite left/right handed transmission line". German Microwave Conference, German Microwave Conference, 12-14 March 2012, pp. 46-49. ISBN: 978-3-9812668-5-6.
4. "Novel microstrip filter with ultra wide stopband," German Microwave Conference, Germany, 2012.
5. "Diplexer based on composite right/left handed TLs". META 2012 Conference, Paris.
6. "Dual-band bandpass filter using open-loop resonators," Asia pacific Microwave Conference, Australia, 2011.
7. "Microwave frequency discriminating devices based on composite right/left-handed transmission-line unit-cell," IET Passive Component Seminar, London Savoy place, UK, pp. 29-37, 2012.

Oral Presentation:

1. "Miniaturized tuneable passive microwave devices based on transmission line metamaterials," IET Passive Component Seminar, Glasgow, UK, 2011.
2. "Microwave frequency discriminating devices based on composite right/left-handed transmission-line unit-cell," IET Passive Component Seminar, London, Savoy Place, UK, 2012.

1.0 INTRODUCTION

1.1 Terminology and Definition

There is rapidly growing interest in engineered materials commonly known as "metamaterials". Metamaterial is an artificially configured material structure which offers distinctive electromagnetic behaviour, such as simultaneous negative permittivity and negative permeability. The prefix "meta" is a Greek word that means "beyond" or "after" [1]. A general description of this concept is explained in this section of the thesis.

1.1.1 Overview on Electromagnetic Metamaterials

Electromagnetic metamaterials (MTM) offer unusual double negative electromagnetic properties and these characteristics result in a negative refractive index, hence metamaterials are also referred to as negative refractive index or left-handed materials [1]. In 1967, V.G. Veselago [1-2], a physicist from the Lebedjev Physical Institute in Moscow, first proposed this unusual metamaterial, however in 1999 Pendry et al. proposed a practical way to realize simultaneously negative permittivity and permeability using a combination of split ring resonator and metal strip structures [1-3]. A split ring resonator (SRR) has inherent capacitance and inductance and so it interacts with an EM wave to create the negative permeability. Thin metal wire (TW) strips arranged in parallel induce a negative permittivity when subjected to an EM wave. The MTM structure is resonant at a particular frequency defined by the dimensions of the TW-SRR structure. It's well known that the quality-factor of the resonant structure is inversely proportional to its bandwidth; however its transmission-loss is inversely proportional to the *Q*-factor. This means a high-*Q* will have a reduced bandwidth which is responsible for a high transmission loss. High-*Q* MTM structures have limited practical use other than as narrow band filters. However, in 2002, Caloz et al. [1-5] investigated the viability of the non resonant transmission-line approach to realize MTM structures. He demonstrated the same electromagnetic properties could be realised using a circuit arrangement of series capacitors and shunt inductors in microstrip technology. The planar configuration displayed low loss and broad bandwidth.

1.2 Research Motivations and Objectives

Following the pioneering work on MTM by Pendry and Smith [1-3][1-4], there has been considerable interest in the practical realisations of novel devices based on MTM. Metamaterial transmission-lines have two main characteristics which make them very attractive for the use in microwave systems, namely (i) line dimensions are independent of wavelength which can lead to size reduction of microwave components, and (ii) zero phase change between the input and output of MTM transmission-line. These properties offer the possibility of developing enhanced performance from microwave components and devices with new functionalities.

The main aim of this research project is to investigate the development of enhanced planar microwave bandpass filters and multiplexers based on planar composite right/-left handed transmission-line unit-cells for application in future wireless communications systems. The investigation addresses some of the key challenges surrounding the design of metamaterial bandpass filters, such as compactness, selectivity, transmission performance, harmonic suppression and tunability. These research objectives were tackled in the stages outlined below.

To date, there is only small number of published works tat show clear evidence that MTMs can be advantageously used to improve the performance of bandpass filters (BPF). Planar filters based on MTM unit-cells have recently been investigated in reference [2-1] [2-2] [2-3]. Though the proposed structures exhibit bandpass filter characteristics they do not meet the stringent requirements for high-performance systems, such as low insertion-loss, high return-loss, sharp-cutoff frequency response, compact size and ease of integration in modern communications systems. To overcome the aforementioned design limitations, the use of a planar transmission-line ladder network consisting of MTM unit-cells was investigated here for bandpass filter design. Each MTM unit-cell comprises of a pair of inter-digital coupled-line capacitors (*IDC*) and a short-circuited inductive line using a via. The decrease in the gap between coupled-lines of the capacitor increases the magnitude of the bandwidth. This property is used to control the filters 3 dB bandwidth. The length of the shunt-line enables the centre frequency of the filter to be finely tuned over a wide range. Moreover, the increase in the number of unit-cells constituting the filter broadens its bandwidth and simultaneously sharpens its passband response. An electromagnetic parameter retrieval technique was used to substantiate the dual negative index nature of the proposed MTM filter structures.

The proposed planar MTM filter's characteristics, e.g. centre frequency, can be altered by changing its physical parameters so that it can be tuned to operate at a desired frequency. However, this technique for low frequency designs can result in a large sized filter structure. A technique was developed here to overcome this shortcoming that is realized by defecting the ground-plane of the MTM filter with a dielectric slot. This technique was verified practically.

In the design of conventional microwave filters there is inevitably a trade-off between compactness, passband loss and selectivity. This is solved by exploiting multilayer technology to design compact devices [3-1]-[3-4]. Although the existing techniques offer sharp selectivity, this is at the expense of insertion-loss. In addition, due to strong coupling effects in conventional multilayer techniques there is an expansion in the filter's bandwidth. To compensate these shortcomings, in this research a novel multilayer technique is proposed that is based on metamaterial technology. The proposed technique is shown to also enhance the filter's selectivity performance.

It is well known that cavity diplexers are an integral part of the modern microwave systems due to their capability of achieving high rejection level between two very close adjacent channels, e.g. GSM 1800 and UMTS 2100. The required rejection level between channels is unattainable with the microstrip technology due to strong electromagnetic coupling between the conventional resonators. In this research it was investigated to determine the feasibility of using microstrip technology to design diplexers using composite right/left-handed transmission-line structures for high rejection between adjacent bands. This investigation eventually led to the development of a multilayer structure that proved to be an an effective solution.

To date, there has been different metamaterial structure proposed to design ultra-wideband bandpass filters. These design concepts are (i) complicated, (ii) difficult to realize, and (iii) occupy a large space; thus rendering them unattractive for modern wireless communication systems. Hence, to overcome these major drawbacks a compact filter structure is proposed and its performance demonstrated for practical applications.

1.3 Fundamentals of the Research

1.3.1 Left-Handed Metamaterial

Left-handed (LH) metamaterial structures are artificial structures that do not exist in nature. These structures are usually constructed from a series of discontinuous sections operating in a restricted frequency range. A typical realization of left-handed transmission-line unit-cell is constructed using quasi-lumped transmission-line consisting of a series capacitor and a shunt inductor.

1.3.2 Basic Physics of Left-Handed Medium

Left-handed term refers to a certain type of plane wave propagation, more precisely to the orientation formed by the electric-field intensity vector E, magnetic-field intensity vector H and the propagation wave vector β [1-2]. As the vectors E, H and Poynting vector S always form a right-handed triplet therefore, the LH nature of the wave can be determined by comparing the directions of S and β.

The direction of the time-averaged power density $P_d = R_e[S]$ and the phase variation of the wave β determine left-handed (LH) and right-handed (RH) propagation, thus:

$$\beta \cdot P_d < 0 \equiv \text{LH propagation}$$

$$\beta \cdot P_d \geq 0 \equiv \text{RH propagation}$$

Consequently, a left-handed medium (LHM) is defined as a medium which is capable of supporting LH propagation. The opposite is a right-handed medium (RHM). It is worth mentioning that the above conditions can be applied both to uniform and non-uniform plane waves. When applied to a uniform plane wave in a simple medium, it can be shown that the condition for LH propagation can be expressed in terms of the wave parameters n and z and medium parameters ε_r and μ_r as follows:

$$\beta . P_d < 0 \longleftrightarrow \frac{z}{n} < 0 \longleftrightarrow \frac{\mu'}{|\mu|} + \frac{\varepsilon'}{|\varepsilon|} < 0$$

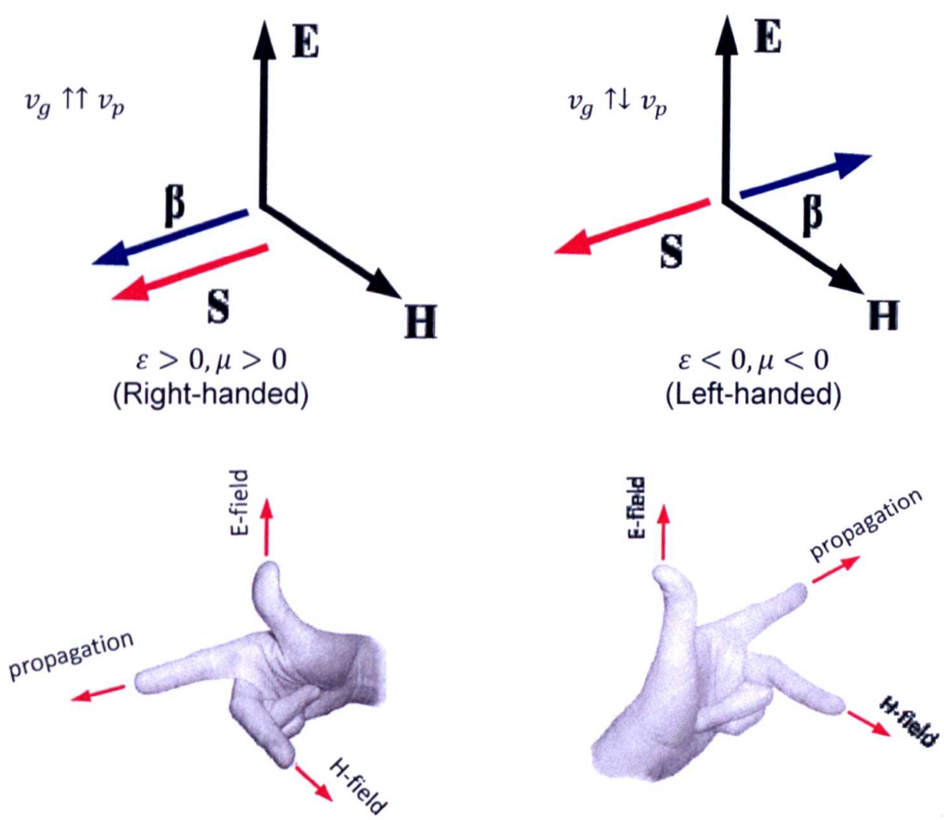

(a) (b)

Fig. 1-0 (a) Left: right-handed medium triad, and (b) Right: left-handed medium triad

In real materials the energy flows in the same direction as the wave propagation (k), and the group and phase velocity are in the direction too. Energy flow is represented by S

(Poynting's vector) and k represents the direction of propagation of the wave. Real materials obey the right-hand rule, where the thumb, the first and the second fingers on the right hand are held so that they are at right angles to each other. The first finger points in the direction of the wave propagation and the thumb in the direction of the electric-field then the second finger will point in the direction of the magnetic-field. In the case of metamaterials the energy of the wave and direction of propagation are opposite to each other. Also its group and phase velocities are opposite to each other. The wave appears to travel backwards.

1.3.3 Wave Propagation In LHM

Maxwell's equations are taken into account in order to verify the wave propagation in left-handed media. A LH material is an electromagnetic medium with simultaneously negative permittivity and permeability. This double negative nature of the constitutive parameters μ, ε results in the propagation of electromagnetic waves exhibiting anti-parallel phase and group velocities. The general form of time varying Maxwell's equations [1-8], [1-9] are:

$$\nabla . E = \frac{-\partial B}{\partial t} - M \text{ (Faraday's law)} \tag{1.1}$$

$$\nabla . H = \frac{-\partial D}{\partial t} + J \text{ (Ampere's law)} \tag{1.2}$$

$$\nabla . D = \rho_e \text{ (Electric Gauss' law)} \tag{1.3}$$

$$\nabla . B = \rho_m \text{ (Magnetic Gauss' law)} \tag{1.4}$$

The quantities represent time varying vector fields and are real functions of spatial coordinates *x, y* and *z*. Here, E (V/m) is the electric-field intensity, H (A/m) is the magnetic-field intensity, D (C/m^2) is the electric flux density, B (W/m^2) is the magnetic flux density, J (A/m^2) is the electric current density, ρ_e (C /m^3) is the electric charge density and ρ_m (C /m^3) is the magnetic charge density.

However, if the medium is linear such that ε, μ are not dependent on E or H and non-dispersive such that ε, μ are not dependent on ω. The relationship between the electric and magnetic-fields intensities and flux densities are related by:

$$D=\varepsilon E=\varepsilon_0 \varepsilon_r E \tag{1.5}$$

$$B=\mu H=\mu_0 \mu_r H \tag{1.6}$$

ε_0= 8.854x10^{-12} F/ m and μ_0= 4πx10^{-7} H/m are permittivity and permeability of free space, respectively. Moreover, Maxwell's equations can be converted to phasor form by assuming an $e^{+j\omega t}$ time dependence therefore, the time derivatives in equation (1.1) is then replaced by $j\omega$ as shown below:

$$\nabla.E = -j\omega \mu H - M \tag{1.7}$$

$$\nabla.H = -j\omega \mu E + J \tag{1.8}$$

$$\nabla.D = \rho_e \tag{1.9}$$

$$\nabla.B = \rho_m \tag{1.10}$$

A plane wave is a wave whose phase is constant over a set of planes whereas a uniform plane wave is a wave that its magnitude and phase are both constant. A uniform plane wave is a transverse electromagnetic wave. It can be assumed that the electric and magnetic-field intensities are given by:

$$E= E_0 e^{-j\beta r} \tag{1.11}$$

$$H=\frac{E_0}{\eta_o} e^{-j\beta r} \tag{1.12}$$

Where η = $|E|/|H|$ denotes the wave impedance. If the medium is lossless then M, J are equal to zero. In regards to this situation, simple Maxwell's equations can be achieved by substituting the plane wave expressions:

$$\beta.E = +\omega \mu H \tag{1.13}$$

$$\beta . H = -\omega \, \varepsilon E \tag{1.14}$$

These expressions represent the right-handed triad (E, H, β), shown in the Fig. 1-0. In the case of LH medium ε and μ <0, and since $|\varepsilon| = -\varepsilon > 0$ and $|\mu| = -\mu > 0$

$$\beta . E = -\omega |\mu| H \tag{1.15}$$

$$\beta . H = +\omega \; |\varepsilon| E \tag{1.16}$$

The above equations represent the unusual left-handed triad shown in Fig. (1).

As frequency is always a positive quantity, the phase velocity is given by

$$v_p = \frac{\omega}{\beta} \tag{1.17}$$

In a LH medium, Equation 1.15 is opposite to the phase velocity in a RH medium as shown in Equation 1.16. Moreover, because the wave number β is known to be positive in a RH medium and is negative in a LH medium. So

RH medium: $\beta > 0 \; (V_p > 0)$

LH medium: $\beta < 0 \; (V_p < 0)$

For generality, Equation 1.15 and Equation 1.16 can be compacted into single relationship:

$$\beta . E = S\omega \, \mu \, H \tag{1.18}$$

$$\beta . H = S\omega \, \varepsilon E \tag{1.19}$$

Where S is a sign function defined as

$$S = \begin{cases} +1 & \text{if the medium is RH} \\ -1 & \text{if the medium is LH} \end{cases}$$

1.4 Realization of LH Metamaterial

The permittivity (ε) is defined as a material's ability to transmit or to permit an electric field [1-9] [1-10]. Permeability (μ) is defined as a material's ability to transmit or to permit a magnetic field. CRLH-TL has important properties which are negative electric permittivity and magnetic permeability. This artificial material can be obtained from SRR-TW and TL. SRR has a positive permittivity (+ε) and a negative permeability (-μ), whereas TW has a negative permittivity (-ε) and a positive permeability (+μ). Therefore, if we combine both of them, a novel material is generated that has properties of a negative permittivity (-ε) and a negative permeability (-μ), as illustrated in Fig.1-1. This unique property is called LHM. In 1999 J.B. Pendry [1-10] first proposed a practical way to realize both negative phenomena by using periodic array of conducting elements, as shown in Fig.1-2.

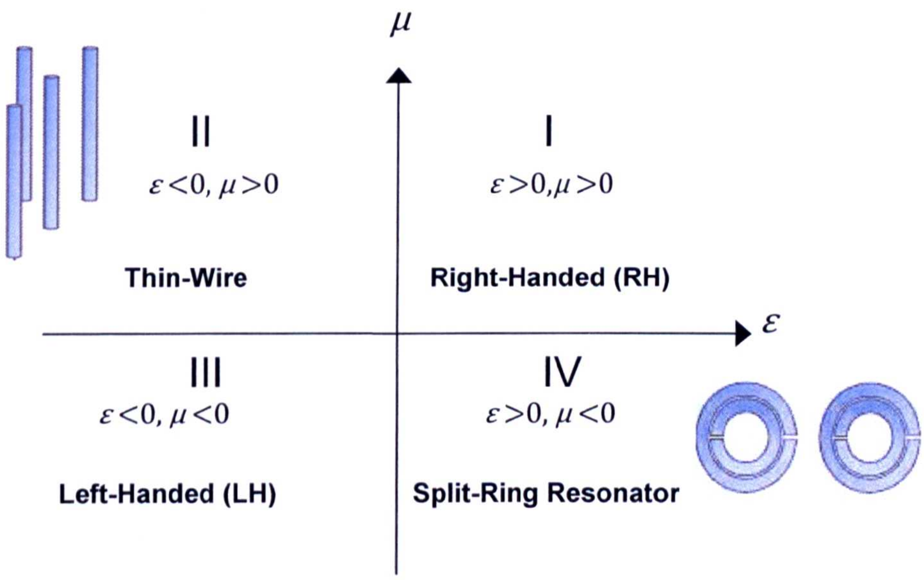

Fig. 1-1 Permittivity-permeability (ε-μ) diagram [1-8, 1-9]

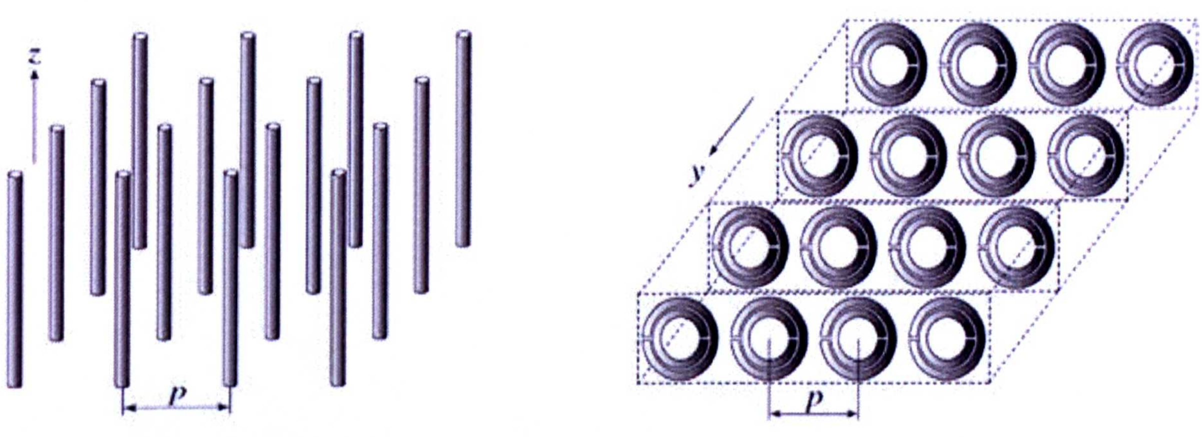

(a) (b)

Fig. 1-2 Thin wire and SRR [9], (a) Thin-wire structure $\varepsilon < 0$, $\mu > 0$ if $E \parallel z$, and (b) split-ring resonator (SRR) structure $\varepsilon > 0$, $\mu < 0$ if $H \perp y$

Natural materials are made of atoms, which are dipoles. These dipoles modify the light velocity by a factor n (the refractive index). ENG MTM is presented by metallic thin wire structure. If the excitation electric-field (E) is parallel to the axis of the wires it induce a current along them and generates electric dipole moments. This MTM exhibits plasmonic type permittivity as function of frequency. MNG type of MTM is presented with a meta split ring resonator structure. If the excitation magnetic-field (H) is perpendicular to the plane of the rings it induces resonating currents in the loop and generates magnetic dipole moments. This MTM exhibits a plasmonic type permeability as function of frequency. The ring and wire units play the role of atomic dipoles; the wire acts as a ferroelectric atom, while the ring acts as an inductor (L) and the open section as a capacitor (C). So the whole ring can be considered as a LC circuit. When the electromagnetic field passes through the ring, an induced current is created and the generated field is perpendicular to the magnetic-field of the EM wave. There is a magnetic resonance so the permeability is negative, and the index is negative too.

In Fig. 1-3, the LHM sample consists of square copper split ring resonators and copper wire strips on fibre glass circuit board material. The rings and wires are on opposite sides of the boards, and the boards have been cut and assembled into an interlocking lattice [1-12].

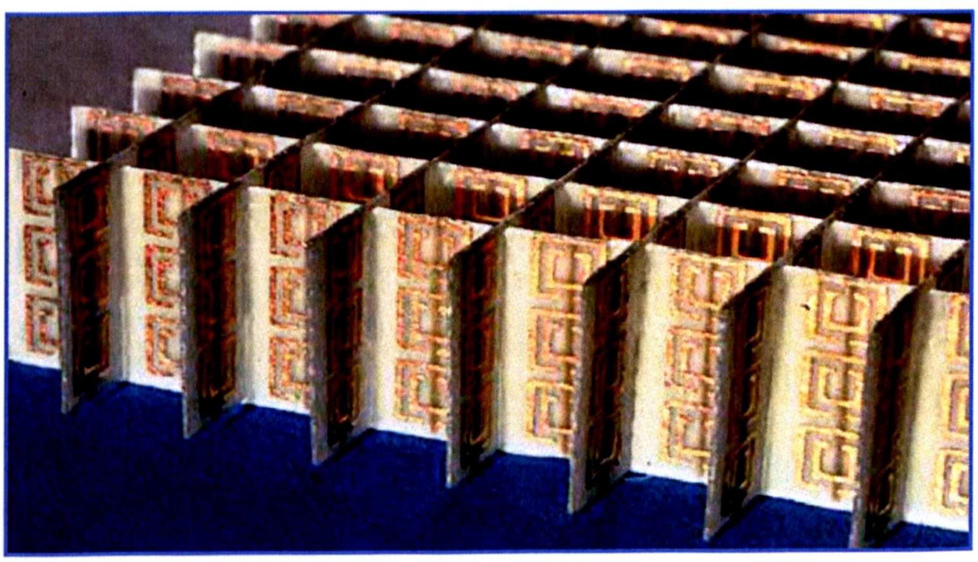

Fig. 1-3 Photograph of the 2-D left-handed metamaterial (LHM) sample [1-10, 1-11]

There has always been a trade-off between bandwidth and transmission level. Minimum transmission loss can be achieved at the resonance frequency by minimizing the system bandwidth. Therefore a structure made of resonating elements doesn't comprise a good transmission medium for a modulated signal and this is due to quality factor intrinsically associated with each resonator [1-13]. The TW-SRR metamaterial structure depicted in Fig. 1-3 is resonant and thus exhibits high-loss and narrow bandwidth. As bandwidth is restricted, signals are usually distorted through the resonating structure. Hence, this type of structures generates little interest for practical engineering applications. Therefore, recognizing the drawbacks of the TW-SRR structure a new architecture based on non resonant nature is proposed in this research. This new planar TL MTMs is designed to exhibit simultaneously low-loss and broad bandwidth.

1.5 Transmission-Line Metamaterial

1.5.1 Metamaterial Unit-Cell

Transmission-line (TL) theory is a powerful analytical tool for analyzing the design of conventional microwave circuits. TL theory can also be applied to analyze composite right/left-handed (CRLH) microwave circuits as shown in ref. [1-5]. The unit-cell of a metamaterial structure is depicted in Fig. 1-4(a). This structure is constituted from a series (inter-digital) capacitor C_L and shunt (stub) inductance L_L. The equivalent circuit model of this structure is shown in Fig.1-4(b). Assuming a loss-less model the complex propagation constant γ , the propagation constant β, the characteristic impedance Z_o, the phase velocity v_p, and group velocity v_g can be shown to be given by

$$\gamma = -j\frac{1}{\omega\sqrt{L_L C_L}} \tag{1.20}$$

$$\beta = -\frac{1}{\omega\sqrt{L_L C_L}} < 0 \tag{1.21}$$

$$Z_o = \sqrt{\frac{L_L}{C_L}} > 0 \tag{1.22}$$

$$v_p = -\omega^2 \sqrt{L_L C_L} < 0 \tag{1.23}$$

$$v_g = \omega^2 \sqrt{L_L C_L} > 0 \tag{1.24}$$

Equation (1.23) and (1.24) shows that the phase and group velocities are unambiguously antiparallel with respect to each other. The phase velocity v_p, associated with the direction of the phase propagation or wave vector β, is negative, whereas the group velocity v_g, associated with the direction of power flow or Poynting vector S, is positive. This left-handed backward wave propagation corresponds to a negative refractive index n, where the permittivity and permeability are negative, given by

$$n = -\sqrt{\varepsilon\mu} \tag{1.25}$$

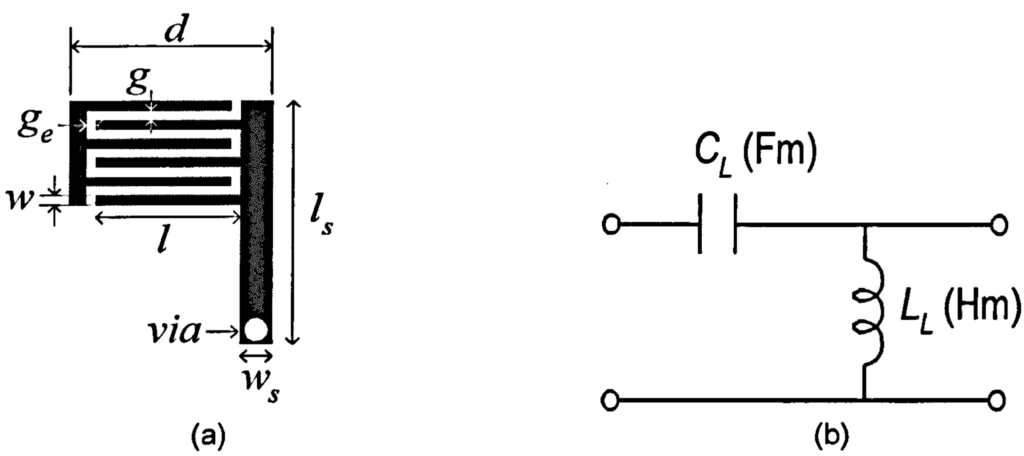

Fig. 1-4 (a) Unit-cell of a microstrip composite right/left-handed (CRLH) metamaterial structure, and (b) equivalent circuit model representing the left-handed (LH) metamaterial unit-cell.

The equivalent circuit of the structure in Fig. 1-4(a) is composed of series capacitor C_L and shunt inductance L_L, shown in Fig. 1-4(b), however as a wave propagates along the structure, the associated current flow along C_L induces magnetic fluxes and therefore a series inductance L_R is also present. Similarly the voltage gradient exists between the upper microstrip conductor and the ground-plane, which corresponds to a shunt capacitance C_R. Hence, a realistic representation of the circuit model in Fig. 1-4(b) with the associate parasitic effects is shown in Fig. 1-5(a), which is referred to as composite right/left-handed (CRLH) metamaterial [1-5].

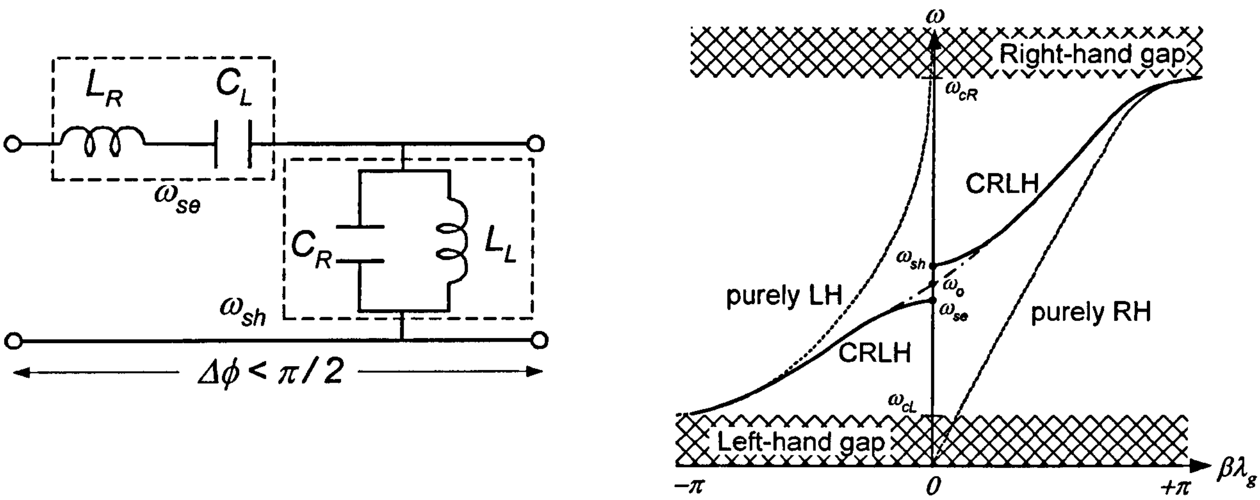

(a) (b)

Fig. 1-5 Composite right/left-handed (CRLH) metamaterial equivalent circuit, (a) unit-cell, and (b) dispersion diagram.

Analysis of the equivalent circuit in Fig. 1-5(a) shows that at low frequencies, L_R and C_R tend to be short and open circuit, respectively, so that the equivalent circuit is essentially reduced to the series C_L shunt L_L circuit, which is LH and has a high-pass frequency response. At high frequencies, C_L and L_L tend to be short and open circuit, respectively, so that the equivalent circuit is essentially reduced to the series L_R shunt C_R circuit, which is right-hand since it has parallel phase and group velocities; this circuit exhibits a low-pass frequency response. Although a CRLH-TL structure has both a LH range and a RH range, the dispersion curve in each of these significantly differs from that of the purely LH and purely RH structures, respectively, because of the combined effects of LH and RH, as shown in Fig. 1-5(b). The series and shunt resonance frequencies corresponding to the CRLH circuit in Fig. 1-5(a) are given by

$$\omega_{se} = \frac{1}{\sqrt{L_R C_L}} \quad \text{rad/s} \tag{1.26}$$

$$\omega_{sh} = \frac{1}{\sqrt{L_L C_R}} \quad \text{rad/s} \tag{1.27}$$

It can be shown the complex propagation constant is

$$\gamma = \pm\sqrt{\left(\frac{\omega}{\omega_R}\right)^2 + \left(\frac{\omega_L}{\omega}\right)^2 - \kappa\omega_L^2} \tag{1.28}$$

The sign is negative in the LH frequency range, and positive in the RH range. The frequency of maximum attenuation, i.e. resonance frequency, ω_o can be derived as the roots of the derivative of the complex propagation constant in (1.28), thus

$$\frac{d\gamma}{d\omega} = \pm\frac{\omega/\omega_R^2 - \omega_L^2/\omega^3}{\sqrt{(\omega/\omega_R)^2 + (\omega_L/\omega)^2 - \kappa\omega_L^2}} = 0 \tag{1.29}$$

Yielding

$$\omega_o = \frac{1}{\sqrt[4]{L_R C_R L_L C_L}} \tag{1.30}$$

The phase velocity v_p and group velocity v_g can be derived from (1.28) to be given by

$$v_p = \frac{\omega}{\beta} = \pm\frac{\omega}{\sqrt{(\omega/\omega_R)^2 + (\omega_L/\omega)^2 - \kappa\omega_L^2}} \tag{1.31}$$

$$v_g = \frac{\sqrt{(\omega/\omega_R)^2 + (\omega_L/\omega)^2 - \kappa\omega_L^2}}{\left|\omega\omega_R^{-2} - \omega^{-3}\omega_L^2\right|} \tag{1.32}$$

In the purely LH case with $L_R = C_R = 0$, then from (1.31) and (1.32), $v_p = -\omega^2/\omega_L$ and $v_g = \omega^2/\omega_L$, showing that phase velocity is negative and that the phase and group velocities are therefore anti-parallel as expected.

The propagation constant of a TL is given by

$$\gamma = \alpha + j\beta = \sqrt{ZY} \tag{1.33}$$

Here, Z and Y are the per-unit length impedance and per-unit length admittance, respectively. Z and Y in CRLH-TL are defined as:

$$Z(\omega) = j\left(\omega L_R - \frac{1}{\omega C_L}\right) \tag{1.34}$$

$$Y(\omega) = j\left(\omega C_R - \frac{1}{\omega L_L}\right) \tag{1.35}$$

Therefore, the dispersion relation for a homogenous CRLH-TL is

$$\beta(\omega) = s(\omega) - \sqrt{\omega^2 L_R C_R + \frac{1}{\omega^2 L_L C_L} - \left(\frac{L_R}{L_L} + \frac{C_R}{C_L}\right)} \tag{1.36}$$

Where,

$$s(\omega) = \begin{Bmatrix} -1 & if\ \omega < min\ (\omega_{se}, \omega_{sh}) \\ +1 & if\ \omega > max\ (\omega_{se}, \omega_{sh}) \end{Bmatrix}$$

The asymmetric metamaterial unit-cells structure of Fig. (1-5) has mismatch effects when connected to external ports. Hence, it was necessary to make the circuit symmetrical, as shown in Fig. 1-6, before it was implemented using microstrip technology. The corresponding layout of the microstrip circuit is shown in Fig. 2-4(a).

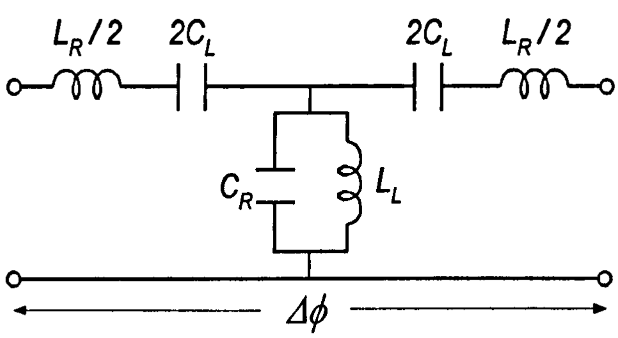

Fig. 1-6 Symmetric unit-cell of the CRLH metamaterial structure in Fig. 1-4.

1.6 Organization Of The Thesis

This chapter provided a backdrop on the fundamentals of metamaterial and the theoretical characterization of the basic unit-cell and its properties.

Chapter two presents a compact transmission-line metamaterial unit-cell configuration that was used in the design of planar microwave filters developed here. It is shown by increasing the number of unit-cells the filter's selectivity and return-loss response can be enhanced. Equivalent electrical circuit models are established for each configuration to aid analyzes. The filters are analyzed and a retrieval method is used to extract the filter's EM properties, such as permittivity, permeability and impedance etc. This chapter also includes a non-electronic tuning mechanism which is implemented using a defected ground-plane (DGP) on the metamaterial unit-cell structure to alter the filter's centre frequency without affecting its size. It is shown by locating the dielectric slot in the ground-plane in the vicinity of the unit-cell can enable substantial tuning as a function of the slot's position.

Chapter three of the thesis explore the use of the metamaterial transmission-line approach to design multiplexers, in particular a diplexer to separate UMTS & GSM signals. This chapter also includes a novel multilayer technique that is shown to simultaneously control of filter's bandwidth and selectivity.

The feasibility of compact wideband and ultra-wideband bandpass filter designs based on composite right/left-handed transmission-line are demonstrated in Chapters four and five, respectively. The fabricated filters are miniature compared to their conventional counterparts and exhibit a good transmission and reflection performance.

1.7 References

[1-0] C. Caloz, T. Itoh, "Transmission line approach of left-handed (LH) materials and microstrip implementation of an artificial LH transmission line," Antennas and Propagation, IEEE Transactions, vol-52, pp. 1159-1166, May. 2004.

[1-2] V.G. Veselago., "The electrodynamics of substances with simultaneously negative values of ε and μ ", Sov. Phys. Usp., vol. 10, no. 4, pp. 509-514, 1968.

[1-3] J.B. Pendry, A.J. Holden, D.J. Robbins, and W.J.Stewart, "Magnetism from conductors and enhanced nonlinear phenomena," IEEE Trans. Microwave Theory Tech. 47, pp. 2075–2084, 1999.

[1-4] D.R. Smith, W.J. Padilla, D.C. Vier, S.C. Nemat-Nasser, and S. Schultz, "Composite medium with simultaneously negative permeability and permittivity," Phys. Rev. Lett. 84, pp. 4184-4187, May. 2000.

[1-5] C. Caloz and T. Itoh, "Electromagnetic Metamaterials: Transmission line theory and microwave applications: the Engineering Approach," John Wiley and Sons, 2006.

[1-6] J. Lee, H. Kim, N. Kang, H. Jung "Effective medium approach of left handed material using a dispersive FDTD method," IEEE Trans. on Magnetics, vol. 41, no. 5, pp. 1484-1487, May. 2005.

[1-7] S. Gündüz, M. Çakır, G. Çakır, L. Sevgi, "A two-dimensional FDTD-based virtual visualization tool for metamnaterial-wave Interaction," Antennas and Propagation Magazine, IEEE, pp. 166 – 175, 2008.

[1-8] M.D. Pozar. Microwave Engineering, third edition, John Wiley & Sons 2004.

[1-9] J.B. Pendry, A.J. Holden, W.J. Stewart, and I. Youngs, "Extremely low frequency plasmons in metallic mesostructures," Phys. Rev. Lett. 76, pp. 4773–4776. 1996.

[1-10] J.B. Pendry, A.J. Holden, D.J. Robbins, and W.J. Stewart, "Magnetism from conductors and enhanced nonlinear phenomena," IEEE Trans. Microwave Theory Tech. 47, pp. 2075–2084, 1999.

[1-11] K. Aydin, K. Guven, and E. Ozbay, "Two-dimensional feft-handed Metamaterial with a negative refractive index," Journal of Physics, Conference Series 36, pp. 6–11, 2006.

[1-12] R.A. Shelby, D.R. Smith, and S. Schultz, "Experimental verification of a negative index of refraction," Science, vol. 292, pp. 77-79, April 2001.

[1-13] R.E. Collin. "Foundations for Microwave Engineering," Second Edition, McGraw-Hill, 1992.

2.0 METAMATERIAL FILTERS

Applications for RF and microwave bandpass filters have grown immensely over the past few decades. In fact, filters have become both vital and indispensible components in modern electronic systems. Filter designers are required to address critical trade-offs between size, passband loss and bandwidth. Planar distributed filters have become hugely popular due to their capabilities of offering size reduction in contrast to relatively bulky filters constructed using waveguide and coaxial media.

Planar filters based on metamaterial unit-cells have recently been investigated. In ref. [2-1], Zagoya-Mellado et al. report high performance filters are reported that are metamaterial ring resonators. Here metamaterial closed loop resonators were used to implement the 3-pole Chebyshev filter, shown in Fig. 2.0, and a 4-pole quasi-elliptic filter at 800 MHz for mobile communications. Although the filters exhibit a good overall response, the dimensions of the filters are relative large (3-pole is ~24x85 mm^2 and 4-pole is ~40x120 mm^2).

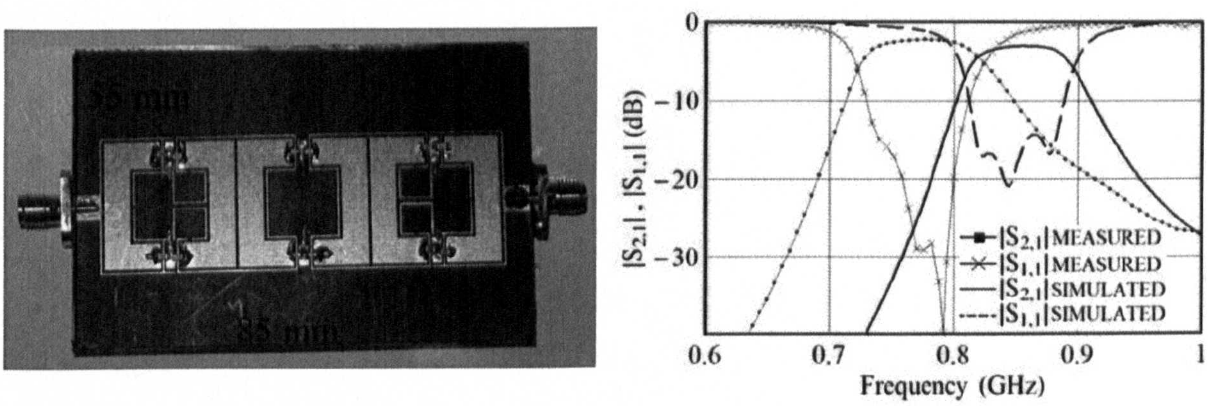

(a) (b)

Fig. 2-0 (a) Photograph of the 3-pole metamaterial ring resonator filter, and (b) simulated and measured response of the filter

Lobato-Morales et al. in [2-2] demonstrate a multiplexer using metamaterial directional filters, shown in Fig. 2-1, for their application in mobile multi-band transceiver front-ends. This technique suppresses harmonic bands without the use of additional high-pass or low-pass filters. However, the circuit occupies a large space area of 110x90 mm^2 and it exhibits high insertion-loss of 2.8 dB; hence, this type of design is not suitable for modern filter applications.

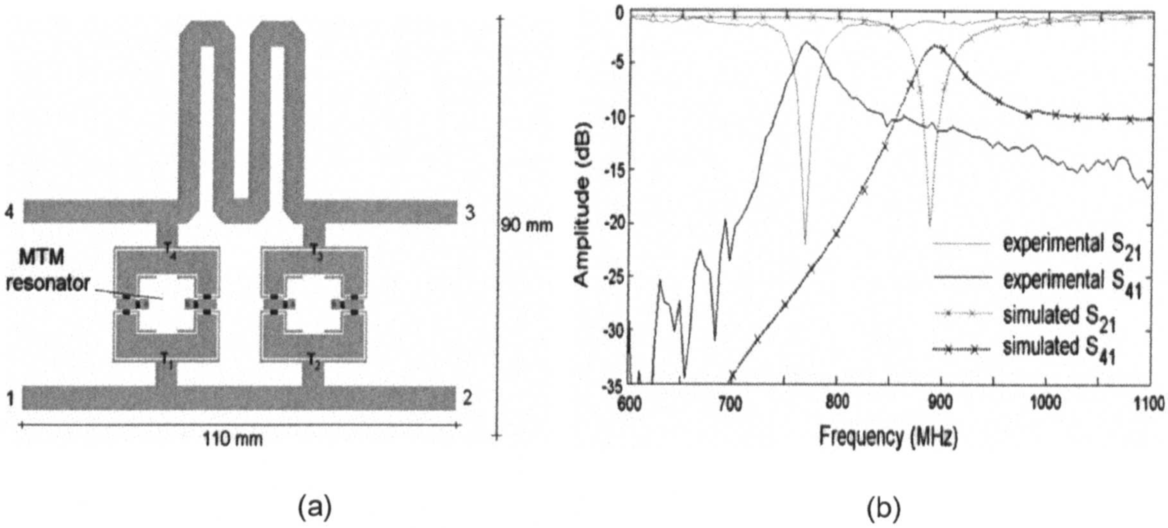

Fig. 2-1 (a) Layout of the metamaterial directional filter, and (b) simulated and measured response of the directional filter

Wiwatcharagoses et al. [2-3] revealed the viability of a filter design using composite right/left-handed metamaterial unit-cell based on split-ring resonators and open split-ring resonators. The unit-cells which are implemented in a microstrip transmission-line configuration incorporate varactor diodes to provide electronic tuning and thus a reconfigurable device. Unfortunately the filters described in [2-2] and [2-3] suffer from the lack of a sharp bandpass response for practical applications.

In this chapter, metamaterial unit-cells have been constructed using planar distributed transmission-lines to tackle the aforementioned critical issues. The chapter investigates the unit-cell's metamaterial characteristics, i.e. electric permittivity and the magnetic permeability, and verifies these parameters using numerically generated *S*-parameters. The retrieval technique used is valid for both symmetric and asymmetric planar microstrip structures comprising of unit-cells whose dimensions are much smaller than the free-space wavelength. The metamaterial properties of the filters are confirmed unlike those described in other published literature [2-1]-

[2-3] where no such verification of metamaterial devices is provided to support the structures unique properties over a given frequency range.

Moreover, this chapter describes a new design methodology for filters based on CRLH-TL unit-cells. The filters include one to four pole bandpass filters, which are compared to their equivalent conventional counterparts.

2.1 CRLH-TL Filters

This section presents one to four pole bandpass filters based on periodic CRLH-TL unit-cell structures which were designed at a centre frequency of 2.2 GHz. The transmission-line approach of LH circuits is based on the equivalent circuit of which is shown in Fig. 1-5(a). The structure of the CRLH-TL unit-cell and its characterizing parameters is shown in Fig.1-4(a). The LH-TL is a composite of RH-TL because of the unavoidable parasitic shunt capacitance and series inductance resulting in a RH contribution. The *L* and *C* components in the structure are dispersive and therefore are likely to introduce some inconsistency with respect to the ideal case. For a shunt-stub the following equation is appropriate [1-5],

$$L_L(\omega) = \left(\frac{Z_0^{stub}}{\omega}\right).tan\left(\omega l\sqrt{\varepsilon_{eff}/C_0}\right) \qquad (2\text{-}0)$$

Where Z_0^{stub} refers to the impedance of the stub, ω and *l* represent the angular frequency and the stub length, respectively. The inductance of the shorted stub naturally becomes a capacitance when the frequency becomes higher than $\pi C_0/\left(4l/\sqrt{\varepsilon_e}\right)$ .Therefore, this LH-TL will have high-frequency limit in addition to a low-frequency limit, which is imposed by the dispersive nature of the L and C components.

The CRLH-TL network shown on Fig. 1-5(a) in first chapter is obviously a filter. When $\omega \rightarrow \infty$ then $|Z| \rightarrow \frac{1}{\omega C_L} \rightarrow \infty$ and $|Y| \rightarrow \frac{1}{\omega L_L} \rightarrow \infty$ and therefore there will be a stopband due to high-pass nature of the LH elements. When $\omega \rightarrow \infty$ then $|Z| \rightarrow \omega L_R \rightarrow \infty$ and $|Y| \rightarrow \omega C_R \rightarrow \infty$. Therefore there will be a stopband due to low-pass nature of the RH elements. A matched passband can exist between these two stop-bands, as illustrated in Fig. 1-5(b). Though the *LC* network implementation of the CRLH-TL results in a simple bandpass filter configuration, it however exhibits the behaviour of a CRLH-TL structure with the following properties:

- Phase response that leads to LH transmission at lower frequencies and RH transmission higher frequencies whereas conventional filters are generally designed to meet magnitude specification and don't reveal a LH range.
- In conventional filter each cell has generally different L and C values to match specifications whereas metamaterial structures can be made of identical cells.
- The phase shifts of a conventional filter may be larger than $\frac{\pi}{2}$ but metamaterial (MTM) structure constituted with unit cells satisfies the homogeneity condition, $|\Delta\varphi| < \frac{\pi}{2}$. The MTM with $\Delta\varphi \ll \frac{\pi}{2}$ or $\Delta z \ll \frac{\lambda_g}{4}$ is an ideal material structure where the dimensions are many orders of magnitude smaller than wavelength.

Filter design flowchart is shown below.

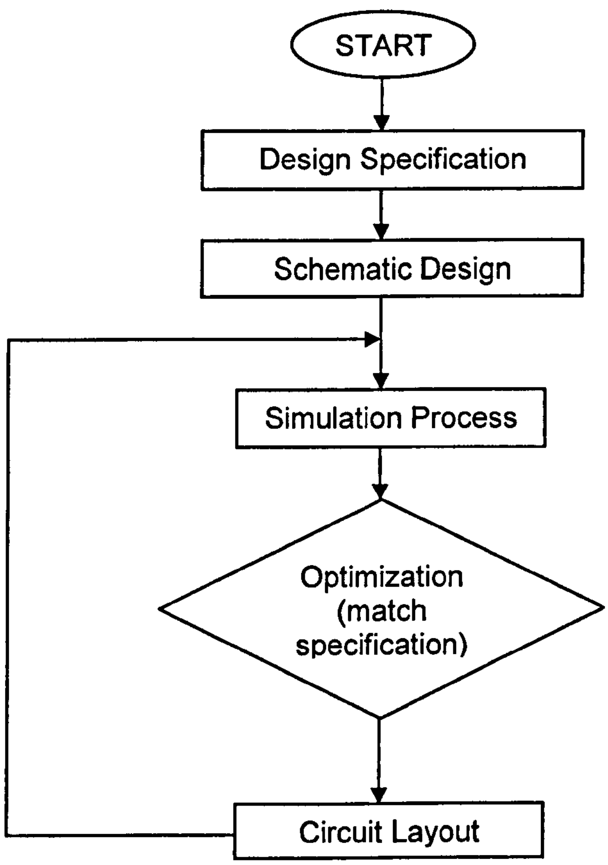

2.2 One-Pole CRLH-TL Filter

In this section, a one-pole bandpass filter configuration based on CRLH transmission-line is presented which was developed at an arbitrary centre frequency of 2.2 GHz with a 3 dB bandwidth of 235 MHz. The CRLH-TL unit-cell structure comprises of two symmetrical inter-digital capacitors (*IDC*) with three fingers and connected to a shunted stub short-circuited to ground using via, as shown in Fig. 2-2(a). In reality, the proposed circuit also comprises of an unavoidable parasitic series inductance and shunt capacitance. In this topology, the series inter-digital capacitor and the short-circuited inductance accounts for left-handedness (high-pass nature) of the structure. The effective inductance of the middle transmission-line section interfaced with the inter-digital lines, and the effective capacitance introduced by the short-circuited inductor represent right-handedness (low-pass nature) characteristics. The filter's 50Ω input and output feed-lines are tapered to enhance impedance matching necessary to improve the filter's passband insertion-loss between 2.08-2.31 GHz.

The actual structure of the one-pole CRLH-TL unit-cell and its characterizing parameters are shown in Fig. 2-2(a). For comparison a conventional parallel coupled-line microstrip filter of identical specifications given in Table 2-1 is shown in Fig. 2-2(b). The one-pole filter design was initially simulated and optimized using two different electromagnetic solvers, i.e. ADS™ (MoM) and Ansoft HFSS (FEM).

Filter Specifications	
Filter Order	1
Centre Frequency	2.2 GHz
Fractional BW (%)	10.68
Source/ Load termination	50 Ω

Table 2-1: One-pole filter specifications

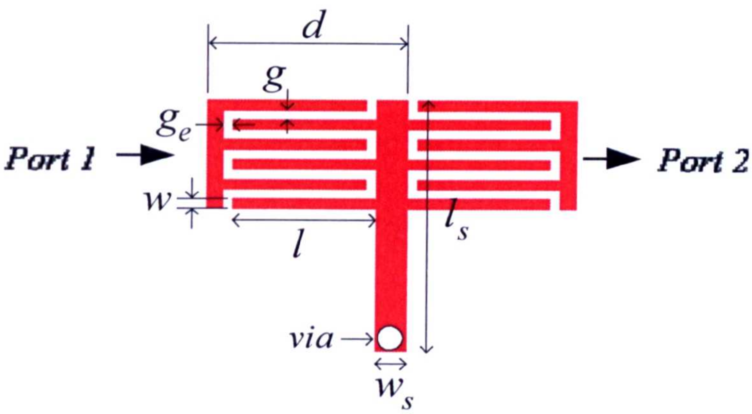

(a)

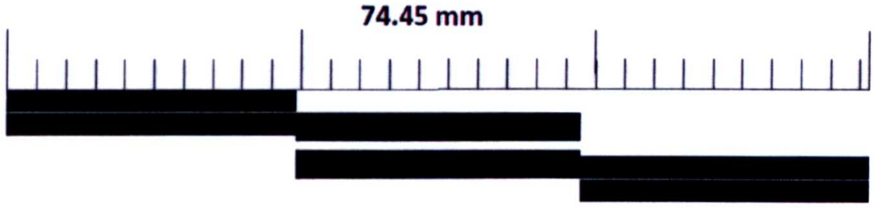

(b)

Fig. 2-2 (a) Physical microstrip layout of the composite right/left-handed (CRLH) metamaterial unit-cell structure, and (b) conventional parallel coupled-line filter with same specification as proposed 1-pole CRLH filter.The proposed one-pole CRLH-TL filter has a length of 13.6 mm whereas the parallel coupled-line filter is 74.45 mm long. The CRLH-TL structure is 72% smaller than the conventional filter.

The equivalent lumped circuit of the proposed CRLH-TL filter structure consists of inductance L_R in series with a capacitance C_L and a shunt capacitance C_R in parallel with an inductance L_L, as shown in Fig. 1-5. The corresponding lumped element components were derived as follows:

For the circuit in Fig. 1-5,

$$\omega C_R = \omega_R + \omega_R\sqrt{1 + \frac{\omega_L}{\omega_R}} \tag{2.1}$$

where ω, ω_L and ω_R represent the angular frequency, partial left-handed (PLH) and partial right-handed (PRH) angular resonance frequencies, respectively. Equation (2.1) can be re-arranged as:

$$\left(\frac{\omega_{C_R}-\omega_R}{\omega_R}\right)^2 = 1+\frac{\omega_L}{\omega_R} \tag{2.2}$$

$$\frac{(\omega_{C_R}{}^2-2\omega_{C_R}\omega_R+\omega_R{}^2)}{\omega_R{}^2} = 1+\frac{\omega_L}{\omega_R}$$

$$\omega_{C_R}{}^2 - 2\omega_{C_R}\omega_R + \omega_R{}^2 = \omega_R{}^2 + \omega_L\omega_R \tag{2.3}$$

The frequency of maximum attenuation, i.e. resonance frequency, ω_o is the roots of PLH and PRH circuits given by $\omega_0 = \sqrt{\omega_L\omega_R}$. Hence, Equation (2.3) becomes:

$$\frac{(\omega_{C_R}{}^2-\omega_0{}^2)}{2\,\omega_{C_R}} = \omega_R \tag{2.4}$$

The characteristic impedance is defined as:

$$Z_0 = \sqrt{\frac{L_R}{C_R}}$$

$$L_R = Z_0^2 C_R$$

The partial RH resonance is given by:

$$\omega_R = \frac{1}{\sqrt{L_R C_R}} = \frac{1}{Z_0 C_R} \tag{2.5}$$

By inserting Equation (2.5) into Equation (2.4) the following equations are obtained:

$$C_R = \frac{2\,\omega_{C_R}}{Z_0\,(\omega_{C_R}{}^2-\omega_0^2)} \tag{2.6}$$

$$L_R = \frac{2\,\omega_{C_R} Z_0}{Z_0\,(\omega_{C_R}{}^2-\omega_0^2)} \tag{2.7}$$

Also, from Equation (2.3) we obtain:

$$\left(\frac{\omega_{C_R}{}^2}{\omega_R} - 2\omega_{C_R}\right) = \omega_L \tag{2.8}$$

The frequency of maximum attenuation, $\omega_0 = \sqrt{\omega_L\omega_R}$. Therefore,

$$\omega_R = \frac{\omega_0^2}{\omega_L} \tag{2.9}$$

At PLH resonance,

$$\omega_L = \frac{1}{\sqrt{L_L C_L}} = \frac{1}{Z_0 C_L} \tag{2.10}$$

Where $$Z_0 = \sqrt{\frac{L_L}{C_L}},\ L_L = Z_0^2 C_L$$

By inserting Equation (2.9) into Equation (2.8) we obtain:

$$\frac{({\omega_{C_R}}^2 \omega_L)}{\omega_0^2} - 2\omega_{C_R} = \omega_L$$

or

$$\frac{({\omega_{C_R}}^2 \omega_L)}{\omega_0^2} - \omega_L = 2\omega_{C_R}$$

$$\omega_L \left(\frac{{\omega_{C_R}}^2}{\omega_0^2} - 1\right) = 2\omega_{C_R}$$

Therefore

$$\omega_L = \frac{2\omega_{C_R}}{\left(\frac{{\omega_{C_R}}^2}{\omega_0^2} - 1\right)} \tag{2.11}$$

By inserting Equation (2.10) into Equation (2.11) one can obtain the following equation:

$$\frac{2\omega_{C_R}}{\left(\frac{{\omega_{C_R}}^2}{\omega_0^2} - 1\right)} = \frac{1}{Z_0 C_L}$$

$$C_L = \frac{(\omega_{UC}/\omega_o)^2 - 1}{2\omega_{UC} Z_o} \tag{2.12}$$

Similarly,

$$L_L = \frac{Z_o\left[(\omega_{UC}/\omega_o)^2 - 1\right]}{2\omega_{UC}} \tag{2.13}$$

The calculated inductance and capacitance of the one-pole CRLH filter parameters defined in Fig. 1.6 are: L_R = 200.6 nH, C_R = 80.23 pF, L_L = 54.8 pH and C_L = 0.022 pF. These lumped elements were implemented using their microstrip equivalent circuit. C_R is the parasitic capacitance in the middle section of the unit-cell in Fig. 2-2(a) constituted from the shunted inductive line. The series and shunt resonance frequencies corresponding to the CRLH-TL circuit are given by

$$\omega_{se} = \frac{1}{\sqrt{L_R C_L}} \text{ rad/s} = 15.08 \times 10^9 \tag{2.14}$$

$$\omega_{sh} = \frac{1}{\sqrt{L_L C_R}} \text{ rad/s} = 15.08 \times 10^9 \tag{2.15}$$

According to the transmission-line theory, the balanced condition for the *LC* network is $\omega_{se} = \omega_{sh}$. The CRLH-TL network is qualitatively a combination of the PRH and PLH network TLs. In the particular, for useful balanced case these cut-off frequencies are given by:

$$f_{cL}^{bal} = f_R \left| 1 - \sqrt{1 + \frac{f_L}{f_R}} \right| \tag{2.16}$$

$$f_{cR}^{bal} = f_R \left| 1 + \sqrt{1 + \frac{f_L}{f_R}} \right| \tag{2.17}$$

Therefore, according to the Equation (2.14) and (2.15) the proposed CRLH-filter structure satisfies the balanced condition where

$$L_R C_L = L_L C_R \text{ and } Z_L = Z_R \tag{2.18}$$

The width of the microstrip-line that corresponded to the calculated capacitance values were determined using:

$$w = \frac{h}{\varepsilon_o \varepsilon_r} \left[2C_p - \frac{\sqrt{\varepsilon_{eff}}}{cZ_o} \right] \tag{2.17}$$

Where *c* is the free-space velocity, ε_0 is permittivity of free-space ε_{eff} is the effective microstrip permittivity and Z_o is the characteristic impedance.

2.2.1 Simulation and Measured Results

The microstrip-line circuit was fabricated using standard photolithographic circuit board techniques on a dielectric substrate with dielectric constant (ε_r) of 2.17, thickness (*h*) of 0.794 mm and loss tangent (tanδ) of 0.0009. The thickness (*t*) of the microstrip conductor is 35 microns. Fig. 2-3 shows the physical layout of the single-pole CRLH metamaterial bandpass filter, which has a length of 13.6 mm. The single-pole bandpass filter was designed using the symmetric unit-cell having the following specifications:

- Centre frequency f_o = 2.2 GHz
- Lower cut-off frequency f_{LC} = 2.10 GHz
- Upper cut-off frequency f_{UC} = 2.33 GHz

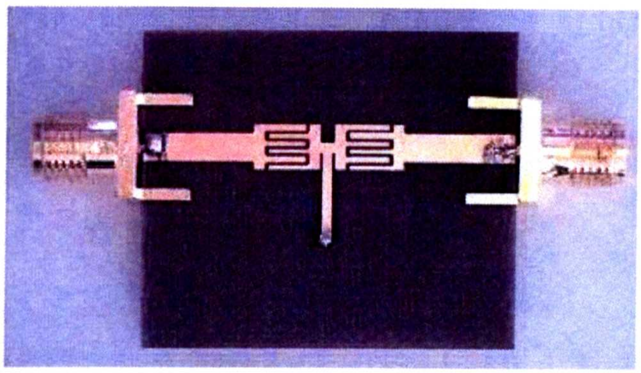

Fig. 2-3 Photograph of the fabricated 1-pole CRLH-TL bandpass filter

The inter-digital capacitor, shown in Fig. 2-3, has the following dimensions:

- Width of each conductor (w) = 0.5 mm
- Space between conductors (g) = 0.5 mm
- Space at end of conductor (g_e) = 0.7 mm
- Length of fingers (l) = 2.49 mm
- Number of fingers (N) = 3

The measured and simulated response of the single-pole CRLH metamaterial bandpass filter is shown in Fig. 2-4. The simulated centre frequency is 2.21 GHz, and the magnitudes of its insertion-loss and return-loss are 0.47 dB and 22.23 dB, respectively. The measured centre frequency is 2.21 GHz, insertion- and return-loss of 0.5 dB and 28.50 dB, respectively. The measured centre frequency is 0.45% below the desired frequency. The slight difference between the measured and simulated results might be due to the high fabrication tolerance and unperfected ground which can be improved by more careful fabrication and measurement technology.

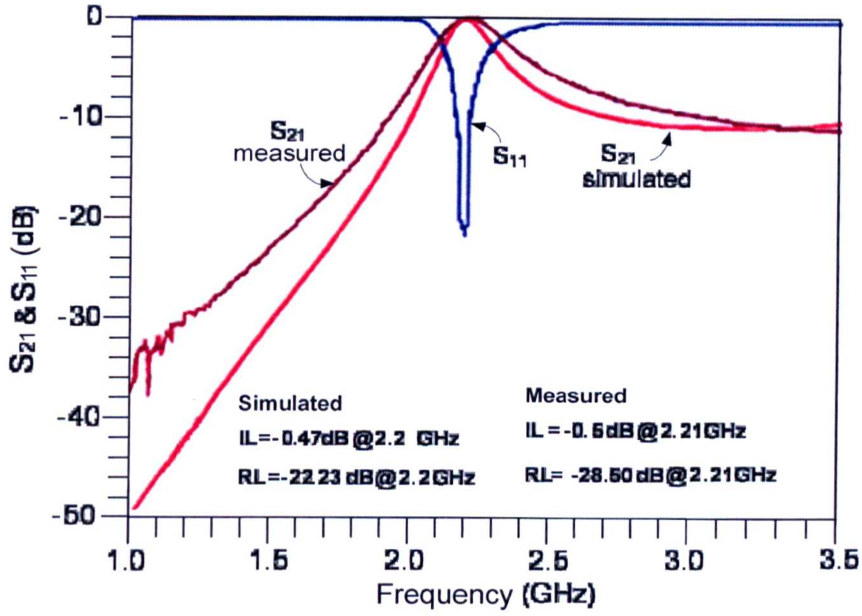

Fig. 2-4 Simulated and measured insertion-loss and return-loss response of the 1-pole CRLH-TL bandpass filter

The symmetrical CRLH-TL unit-cell in Fig. 2-3 can be tuned by controlling the width and length of the inter-digital fingers. These changes in the dimensions will affect the *LC* parameters associated with the microstrip-line to affect the resonant frequency of the unit-cell. The graph in Fig. 2-5 shows that by varying the finger length and width of the inter-digital capacitor has a linear effect on the resonant frequency of the proposed filter. In both cases a tuning range is 23% at f_o is achieved by changing the finger length or width. The insertion-loss remains virtually unaffected with a magnitude of less than 0.6 dB, and the return-loss is greater than 20 dB across the entire tuning range.

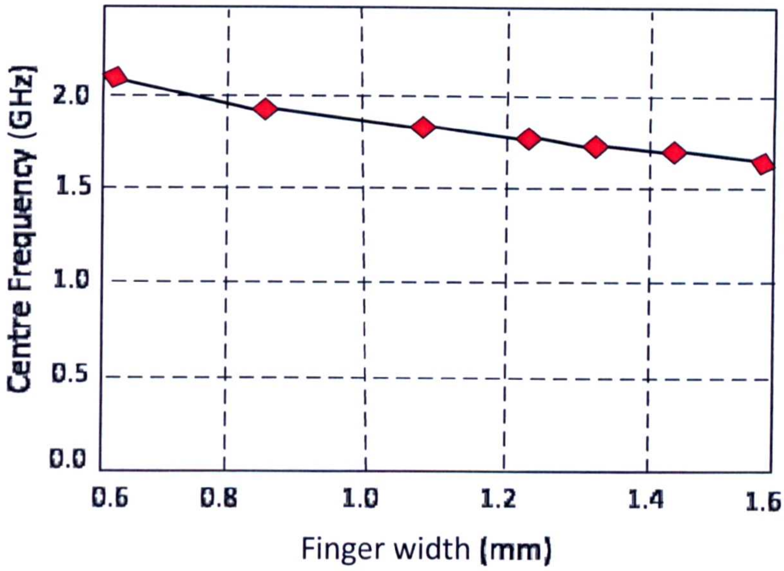

(a)

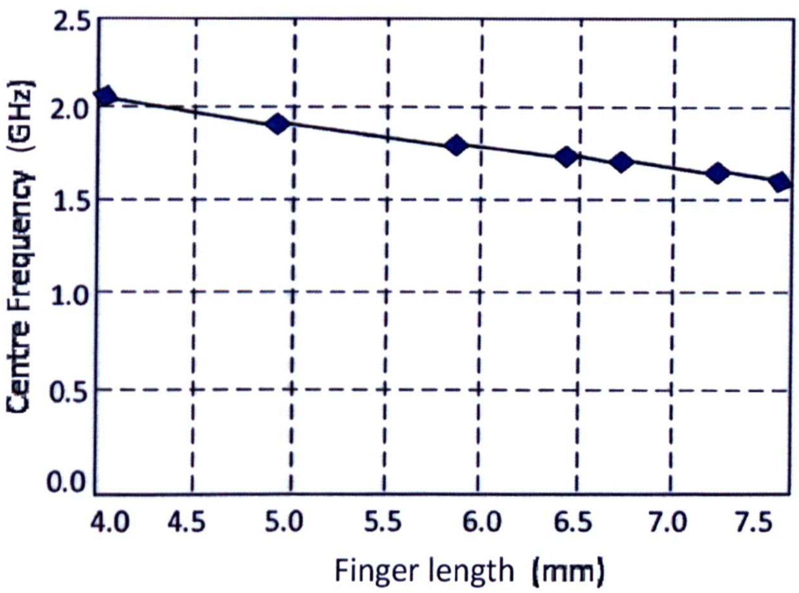

(b)

Fig. 2-5 (a) Metamaterial unit-cell's resonant frequency as a function of finger width, and (b) metamaterial unit-cell's resonant frequency as a function of finger length.

The simulation results in Fig. 2-6 show that the length of the short-circuited stub (l_s), in Fig. 2-2(a), can provide a significant tuning range in the order of 21% without significantly affecting the filter's Q-factor.

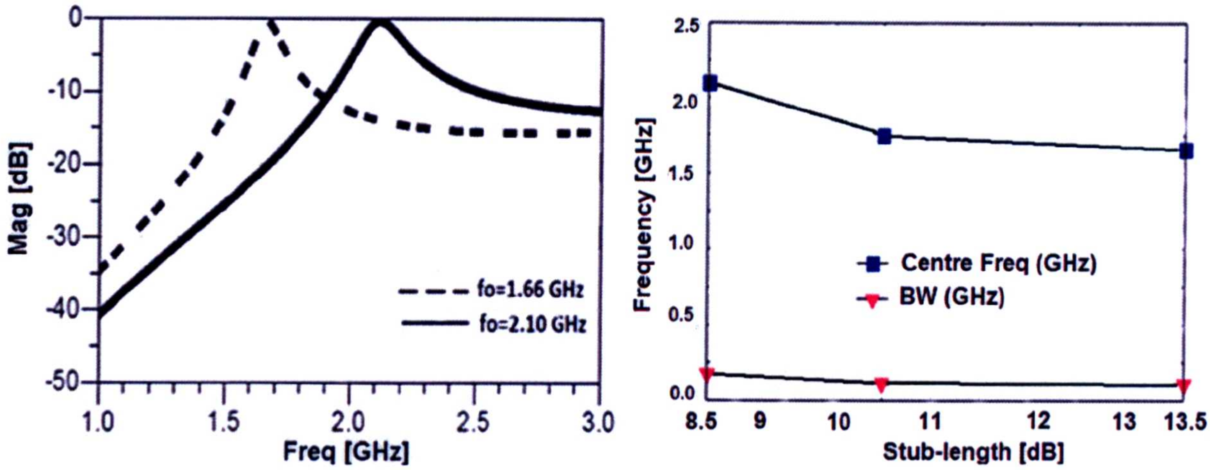

(a) (b)

Fig. 2-6 1-pole CRLH-TL filter, (a) Insertion-loss response, and (b) resonant frequency as a function of inductive stub length

The simulation analysis in Fig. 2-5 and Fig. 2-6 indicates that the dimensions of the filter increase significantly to achieve tuning range from 1.66 GHz to 2.10 GHz. The electromagnetic properties will consequently change too. Conversely, the size of the filter plays the significant role towards the low cost fabrication and circuit miniaturization. It is also well known that changes in dimensions affect the conventional filter's centre frequency. It is shown later a novel technique that allows a wide tuning range (27.3%) to be achieved while maintaining almost similar transmission characteristics without changing size of the filter.

2.2.2 Retrieval Of Electromagnetic Properties Using S-parameters

In the microwave regime once a negative refractive index metamaterial structure has been designed, it is vital to validate the design properties to substantiate the metamaterial characteristics. This can be attained through demonstration of the negative index of refraction. In the proposed meta-structure filter, passband is caused by the combination of negative permittivity (ε) and permeability (μ) that gives rise to a negative effective index of refraction ($n <$ 0) and thus to left-handed propagation of electromagnetic waves. The retrieval method employed in this section is used to characterise the metamaterial unit-cell in terms of its permittivity and permeability. This method is a modification based on the approach used by Smith et al. [2-4] that enables characterisation of either a symmetric or asymmetric planar microstrip structure comprising the unit-cell whose dimensions are much smaller than the free-space wavelength, where the phase across the unit-cell can vary significantly at the operational frequencies.

Metamaterials have been characterized in terms of the index of refraction by computing the average field strengths [2-5] and by tracking the phase inside the metamaterial [2-6]. Both of these methods require knowledge of the electromagnetic field distribution inside the metamaterial; however, these methods cannot be implemented practically through measurements. In addition, reflection (S_{11}) and transmission (S_{21}) coefficients can be used to retrieve the permittivity and permeability and various methods have been developed to do this. In one of these methods the measured S-parameter data is parametrically fitted to known permittivity and permeability models. Shelby et al. [2-5] used this approach to extract permittivity and permeability data of the rod and split-ring resonator metamaterials using the Drude and Lorentz models, respectively [2-7] [2-8]. In this section the reflection and transmission coefficients are derived for a metamaterial circuit implemented on a planar microstrip substrate. It is assumed that the incident wave is TE polarized with a propagation factor e^{ikz}. Hence, the fields in the three regions are given by:

$$E_{0x} = e^{ik_0 z} + Re^{-ik_0 z} \tag{2.17}$$

$$H_{0y} = \frac{k_0}{\omega\mu_0}\left[e^{ik_0 z} - Re^{-ik_0 z}\right] \tag{2.18}$$

$$E_{1x} = Ae^{ik_1 z} + Be^{-ik_1 z} \tag{2.19}$$

$$H_{1y} = \frac{k_1}{\omega\mu_1}\left[e^{ik_1 z} - Re^{-ik_1 z}\right] \tag{2.20}$$

$$E_{2x} = Te^{ik_0 z} \tag{2.21}$$

$$H_{2y} = T\frac{k_0}{\omega\mu_0}e^{ik_0 z} \tag{2.22}$$

where R and T represent the reflection and transmission coefficients, respectively. The metamaterial substrate is characterised by ε_1 and μ_1. The substrate boundaries are at $z = 0$ and $z = d$. Applying the boundary conditions yields the following equations,

$$1 + R = A + B \tag{2.23}$$

$$1 - R = \eta(A - B) \tag{2.24}$$

$$Ae^{ink_0d} + Be^{-ink_0d} = Te^{ik_0d} \tag{2.25}$$

$$Ae^{ink_0d} - Be^{-ink_0d} = \frac{1}{\eta}Te^{ik_0d} \tag{2.26}$$

where the normalised impedance is defined as,

$$\eta = \frac{\eta_1}{\eta_0} = \sqrt{\frac{\varepsilon_0\mu_1}{\varepsilon_1\mu_0}} \tag{2.27}$$

and the index of refraction of the metamaterial substrate is defined as,

$$n = \sqrt{\frac{\varepsilon_1\mu_1}{\varepsilon_0\mu_0}} \tag{2.28}$$

Elimination of the coefficients A and B leads to the following expressions for R and T,

$$2R = \left[\frac{1}{2}(1-\eta)\left(1+\frac{1}{\eta}\right)e^{ink_0d} + \frac{1}{2}(1+\eta)\left(1-\frac{1}{\eta}\right)e^{-ink_0d}\right]Te^{ik_0d} \tag{2.29}$$

$$2 = \left[\frac{1}{2}(1+\eta)\left(1+\frac{1}{\eta}\right)e^{ink_0d} + \frac{1}{2}(1-\eta)\left(1-\frac{1}{\eta}\right)e^{-ink_0d}\right]Te^{ik_0d} \tag{2.30}$$

Solving for R and T yields the following expressions,

$$\frac{1}{S_{21}} = cos(nk_0d) - \frac{i}{2}\left(\eta + \frac{1}{\eta}\right)sin(nk_0d) \tag{2.31}$$

$$\frac{S_{11}}{S_{21}} = -\frac{i}{2}\left(\eta - \frac{1}{\eta}\right)sin(nk_0d) \tag{2.32}$$

The S-parameters are defined in terms of the reflection and transmission coefficients as,

$$S_{11} = R \tag{2.33}$$

$$S_{21} = Te^{ik_0 d} \tag{2.34}$$

The material parameters of the medium are obtained by inverting (2.31) and (2.32) in terms of S_{11} and S_{21} to obtain:

$$\eta = \pm\sqrt{\frac{(1+S_{11})^2 - S_{21}^2}{(1-S_{11})^2 - S_{21}^2}} \tag{2.35}$$

$$Re(n) = \pm Re\left\{\frac{\cos^{-1}\left(\frac{1}{2S_{21}}\left[1-\left(S_{11}S_{22}-S_{21}^2\right)\right]\right)}{k_0 d}\right\} + \frac{2\pi m}{k_0 d} \tag{2.36}$$

$$\mathrm{Im}(n) = \pm \mathrm{Im}\left\{\frac{\cos^{-1}\left(\frac{1}{2S_{21}}\left[1-\left(S_{11}S_{22}-S_{21}^2\right)\right]\right)}{k_0 d}\right\} \tag{2.37}$$

Where m is an integer corresponding to the number of cycles a wave goes through the substrate. Equation (2.36) and (2.37) show that regardless of the wavelength to unit-cell ratio ($k_o d$), an effective refractive index can be recovered from all elements of the S-parameters irrespective of the structure's configuration. Although the retrieval of n is complicated by arccosine function in (2.36) and (2.37); however, this is not the case when the wavelength within the medium is much larger than the length [2-9]. Once the impedance and index of refraction have been retrieved, the relative permittivity and permeability of the substrate can be directly calculated by $\varepsilon_{1r} = n/\eta$ and $\mu_{1r} = n\eta$.

The normalised impedance was computed using:

$$\eta = \pm\sqrt{\frac{(1+S_{11})^2 - S_{21}^2}{(1-S_{11})^2 - S_{21}^2}} \tag{2.38}$$

The index of refraction of the metamaterial substrate was computed using:

$$Re(n) = \pm Re\left\{ \frac{\cos^{-1}\left(\frac{1}{2S_{21}} \left[1 - \left(S_{11}S_{22} - S_{21}^{2} \right) \right] \right)}{k_{0}d} \right\} + \frac{2\pi m}{k_{0}d} \tag{2.39}$$

$$Im(n) = \pm Im\left\{ \frac{\cos^{-1}\left(\frac{1}{2S_{21}} \left[1 - \left(S_{11}S_{22} - S_{21}^{2} \right) \right] \right)}{k_{0}d} \right\} \tag{2.40}$$

Equation (2.40) indicates that regardless of the wavelength to unit-cell ratio ($k_o d$), an effective index can be recovered from all elements of the *S*-parameters irrespective of the structure's configuration. An optimization process has been introduced along the simulation procedure focusing on the filter dimension in order to improve the response of the filter. For the structure in Fig. 2-3, its material properties and impedance were computed using Ansoft's HFSS™ a 3D full-wave electromagnetic field solver based on Equations (2.38)-(2.40). The structure was excited between ports 1 and 2, and the HFSS™ representation of the metamaterial distributed transmission-line circuit is shown in Fig. 2-7.

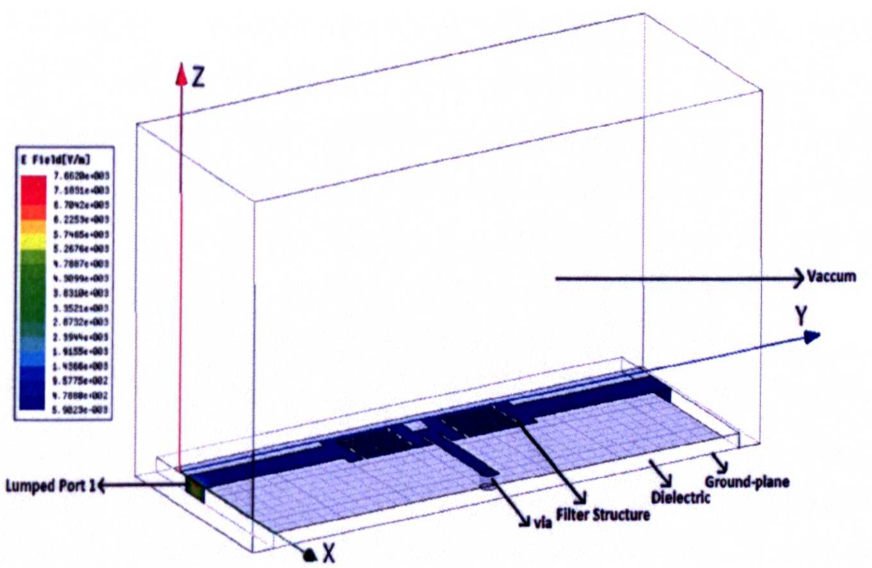

Fig. 2-7 Layout of the metamaterial unit-cell in Ansoft HFSS™

The aforementioned retrieval method using S-parameter was used to show the planar composite structure of Fig. 2-7 exhibited negative refractive index across a defined frequency band. The structure's material properties and impedance were computed using Ansoft's HFSS™ a 3D full-wave electromagnetic field solver based on finite element method. The structure was excited between input and output ports 1 and 2, in Fig. 2-7. It should be noted the retrieval method is applied to geometries of infinite extent in the two directions perpendicular to the direction of propagation, which can be modelled numerically by using periodic boundary conditions, as implemented in the FDTD and MoM techniques. In practice these types of geometries can be realised by surrounding the finite sized substrate with microwave absorbing material or by using a single-mode waveguide. The two segments of microstrip-line besides the CRLH at the two ports will change the phase of S-parameters. Hence, their length was adjusted to negate this effect. The resulting characterising properties of the structure are shown in Fig. 2-8, where the permittivity and permeability are simultaneously negative between 2.23 to 2.40 GHz; hence the index of refraction of the unit-cell is negative across this frequency band. The structure's normalised impedance magnitude (real), shown in Fig. 2-8(c), varies between 0.4 and 1.28 across the 2.23 to 2.40 GHz, however the imaginary part of the impedance is zero.

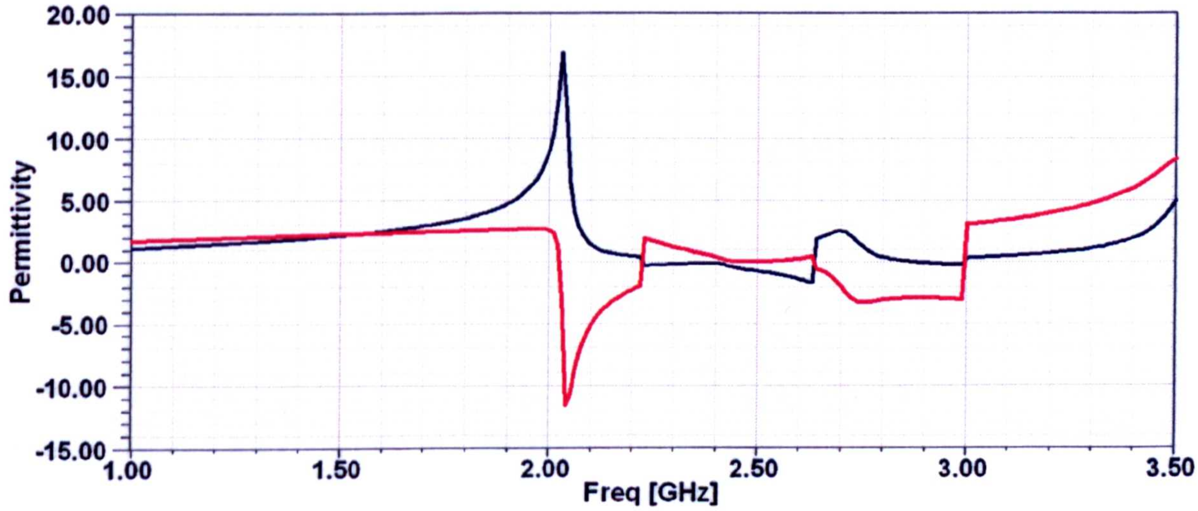

(a) Permittivity (Re[ε] is the blue curve, Im[ε] is the red curve)

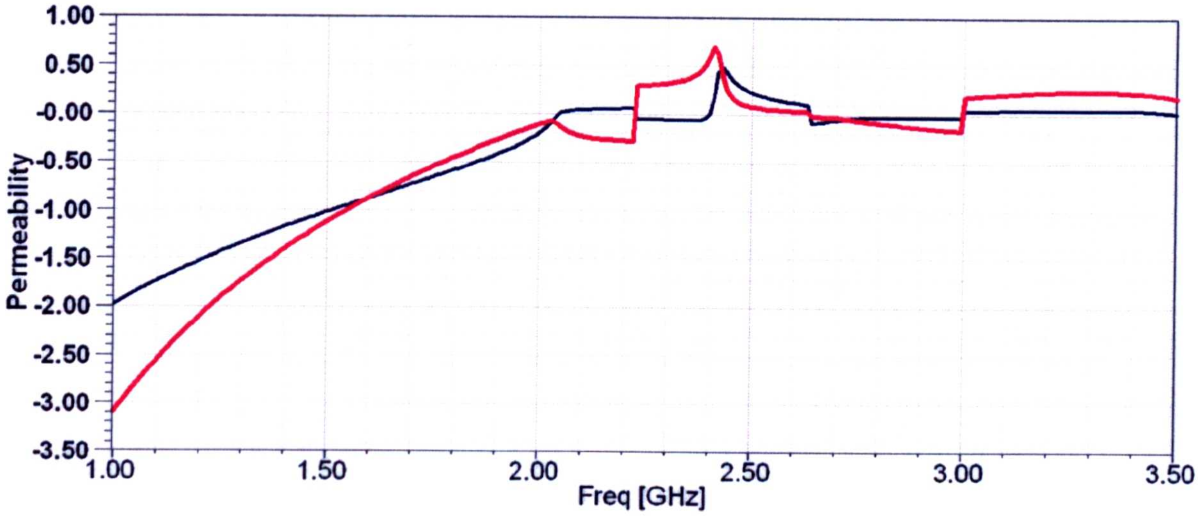

(b) Permeability (Re[μ] is the blue curve, Im[μ] is the red curve)

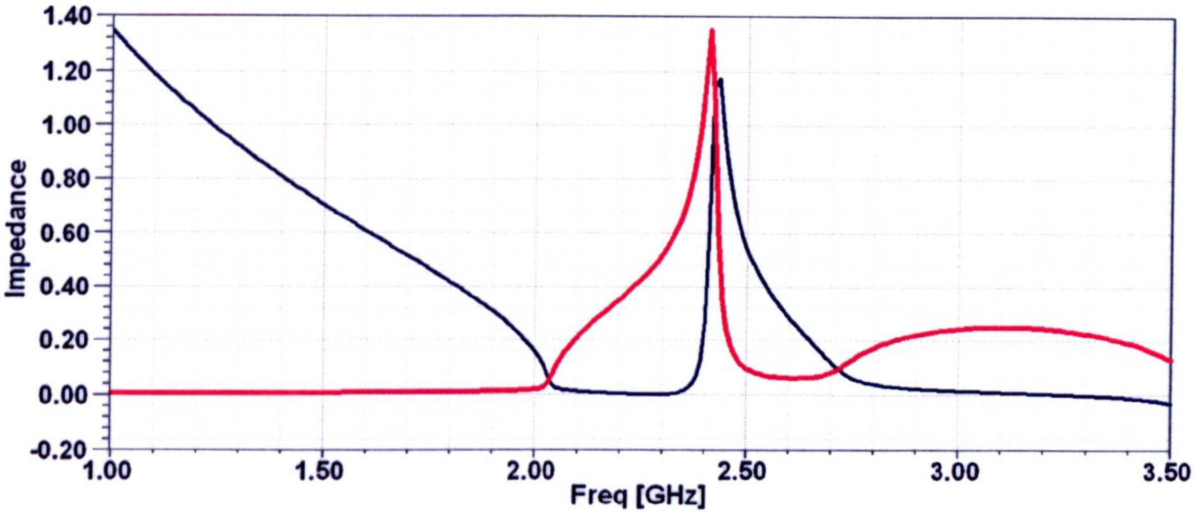

(c) Impedance magnitude (Re[Z] is the blue curve, Im[Z] is the red curve)

Fig. 2-8 CRLH metamaterial unit-cell's electrical properties as a function of frequency: (a) permittivity, (b) permeability, and (c) impedance magnitude

2.3 Two-Pole CRLH-TL Filter

In this section, a two-pole bandpass filter based on CRLH-TL is presented that was designed at a centre frequency of 2.2 GHz with a 3 dB bandwidth of 278 MHz. Other specifications of the filter are given in Table 2-2. The CRLH-TL unit-cell structure of the filter comprises of three asymmetric inter-digital capacitors (*IDC*) with inductive stubs short-circuited to the ground using vias. The stubs are connected at the junction between the adjacent capacitors as shown in Fig. 2-9. According to the simulation analysis, the capacitive gaps between the inter-digitally coupled fingers can enhance the filter's transmission performance, i.e. bandwidth and insertion-loss. In particular, the capacitive gap of the first and last inter-digital capacitors (*IDC1* and *IDC3*) control the passband loss, whereas the gap of the middle inter-digital capacitor (*IDC2*), shown in Fig. 2-11(b), controls the filter's passband bandwidth. The grounded stub inductor length must have the same dimensions to ensure that acceptable filter response is obtained, and this was substantiated through a rigorous optimization process.

The filter's design was initially simulated and optimized using ADS™ (MoM) before fabrication. Its performance was confirmed through measurement as shown in Fig. 2-10. The filter's 50Ω input and output feed-lines are tapered to improve its passband insertion-loss between 2.08-2.36 GHz. The two-pole filter, shown in Fig. 2-10(a) is 80% smaller than a conventional edge-coupled filter with the same specifications.

Filter Specifications	
Filter Order	2
Centre Frequency	2.2 GHz
Fractional BW (%)	12.63
Source/ Load termination	50 Ω

Table 2-2: Two-pole filter specifications

The lumped element components of the equivalent electrical circuit, shown on Fig 2-9(b), were calculated using Equation (2.6), (2.7), (2.12) and (2.13). The calculated inductance and capacitance values were: L_R = 20.69 nH, C_R = 16.55 pF, L_L = 0.265 nH, C_L = 0.212 pF, L_{R1} = 41.41 nH and C_{L1} = 0.106 pF. C_R and L_R are the parasitic capacitance and inductance, respectively, of the shunted inductive line and the middle section of the unit-cell in Fig. 2-9(a). The corresponding dimensions of unit-cells elements *IDC1* and *IDC3*, defined in Fig. 2-2, are: w = 0.5 mm, g = 0.2 mm, g_e = 0.25 mm, and l =3.5 mm. For *IDC2*, the dimensions are: w = 0.5 mm, g = 0.73 mm, g_e = 0.25 mm, l = 2.40 mm. The length and the width of the stub inductors are 8.4 mm and 1 mm, respectively. The proposed microstrip filter structure occupies an area of $19.99 \times 12.40\ mm^2$.

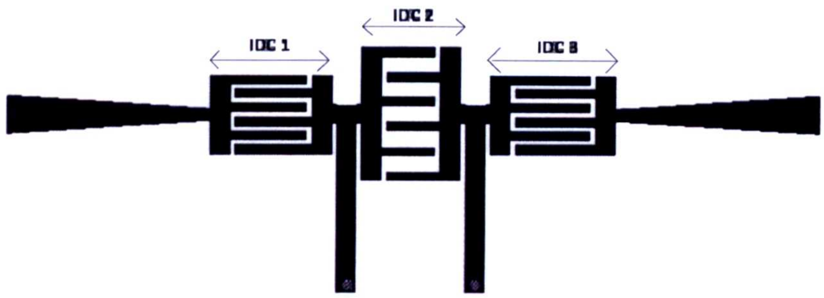

(a)

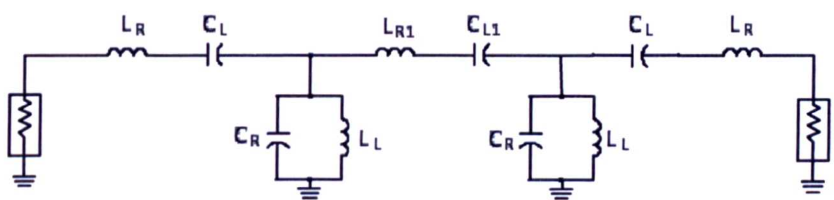

(b)

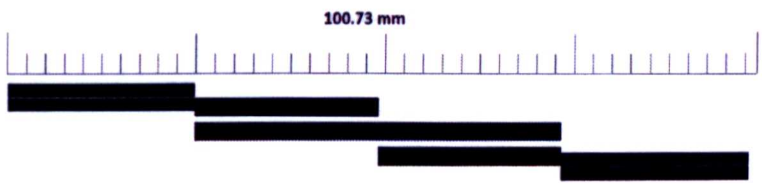

(c)

Fig. 2-9 (a) Physical layout of the composite right/left-handed metamaterial unit-cell structure of the 2-pole filter, (b) equivalent circuit, and (c) conventional parallel coupled-line filter layout designed using the same specifications as the proposed 2-pole CRLH filter

(a)

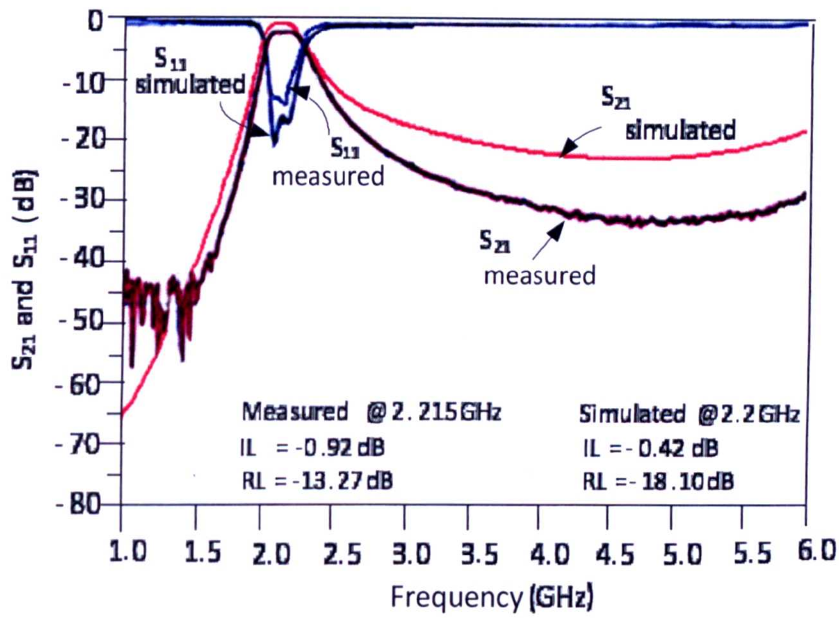

(b)

Fig. 2-10 (a) Photograph of the 2-pole CRLH-TL filter, and (b) simulated and measured insertion-loss and return-loss response of the filter

2.4 Three-pole CRLH-TL Filter

This section describes the design of a three-pole bandpass filter. The design procedure follows the two-pole design in section 2.3. Here three CRLH-TL unit-cells are connected in a cascade to create the filter. The main objective in this case was to achieve the followings requirements:

- Develop a filter with a bandwidth of 230 MHz
- Attain a low insertion-loss and high return-loss characteristics
- Attain a sharper passband edge selectivity

The filter's specifications are given in Table 2-3. The layout geometry of the CRLH-TL filter, shown in Fig. 2-11, includes the following set of identical elements *IDC2* and *IDC3*, and *IDC1* and *IDC4*. Simulation analysis shows that the gap between the inter-digitally coupled fingers of *IDC2* and *IDC3* control the filter's bandwidth, and the length of the shunted stub inductors controls its centre frequency. The length and the impedance of the shunted stubs were made to be equal to ensure an acceptable bandpass filter response. This was confirmed through a simulation analysis. Fig. 2-12 shows that the stub length can be used to tune the filter's centre frequency without adversely affecting its bandwidth and selectivity. A substantial tuning range of 1 GHz can be achieved. The filter's 50Ω input and output feed-lines are tapered to improve its passband insertion-loss between 2.08-2.31 GHz. The 3-pole filter, shown in Fig. 2-11(a) is 72% smaller than a conventional parallel edge-coupled filter designed with the same specifications on the same dielectric medium.

Filter Specifications	
Filter Order	3
Centre Frequency	2.2 GHz
Fractional BW (%)	10.45
Source/ Load termination	50 Ω

Table 2-3: 3-pole filter specifications

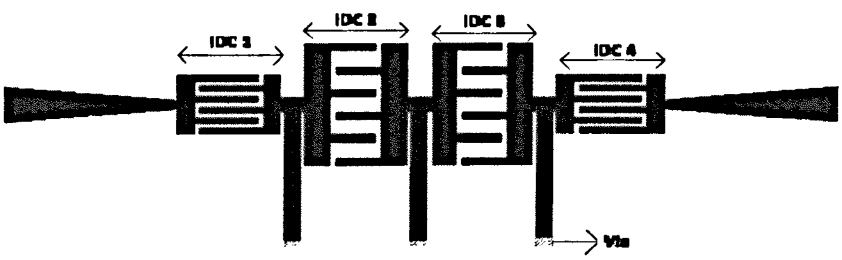

(a)

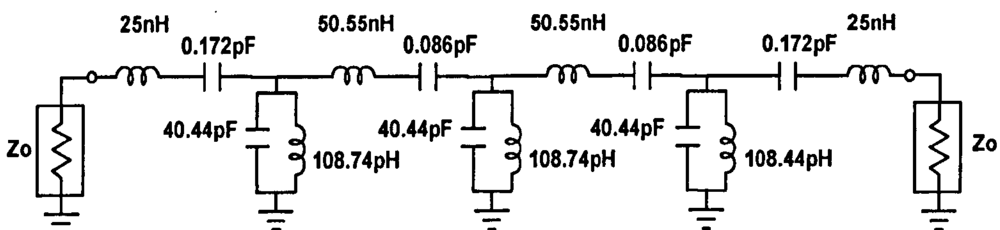

(b)

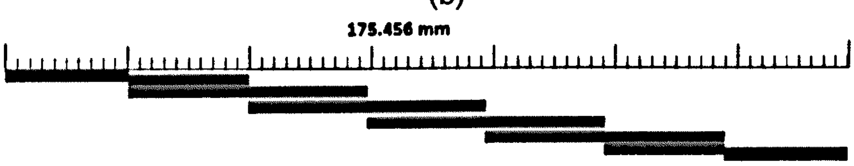

(c)

Fig. 2-11 (a) Physical layout of the CRLH-TL 3-pole filter, (b) equivalent circuit model of the 3-pole filter, and (c) conventional parallel coupled-line filter with same specifications as proposed 3-pole CRLH filter

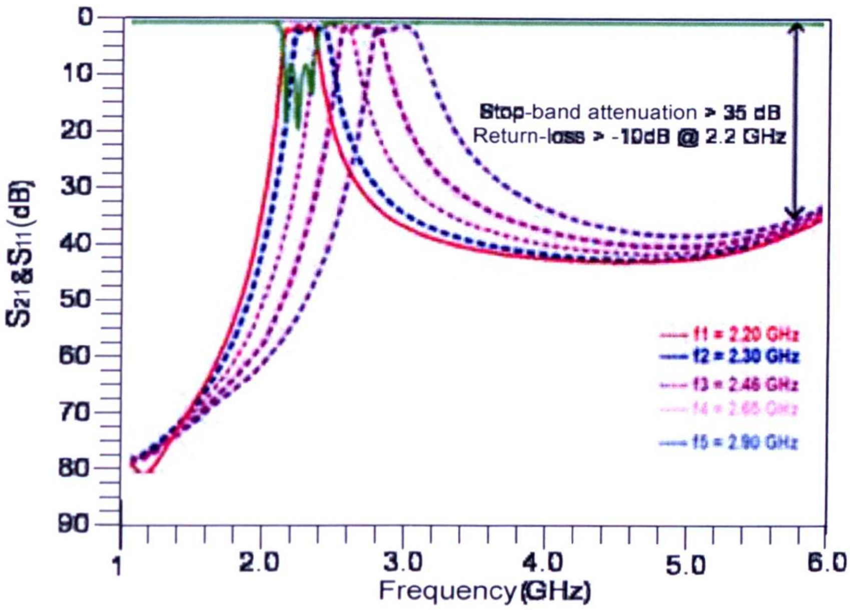

Fig. 2-12 Filter response as a function of stub length

The lumped element components of the circuit in Fig. 2-11(b) were calculated using Equation (2.6), (2.7), (2.12) and (2.13). The calculated inductance and capacitance values are: L_R = 68.07 nH, C_R = 27.48 pF, L_L = 0.189 nH, C_L = 0.0758 pF, L_{R1} = 136.14 nH, and C_{L1} = 0.0379 pF. The input impedance of each unit-cell will differ as it's not a symmetrical structure. The corresponding inter-digital capacitors elements, shown in Fig. 2-11, have dimensions given below. For *IDC1* and *IDC4*: w = 0.5 mm, g = 0.65 mm, g_e = 0.25 mm, and l =3.7 mm. For IDC2 and IDC3: w = 0.5 mm, g = 0.65 mm, g_e = 0.25 mm, and l = 2.40 mm. Length and the width of the stub inductors are 8.6 mm and 1 mm, respectively.

(a)

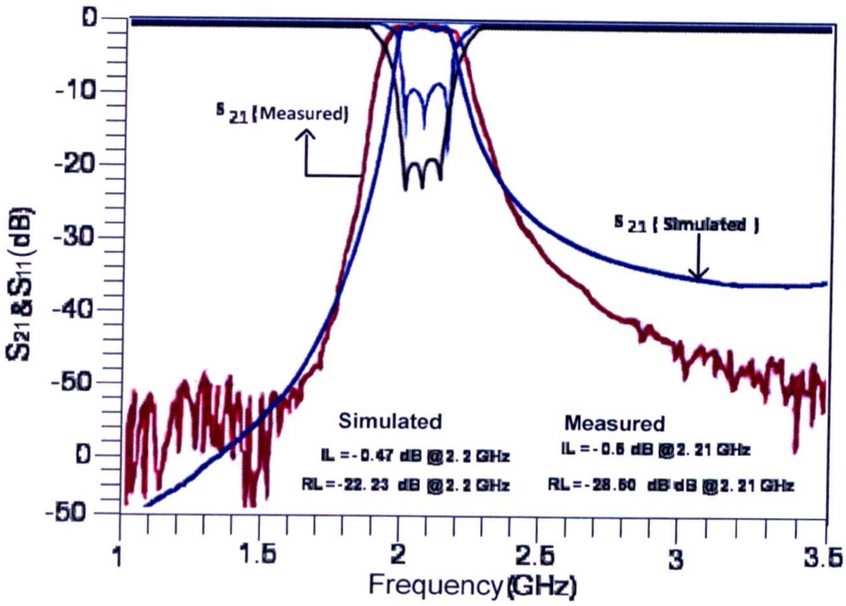

(b)

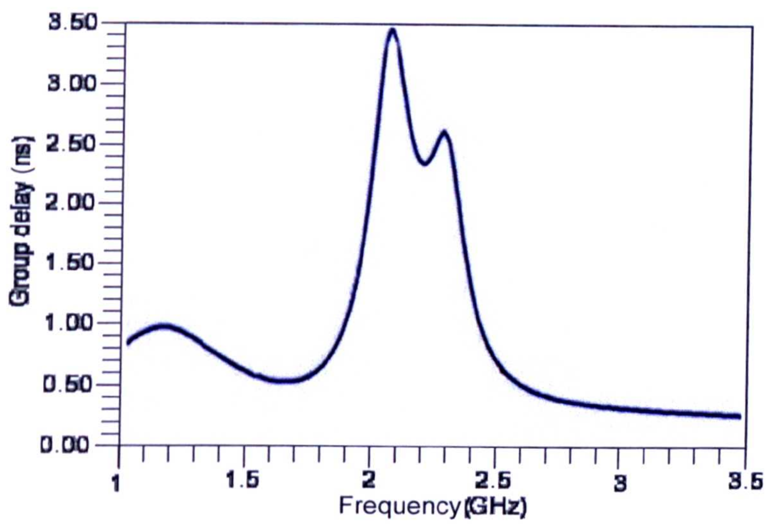

(c)

Fig. 2-13 (a) Photograph of the 3-pole CRLH-TL filter, (b) simulated and measured performance, and (c) group delay (simulated)

A photograph of the 3-pole CRLH-TL filter is shown in Fig. 2-13(a). The microstrip filter has an area of 28.16x12.50 mm^2. The simulated and measured performance of the filter, shown in Fig. 2-13(b), shows good correlation. The filter's simulated centre frequency is 2.2 GHz whereas its actual measured results is 2.13 GHz, which is 2.32% below the desired frequency. The magnitude of measured insertion-loss and return-loss are 0.7 dB and 9.25 dB, respectively. The return-loss can be improved by more carefully designing the feed-line matching network to the filter. The group-delay in the passband varies by ~1.1 ns, which is considered acceptable for practical applications.

2.5 Four-Pole CRLH-TL filter

This section gives insight to the design of a higher order CRLH-TL filter developed to operate at a centre frequency of 2.2 GHz with a bandwidth of 249 MHz. The proposed structure is composed of four microstrip CRLH-TL unit-cells, where each unit-cell consists of a pair of inter-digital capacitors with a short-circuited inductive stub. The impedance of the inductive stub was found to control the centre frequency of the filter. In addition, a curved high impedance feed-line results in an enhancement in the filter's passband insertion-loss and suppression of high order spurii.

The 4-pole CRLH-TL filter's lumped elements, shown in Fig. 2-14, were calculated using Equation (2.6), (2.7), (2.12) and (2.13) for the given specifications. The dimensions of the inter-digital capacitors forming the filter are given in Table 2-4. The inductive line has a length of 11.3 mm and width of 1 mm, which was determined through simulation analysis. Fig. 2-15 shows the layout of the filter.

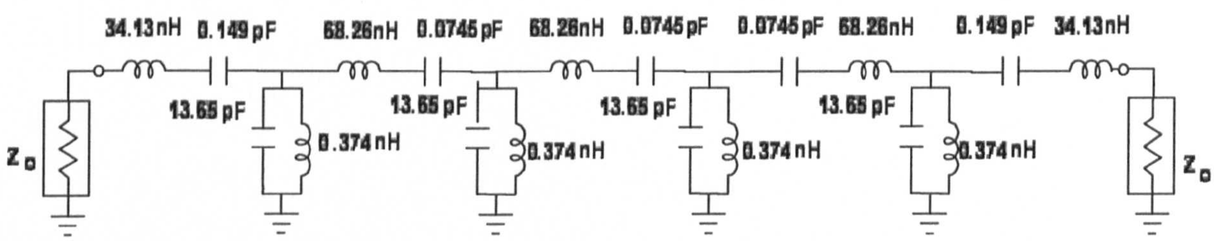

Fig. 2-14 Equivalent electrical circuit of the 4-pole filter

IDC	w (mm)	g (mm)	g_e (mm)	l (mm)	N
1 & 5	0.25	0.2	0.25	3.7	3
2,3,& 4	0.55	0.2	0.25	2.4	3

Table 2-4: Dimensions of inter-digital parameters for the 4-pole filter

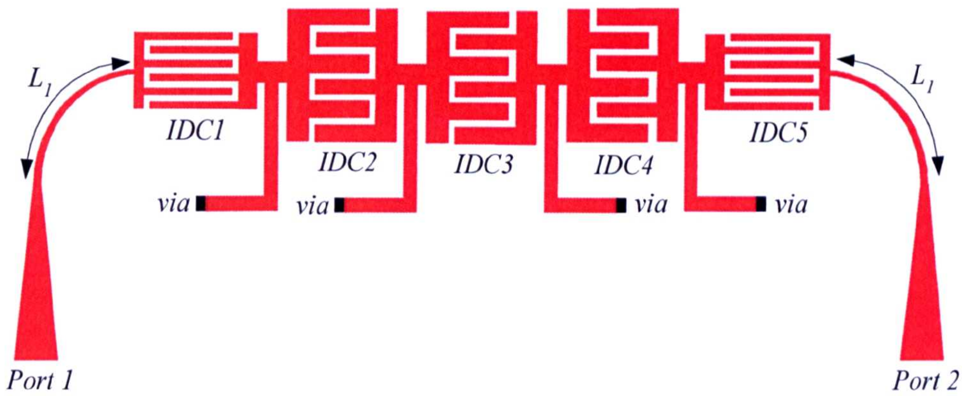

Fig. 2-15 Layout of the CRLH-TL 4-pole filter

Conventional resonant structure's *Q*-factor is inversely related to its bandwidth, and directly related to its loss. Therefore there is a trade-off between the fractional bandwidth and loss. In [2-10] the filter's bandwidth is improved by increasing the number of unit-cells. However, the simulation results in Fig. 2-16 show that by altering the gap (*g*) between the fingers of the inter-digital capacitors the bandwidth of the filter can be changed without adversely affecting its selectivity, *Q*-factor and loss performance. Also it is not necessary to increase the number of unit-cells. Table 2-5 gives the stub length and characterising other parameters corresponding to various gaps defined in Fig. 2-16.

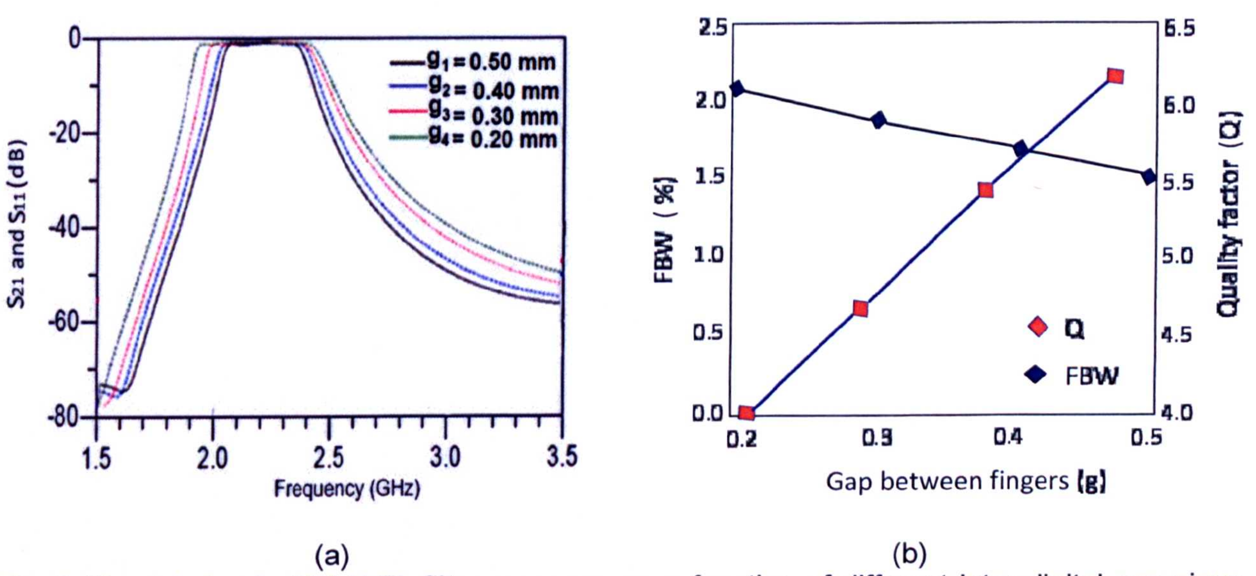

Fig. 2-16 (a) 4-pole CRLH-TL filter response as a function of different inter-digital gap sizes, and (b) *Q*-factor and fractional bandwidth vs gap size

Gap	Stub length (mm)	Fractional BW (%)	IL (dB)	RL (dB)	Q-factor
g_1	10.5	15.90%	0.984	12.45	6.11
g_2	11.5	18.18%	0.778	14.00	5.50
g_3	10.8	21.09%	0.573	20.00	4.68
g_4	8.30	24.54%	0.561	20.00	4.00

Table 2-5: Parameters of 4-pole CRLH-TL filter for different inter-digital finger gaps

Fig. 2-17 confirms good agreement between the simulation and measured results. The measured results show the worst case passband insertion-loss is 0.5 dB and return-loss is better than 10 dB. The out-of-band rejection level at the lower and upper passband edges is > 40 dB/GHz and the fractional bandwidth of the filter is 15.9%.

The 4-pole CRLH-TL filter is 42.50 mm in length whereas conventional parallel edge-coupled filter, shown in Fig. 2-18, with similar performance has a length of 258.07 mm. This confirms that ~86% reduction in size is achieved with the proposed filter configuration.

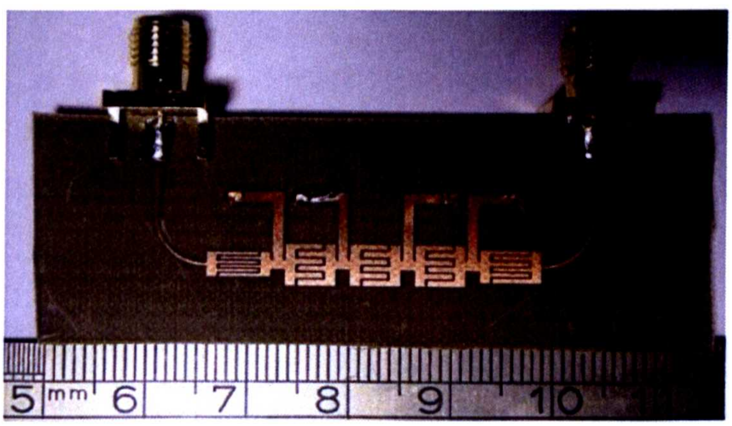

(a)

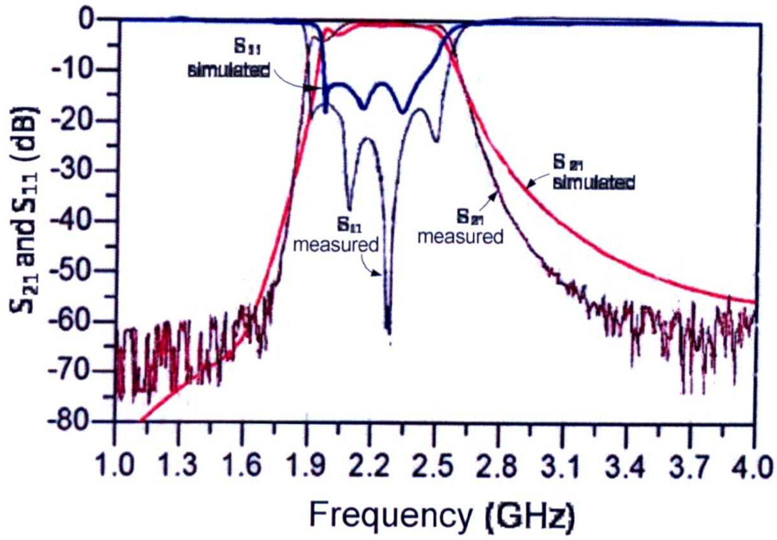

(b)

Fig. 2-17 (a) Photograph of the 4-pole CRLH-TL filter, and (b) simulated and measured response of the filter

Fig. 2-18 Layout of a conventional parallel coupled-line filter designed for the same specifications as the proposed 4-pole CRLH filter

2.6 Prefabrication Tuning of CRLH-TL Unit-Cell

This section explores a technique to tune the centre frequency of the CRLH-TL unit-cell without affecting the unit-cell structure's pre-determined physical attributes. This was achieved by defecting the ground-plane of the unit-cell with a rectangular dielectric slot. The proposed structure is shown to exhibit substantial tuning of the unit-cell's resonant frequency in the order of 26.5%, which is realized as a function of the slot location underneath the unit-cell. It is demonstrated that this prefabrication tuning methodology enables quick and accurate adjustment of the center frequency of filters developed using this resonant structure; thus compensating for the effects of unwanted parasitics. This is because the technique proposed has minimal effect on the unit-cell's, and therefore the filter's, insertion and return-loss performance, and its selectivity. Normally the filter's performance is acutely sensitive to the dimensions of the unit-cell; relatively small changes to the dimensions of the structure can adversely affect the filter's bandpass performance. The advantage of the proposed technique is that it permits the filter to be tuned by merely adjusting the position of the dielectric slot. In addition, it eases the trade-off constraints and makes possible the realization of challenging filter specifications using CRLH unit-cells constituted from microstrip distributed transmission-lines.

2.6.1 CRLH-TL Unit-Cell With Defected Ground-Plane Structure

The resonant frequency of the CRLH-TL unit-cell can be adjusted or tuned by defecting the ground-plane of the metamaterial structure with a rectangular dielectric slot orientated orthogonal to the inductive line as illustrated in Fig. 2-19. The electromagnetic interaction between the dielectric slot and the inductive line perturb the *LC* parameters associated with the microstrip-line to affect the resonant frequency of the unit-cell. The rectangular area etched in the dielectric substrate's metallic ground-plane reduces the effective electric field within the microstrip configuration due to the absence of the base metal section. Thus, the effective capacitance of the short-circuited shunt stub in the region of the slot is increased. Furthermore, the rectangular slot behaves as a resonant structure that is inductively coupled with the shunt stub. The inclusion of the slot introduces a loss of 0.42 dB. The graph in Fig. 2-20 shows how the normalised resonant frequency of the unit-cell is affected by altering the vertical position of the slot along the vertical y-axis in relation to the unit-cell, as indicated in Fig. 2-19(a). The graph is valid for a slot length and width of 13.6 mm and 1.5 mm, respectively, constructed on a dielectric substrate with dielectric constant of 2.17 and thickness of 0.794 mm. The inter-digital capacitor, shown in Fig. 2-19, has the following parametric dimensions:

- Width of each conductor (w) = 0.5 mm
- Space between conductors (g) = 0.5 mm
- Space at end of conductor (g_e) = 0.7 mm
- Length of fingers (l) = 2.49 mm
- Number of fingers (N) = 3

The filter's design was initially simulated and optimized using electromagnetic solver ADS^{TM} (MoM).

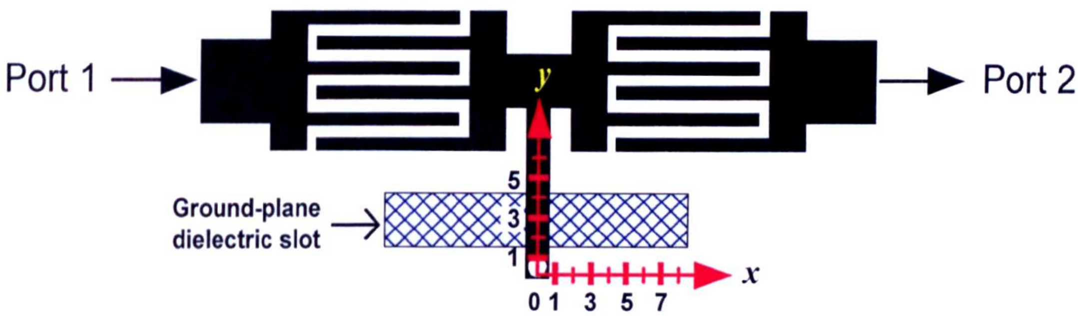

(a)

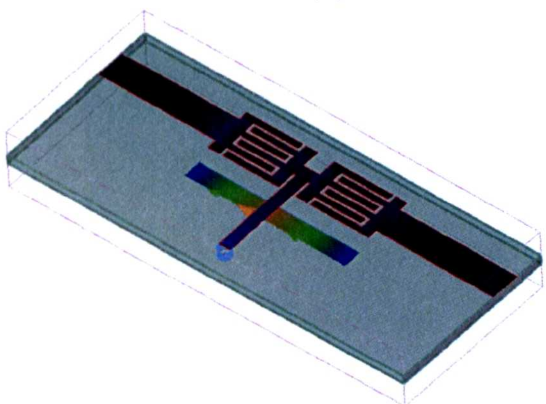

(b)

Fig. 2-19 Metamaterial unit-cell with ground-plane dielectric slot, (a) Plain-view, and (b) perspective view

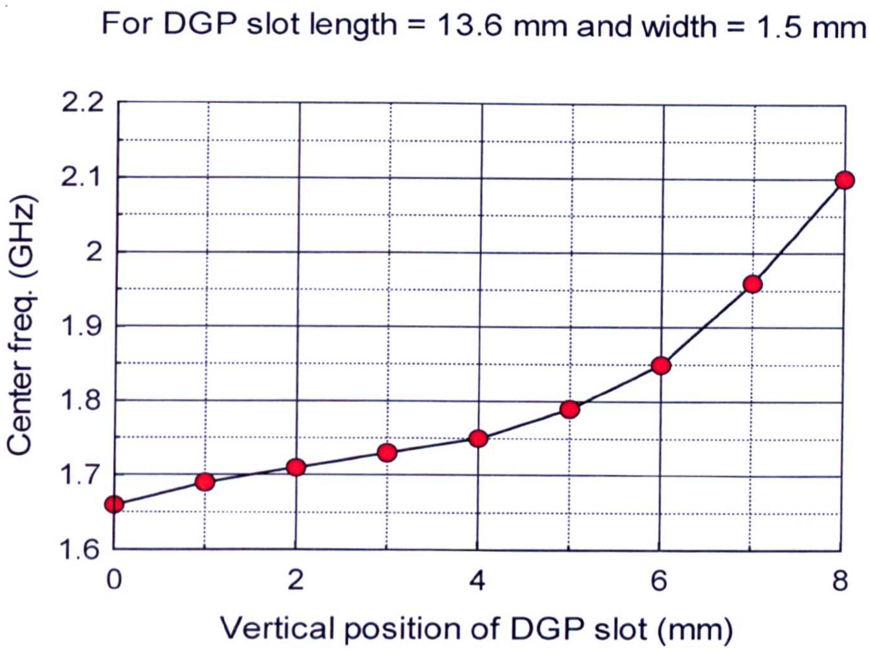

Fig. 2-20 Metamaterial unit-cell's normalised resonant frequency as a function of vertical position of the defected ground-plane (DGP) slot for a slot length and width of 13.6 mm and 1.5 mm, respectively

In Fig. 2-20 shows the tuning to increase with vertical position of the slot, which follows a second degree polynomial function. A tuning range of 26.5% at f_o is achieved by moving the dielectric slot 8 mm from the defined datum point. Fig. 2-21 shows that the insertion-loss is virtually unaffected and whose magnitude is less than 0.4 dB and the return-loss is greater than 18 dB across the entire tuning range. Fig. 2-22 shows that the 3 dB bandwidth of the unit-cell gradually increases with the vertical position of the slot. The bandwidth increases from 120 to 200 MHz with increase in vertical position of slot from 0 to 8 mm.

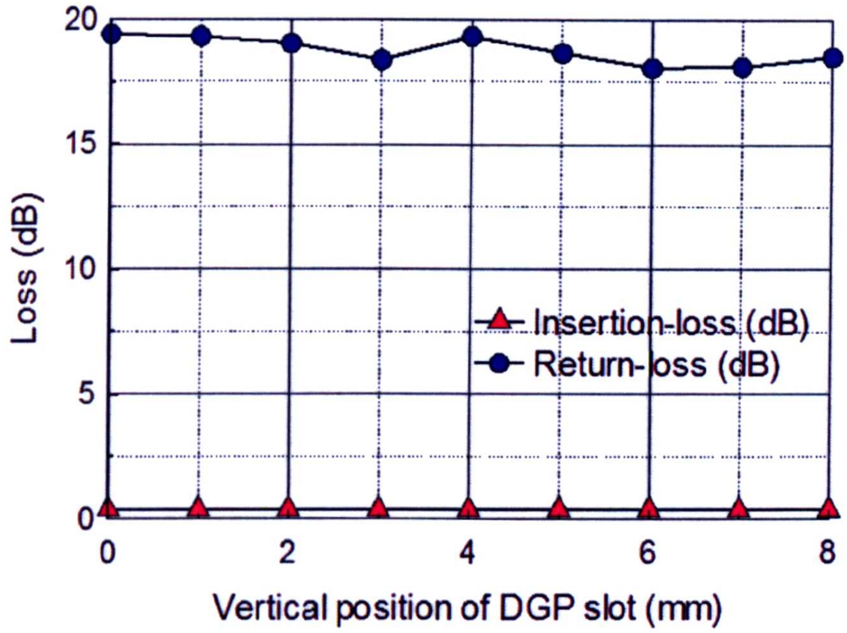

Fig. 2-21 Metamaterial unit-cell's insertion-loss and return-loss as a function of vertical position of ground-plane dielectric slot for a slot length and width of 13.6 mm and 1.5 mm, respectively.

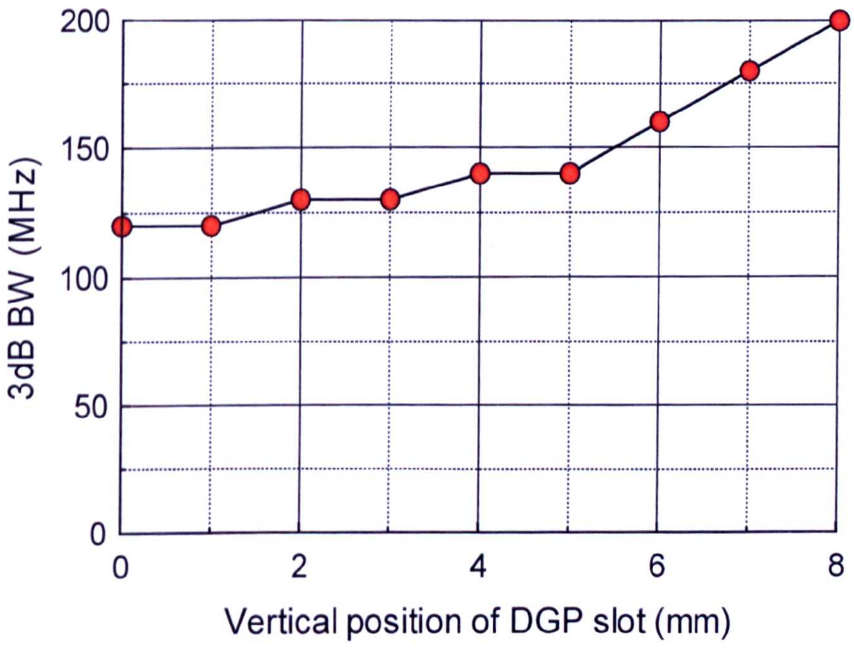

Fig. 2-22 Metamaterial unit-cell's 3 dB bandwidth as a function of vertical position of ground-plane dielectric slot for a slot length and width of 13.6 mm and 1.5 mm, respectively.

2.6.2 Fabrication and Measurement

Fig. 2-23 shows a photograph of the fabricated CRLH-TL unit-cell with a defected ground-plane (DGP) structure, and its measured response with and without the DGP slot. In the measurement the horizontal dielectric slot was located 1 mm above via (reference point). According to the measured results in Fig. 2-23(c), the centre frequency shifts to from 2.2 GHz to 1.66 GHz with the slot with no adverse affect on the unit-cell's overall response. This validates the effectiveness of the proposed technique.

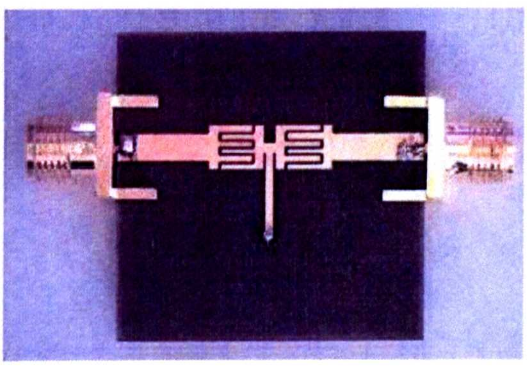

(a)

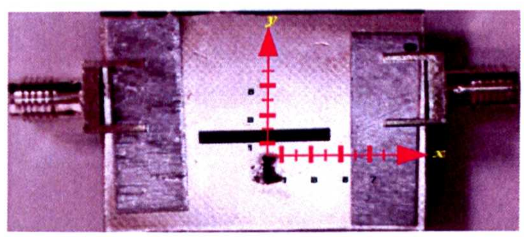

(b)

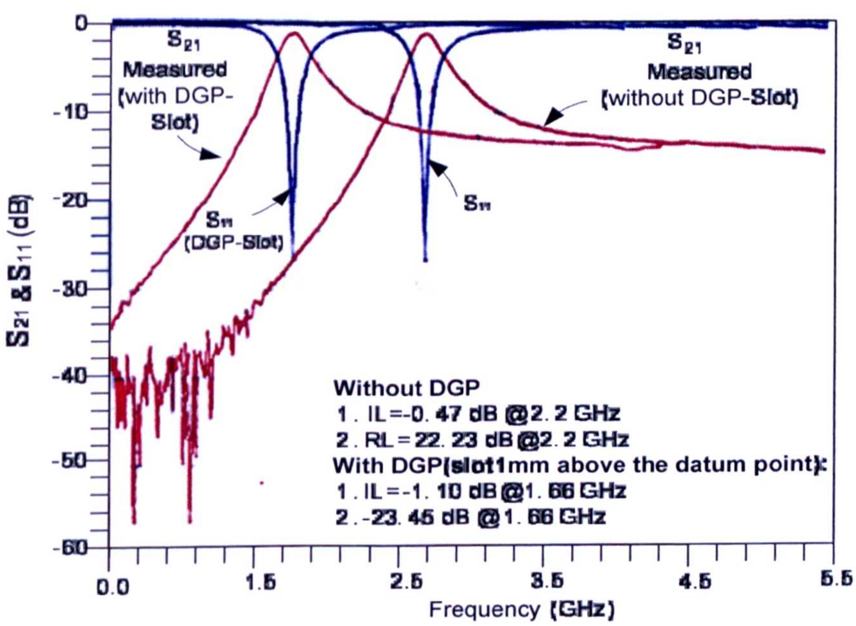

(c)

Fig. 2-23 Photographs of the fabricated 1-pole CRLH-TL unit-cell with defected ground-plane (DGP), (a) top view, (b) bottom view, and (c) measured response with and without DGP

2.7 Two-Pole CRLH-TL Filter with DGP Slot

This investigation analyses the effect of the ground-plane dielectric slots on higher order filters based on CRLH-TL unit-cell structures. The unit-cell structure is shown in Fig. 2-24(a). Its resonant frequency is perturbed by defecting the ground-plane of the unit-cell structure with three rectangular dielectric slots orientated orthogonal to the shunt inductive lines and located immediately below the slots. The electromagnetic interaction between the dielectric slot and the inductive line perturb the *LC* parameters associated with the microstrip-lines to affect the resonant frequency of the structure. A simulation analysis was carried out below using ADS.

The graph in Fig. 2-24(b) shows the response of the 2-pole CRLH-TL filter can be tuned by changing the vertical position of the dielectric slots under the filter's inductive stubs. In fact, the slot positions are identical with respect to the shunted inductive stubs. A tuning range of 9% at f_0 is achieved by moving the dielectric slots by 8 mm from the defined datum point (i.e. via). These results show that there is no adverse affect on the filter's response in terms of insertion-loss, return-loss, bandwidth and selectivity. The importance of this is significant especially in the design of metamaterial bandpass filters that are required to meet stringent design specifications where the equivalent microstrip representation of the lumped elements is not easily realisable using conventional MIC technology. The proposed tuning mechanism relaxes the design of metamaterial filter for practical implementation.

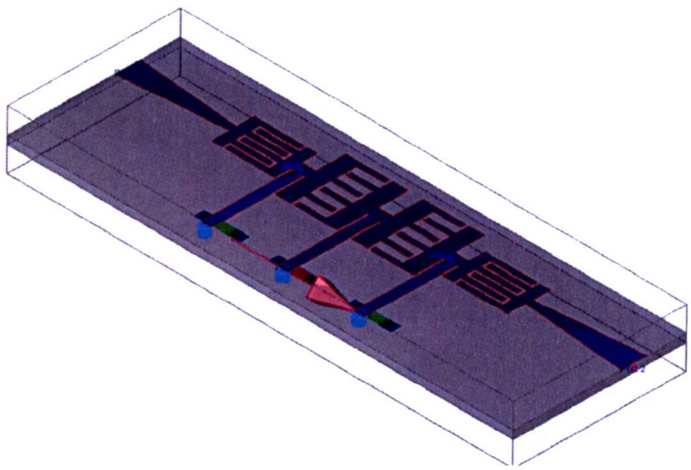

(a)

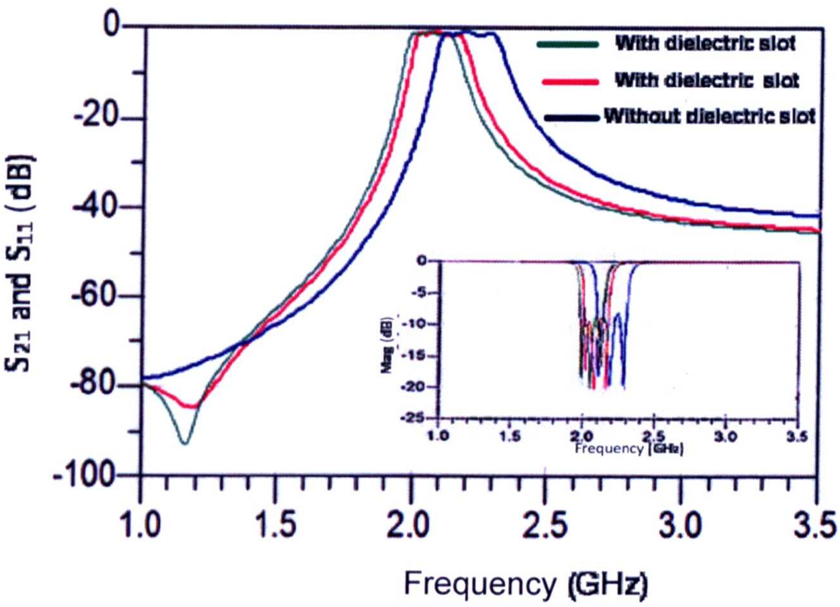

(b)

Fig. 2-24 (a) Structure of the 2-pole CRLH-TL filter, and (b) response of 2-pole CRLH-TL filter with and without ground-plane dielectric slot

2.8 Conclusion

A detailed analysis of the 1-4 pole bandpass filters based on composite right/left-handed (CRLH) metamaterials has been presented in this chapter. The partial left-handedness and partial right-handedness effect in the proposed CRLH ladder network is shown to offer the desired bandwidth, passband loss and selectivity performance. In addition, it was shown the coupling gap of the fingers in the inter-digital capacitor control the filter's bandwidth and transmission-loss performance. Also the length of the short-circuited inductive stub controls the centre frequency of the filter, enabling fine tuning over a relatively large frequency range. An investigation done by Caloz et al. in [2-10] using the CRLH-TL ladder network of unit-cells show the bandwidth of the filter can be increased by increasing the number of unit-cells. However, it has been shown in this chapter that with the proposed CRLH-TL filter structures the bandwidth of the filter can be adjusted by merely changing the gap between the fingers of the inter-digital capacitors without adversely affecting the filter's overall performance. This technique is shown to substantially reduce the filter's size, thus aiding miniaturisation. Moreover, these filter configurations generate no higher order spurii closer to the passband. It was shown that higher order CRLH-TL filters exhibit sharper passband selectivity. Hence, this filter design technique was used to develop novel wideband and ultra-wideband filters.

Planar CRLH-TL metamaterial unit-cell whose ground-plane is defected with a dielectric slot is shown to exhibit substantial tuning properties as a function of the slot position with no adverse effect on its insertion-loss, return-loss, bandwidth and selectivity characteristics. It was shown that this technique provides the necessary tuning mechanism that relaxes the trade-off constrains for filter realisation using distributed transmission-line technology, especially for designs requiring stringent specifications.

2.9 References

[2-1] I. Zagoya-Mellad, A Corona-Chave, I. Llamas-Garro, "Miniaturized metamaterial filters using ring resonators," IEEE International Microwave Workshop Series on Signal Integrity and High-Speed Interconnects, pp.45-48, 2009.

[2-2] H. Lobato-Morales, A. Corona-Chavez, J. Rodriguez-Asomoza, "Novel channelization multiplexer using Metamaterial filters," IEEE 10th Annual conference on Wireless and Microwave Technology, pp.1-4, 2009.

[2-3] N. Wiwatcharagoses, P. Chahal, "A novel reconfigurable metamaterial unit cell based Composite Right/Left Handed microstrip design," IEEE International Symposium on Antennas and Propagation, pp.2954-2957, 2011.

[2-4] D.R. Smith, S. Schultz, P. Markos, C.M. Soukoulis, "Determination of effective permittivity and permeability of Metamaterials from Reflection and Transmission Coefficients," Phys. Rev. B, 65, 195104, 2002.

[2-5] D.R. Smith, D.C. Vier, N. Kroll, S. Schultz, "Direct calculation of permeability and permittivity for a left-handed metamaterial", Appl. Phys. Lett., 77, pp. 22-46, 2000.

[2-6] C.D. Moss, T.M. Grzegorczyk, Y. Zhang, and J.A. Kong, "Numerical studies of left handed metamaterials," PIER, 35, pp.315-334, 2002.

[2-7] R.A. Shelby, D.R. Smith, and S. Shultz, "Experimental verification of a negative index of refraction," Science, 292, pp.77-79, 2001.

[2-8] R.A. Shelby, D.R. Smith, S.C. Nemat-Nasser, and S. Shultz, "Microwave transmission though a two-dimensional, isotropic, left-handed metamaterial," Appl. Phys. Lett., 78, pp.489-491, 2001.

[2-9] J.B. Pendry, "Negative refraction," Contemporary Physics, vol. 45, No.3, pp.191-202, January-February. 2004.

[2-10] C. Caloz and T. Itoh, "Novel microwave devices and structure based on the transmission line approach of metamaterials," in IEEE-MTT Int'l Symp., vol.1, Philadelphia, PA, pp. 195-198, Jun. 2003.

3.0 MULTILAYER FILTERS AND MULTIPLEXERS

The microwave filter is the fundamental component in RF/microwave systems, and its characteristics can contribute towards the overall performance of the system. Filters can be designed and fabricated on various materials using standard photolithography and printed circuit board technologies. In low frequency applications, circuit dimensions of conventional filters implemented on a single layer become too large to satisfy the requirements of circuit size reductions [3-1]. To resolve this problem, engineers are now exploring the multilayer technology that offers an extra degree of freedom for designing microwave and millimetre wave components. In multilayer technology, the arrangement of the different layers can reduce the overall circuit size of the circuit. Single layer filter design requires a trade-off between the circuit size and filter performance. However using the multilayer approach, the performance of a filter can be enhanced and its size reduced.

Although the multilayer technique can be used to reduce the circuit size however the additional layers introduce extra dielectric loss that can further degrade the filter's insertion-loss performance. In [3-2] the authors proposed a compact multilayer hairpin bandpass filter and managed to reduce its size by more than 50% when compared with a single layer implementation. However, the filter's insertion-loss of > 4 dB is not practically acceptable. Several techniques have been previously considered to improve a filter's selectivity [3-3] [3-4] using cross-coupling between non-adjacent resonators to create a pair of transmission zeros. However, these filters are still considered too large for practical applications. The multilayer technique proposed in this chapter offers signification miniaturization without detrimental effect on the overall performance of the filter.

3.1 Multilayer Filter Design

The CRLH-TL unit-cell in chapter 2 was used in the development of the multilayer filter. Motivation was to mitigate the limitations of the conventional single layer implementation, in particular, to concurrently achieve controllable bandwidth, selectivity and size reduction. Here the multilayer comprises of two stacked substrate layers, where a single CRLH-TL filter structure is etched on the top of first substrate and an identical CRLH-TL structure is etched on the bottom side of the same substrate. The input/output ports and feed-lines are located on the top layer. The feed-lines are tapered from the 50Ω ports and transformed into a curved high impedance line that connects with the CRLH-TL structure. This feed-line network achieves an excellent match with the filter structure and minimizes the creation of unwanted spurii. The metallic tracks of the top substrate are connected with the bottom layer through vias. The bottom circuit is placed on an identical substrate whose top layer contains no metallization and the bottom layer includes the ground-plane, as illustrated in Fig. 3-1.

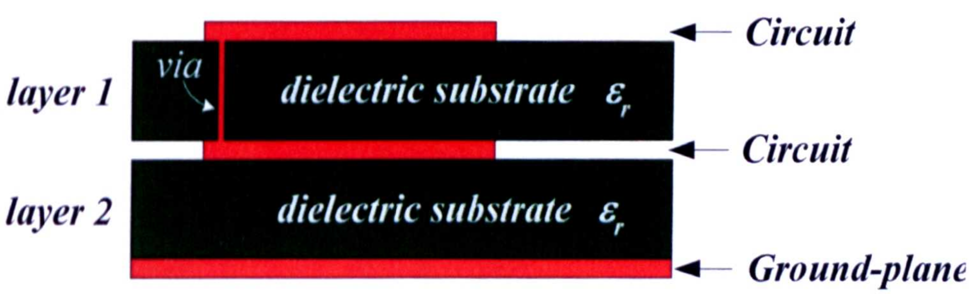

Fig. 3-1 Proposed multilayer substrate stack implementation.

3.1.1 3-Pole Multilayer Filter Design

The structure of the 3-pole CRLH-TL bandpass filter is shown in Fig. 3-2(a). The multilayer design process involves the construction of the 3-Pole CRLH-TL filter structure on the top and bottom layers of the substrate such that they appear superimposed, as shown in Fig. 3-2(b). The filter's specifications and details on its design are given in chapter 2, section 2.4. The input/output feed-line is tapered to a high-impedance line (154 Ω) to enhance matching with the filter. The proposed multilayer technique shifts unwanted harmonics far away from the filters operating frequency. Electromagnetic coupling interaction between the duplicated CRLH-TL filter structures that are separated by the dielectric medium is very tight, which creates a transmission zero at the lower passband edge (1.88 GHz), as shown in Fig. 3-2(c). It is observed the fractional bandwidth of the filter is reduced by approximately 50%; however the filter selectivity improves significantly. The affect observed on the filter's bandwidth is converse to that when the technique is applied on a conventional filter.

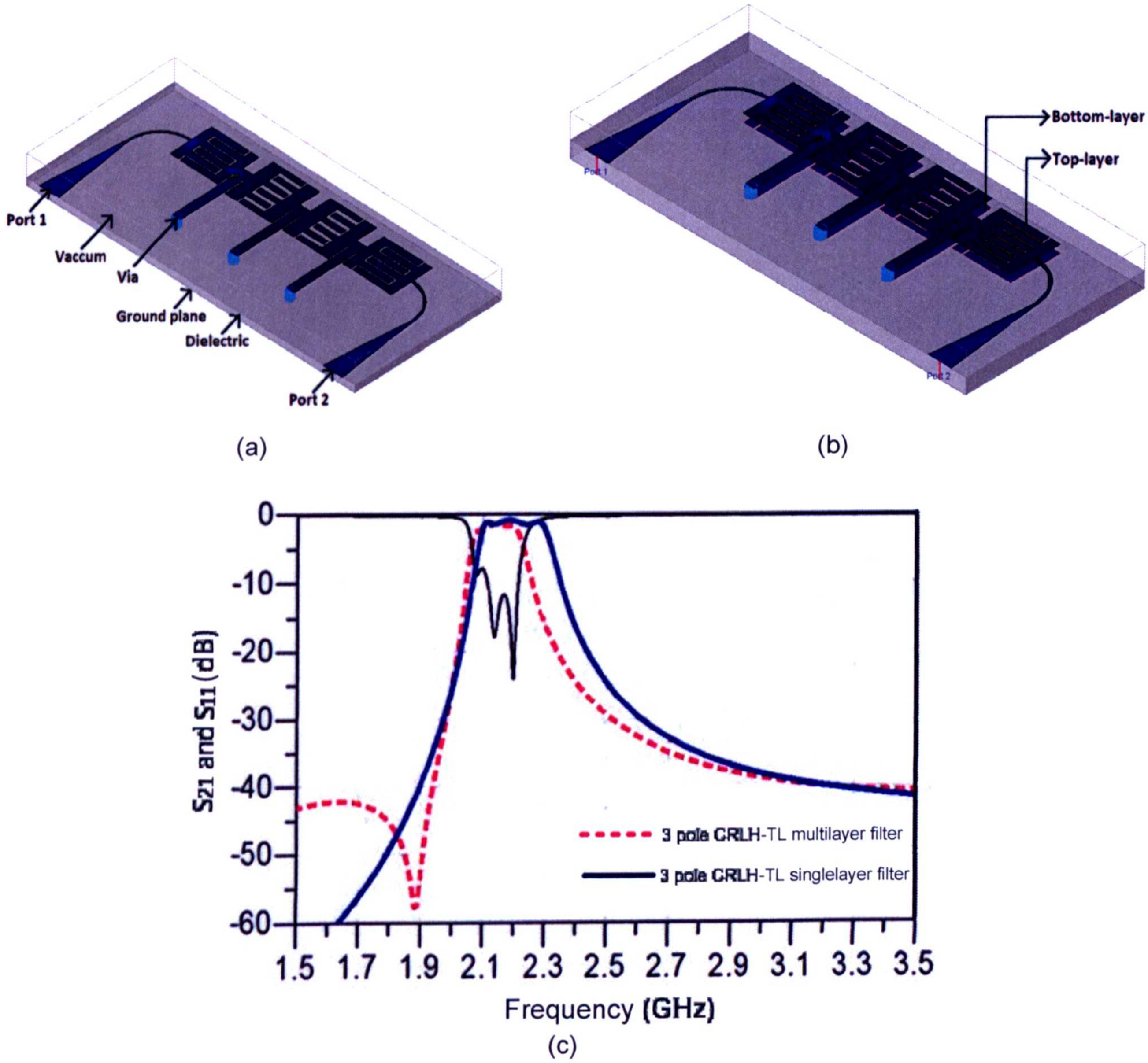

Fig. 3-2 (a) 3-pole CRLH-TL filter implemented on a single-layer, and (b) 3-pole CRLH-TL filter implemented on multilayer, and (c) Insertion-loss and return-loss response of the single layer and multilayer filters

3.1.2 4-Pole Multilayer Filter Design

The design methodology of the 4-pole CRLH-TL multilayer filter, shown in Fig. 3-3, is identical to the 3-pole design described in the previous section. Details of the 4-pole CRLH-TL filter design is given in chapter 2, section 2.5. The proposed multilayer filter's response was optimized using ADS (MoM), and realized using conventional microstrip integrated circuit technology. A simple electrical equivalent circuit representing the multilayer structure is shown in Fig. 3.3(b). The filter's transmission-loss response is shown in Fig. 3.3(c).

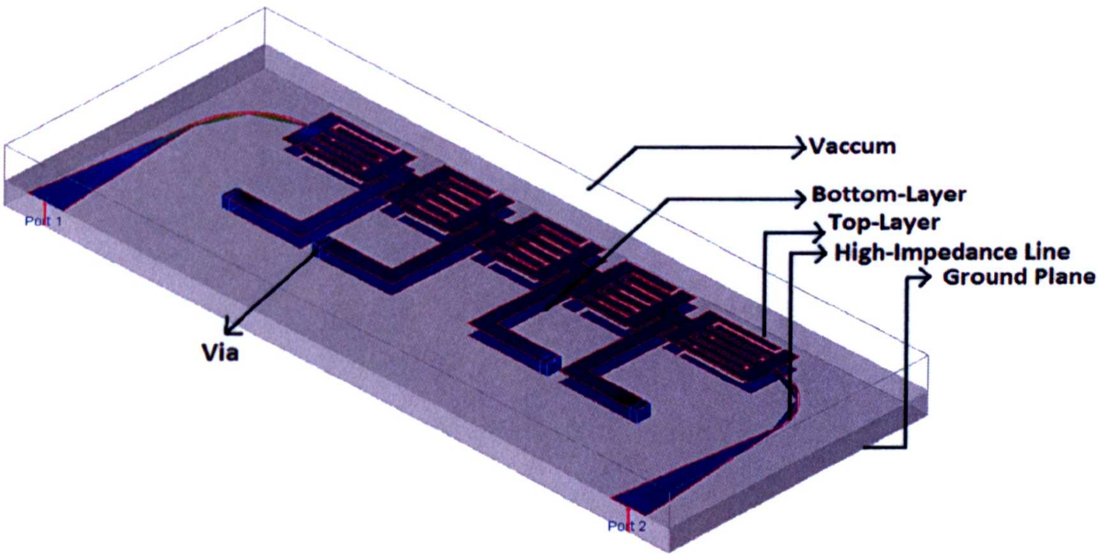

(a)

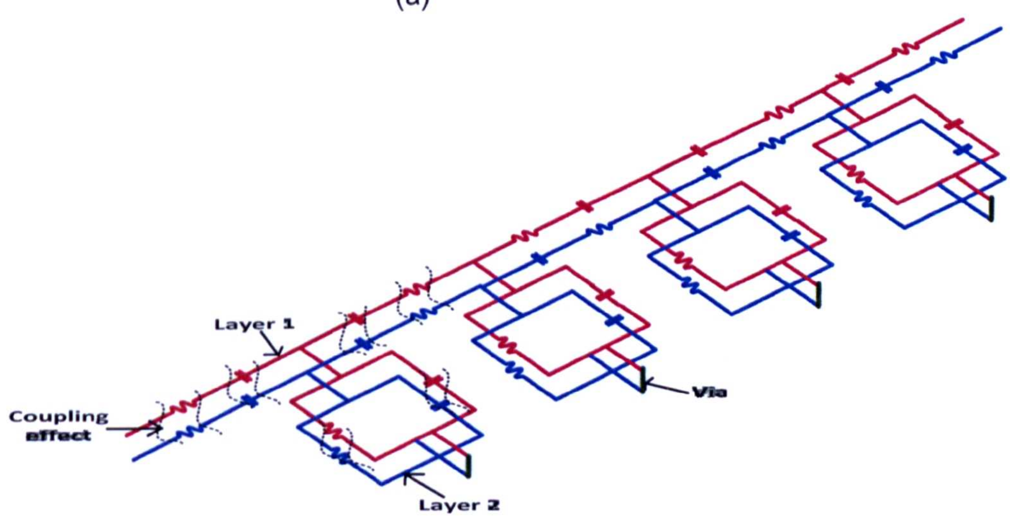

(b)

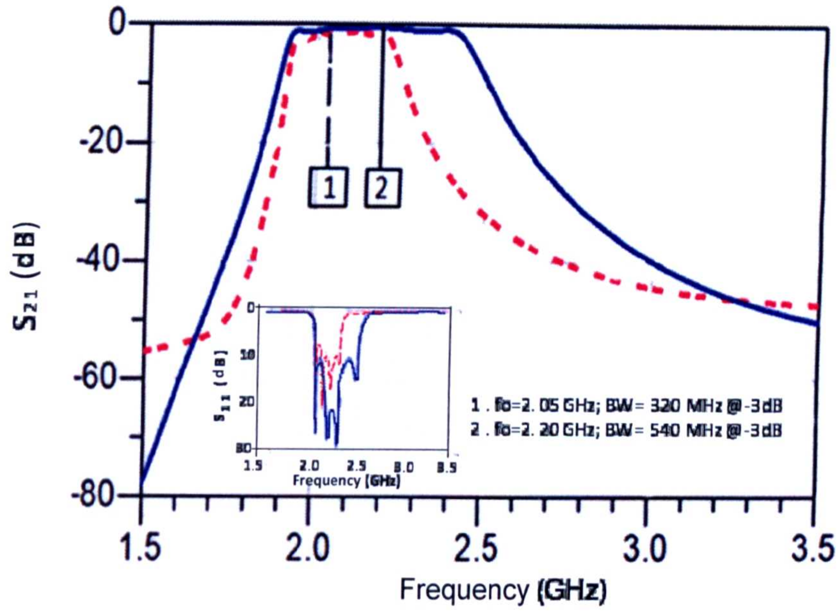

(c)

Fig. 3-3 (a) Microstrip layout of the 4-pole CRLH-TL multilayer filter configuration, (b) equivalent electrical circuit of the filter, and (c) insertion-loss and return-loss response of the multilayer filter

Design of CRLH-TL filter on a single layer, as shown in chapter 2, offers appreciable reduction in the overall size of the filter when compared with a conventional filter. A multilayer structure provides further reduction in circuit size. The proposed multilayer filter configuration has a bandwidth of 320 MHz bandwidth and length 32.50 mm. A conventional parallel coupled filter developed on a single layer with a similar bandwidth characteristic has a length of 238.84 mm; hence the multilayer CRLH-TL filter provides significant size reduction of 86.39%.

3.1.3 Fabrication and Measurement

The practical feasibility of the proposed multilayer technique for filter application is now demonstrated. The filter was constructed on 3M Cu-clad217 substrate from Arlon with ε_r = 2.17 and h = 0.794 mm. The steps involved showing the implementation of the 4-pole CRLH-TL multilayer filter are depicted in Fig. 3-4(a) and (b).

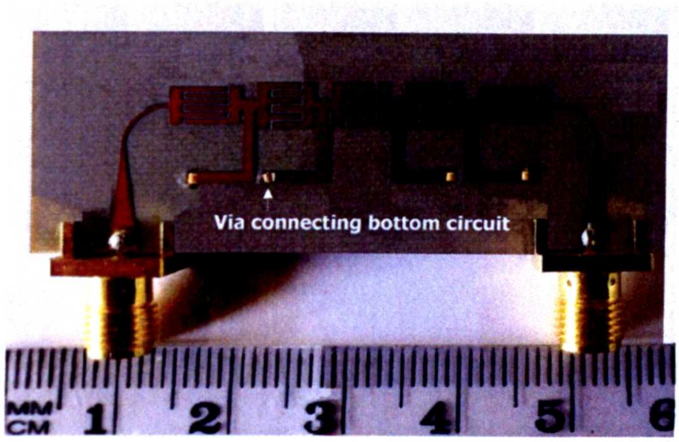

(a)

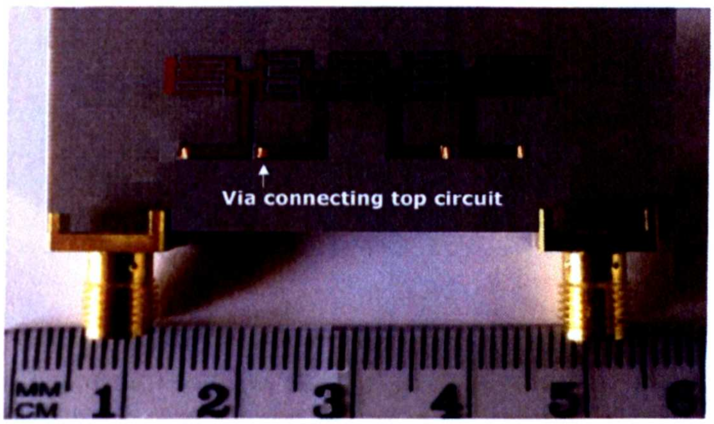

(b)

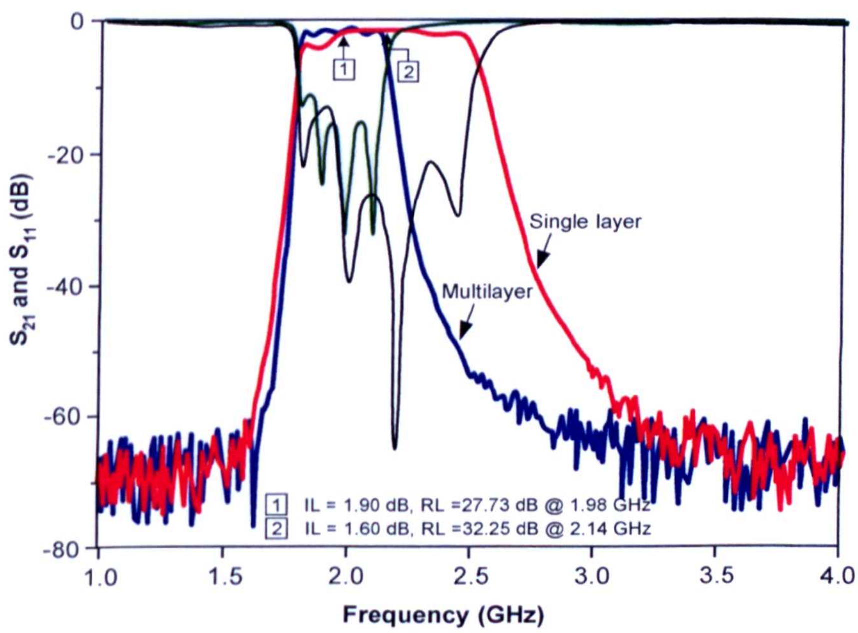

(c)

Fig.3-4 Fabricated 4-pole CRLH-TL multilayer filter, (a) filter implementation on the top of layer 1, (b) duplicate filter structure implemented on the bottom side of layer 1, and (c) measured insertion-loss and return-loss response of the single layer and multilayer filter with identical specifications

The measurement results for a single and multilayer CRLH filter structures in Fig. 3-4(c) show the multilayer technique reduces the passband bandwidth to almost a half however the rejection level is substantially improved. Hence, in designs the bandwidth will need to be doubled to achieve the desired bandwidth using the proposed technique. This technique was employed in the implementation of a diplexer in the next section.

3.2 Multiplexer Based on CRLH-TL

Diplexers/triplexers are essential components for channel separation in communications and radar systems. These devices provide isolation between transmit and receive channels by assigning a different frequency band to each channel. The integration of bandpass filters with circulators makes possible the realization of diplexers/triplexers. These devices find application in RF transceiver's front-end of multi-service and multi-band mobile communications systems. The design of a conventional diplexer/triplexer comprises of two parts, i.e. the design of individual filters to the required specifications, and the amalgamation of the filters using circulators. Although circulators provide appropriate isolation between the filters, however this substantially inflates the cost and size of the diplexer/triplexer. Also dimensions of conventional microwave filters are fixed to the signal's wavelength, which can result in large multiplexer designs [3-5]-[3-6]. An example of a typical multiplexer is shown in Fig. 3-5.

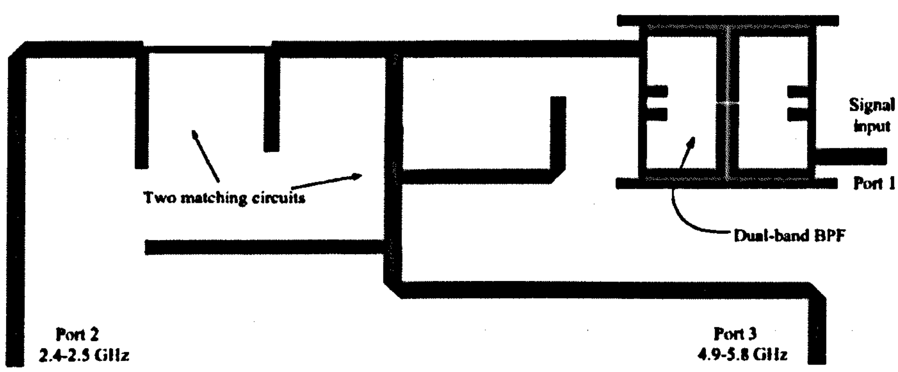

(a)

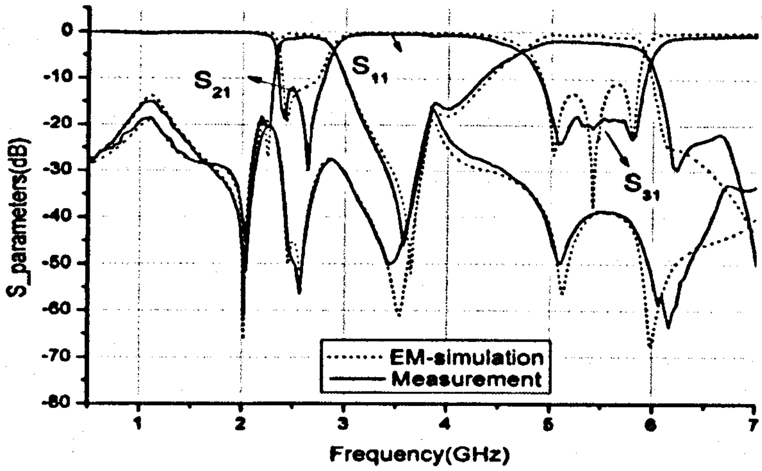

(b)

Fig. 3-5 (a) Conventional diplexer layout, and (b) *S*-parameter response of the diplexer [3-5]

Composite right/left-handed transmission-line filters eliminates such restrictions and unlocks the possibilities of designing compact filters which could make significant contribution with regard to design a miniaturized compact multiplexers [3-7].

In this section, design guideline is provided for CRLH-TL multiplexers (diplexer and triplexer). An integrated matching network is developed for the multiplxers is simple and easily fabricated. The three passband channels of the triplexer have a common input splitter. Relatively high isolation between the channels is critical in order to prevent undesired interaction that would otherwise adversely affect the triplexer's passband response. The isolation was achieved using stepped-impedance lines (SIL). It is shown by simply curving the SIL results in enhancement of the triplexer's passband insertion-loss performance and bandwidth, as well as suppression of high order spurii. The performance of the multiplexers were verified experimentally.

3.2.1 Diplexer Design Using CRLH-TL Filters

This section present a diplexer design based on CRLH-TL filters. The diplexer is shown to exhibit low passband insertion-loss and good isolation between the channels. The diplexer also suppresses higher order spurii. The first step is to design the two 2-pole CRLH-TL filters.

The second step is to combine the filters using a matching network, as illustrated in Fig. 3-6. The proposed diplexer implemented is compact than conventional diplexers [3-7] [3-8]-[3-10].

The conditions of the impedance matching network for the diplexer, shown in Fig. 3-6, are: Z_{in1} (f_a) $=50\Omega$ Z_{in1} $(f_b) = \infty$ and Z_{in2} $(f_b) = 50\Omega$ Z_{in2} $(f_a) = \infty$.

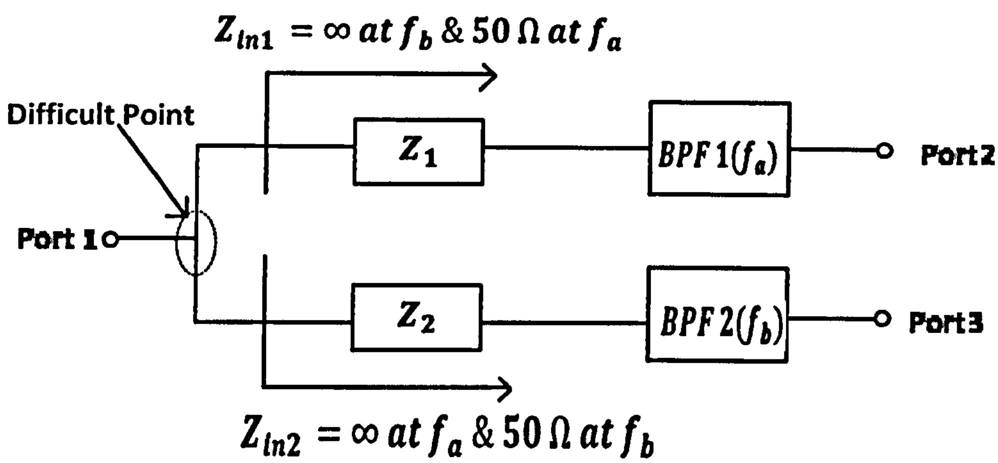

Fig. 3-6 Schematic of the diplexer

The two 2-pole CRLH-TL filters were designed at the GSM band (*fo* = 1.79 GHz and *BW* = 170 MHz) and at the UMTS band (*fo* = 2.02 GHz, *BW* = 250 MHz). The filters were combined with a common matching line network, as shown in Fig. 3-7(a). The matching was optimized using a curved stepped-impedance line to minimize passband loss. SIL consists of tri-sections, as shown in Fig. 3-7(b), to provide a good match to the filters. This SIL matching technique allows the integration of the filters to create a diplexer without the use of isolators; thus saving cost and space, as no isolator is employed. In addition, the SIL match also suppresses undesired high order harmonics.

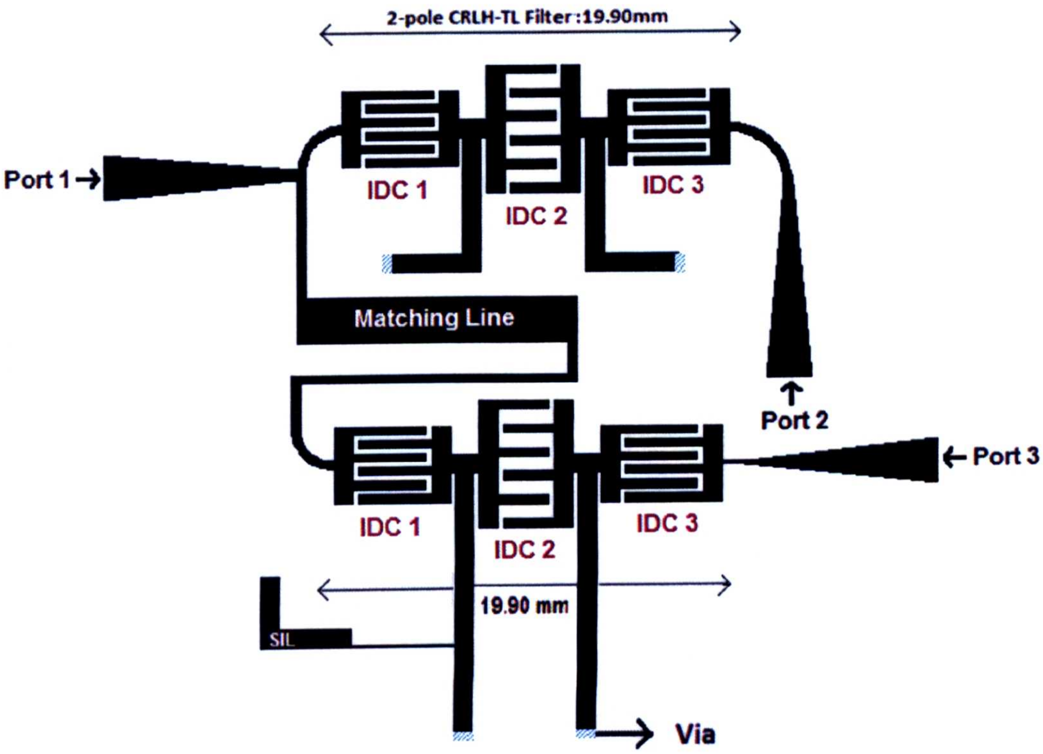
2-pole CRLH-TL Filter :19.90mm
Port 1
IDC 1
IDC 2
IDC 3
Matching Line
Port 2
Port 3
IDC 1
IDC 2
IDC 3
19.90 mm
SIL
Via

(a)

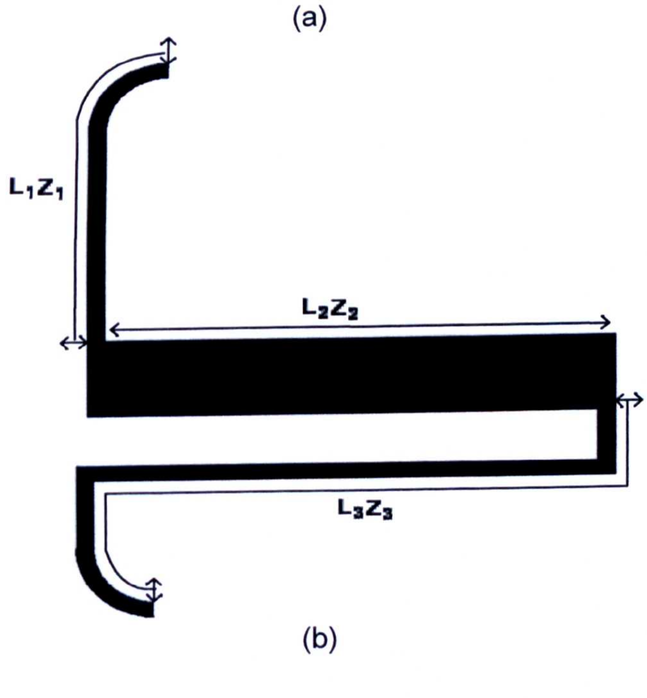
L_1Z_1
L_2Z_2
L_3Z_3

(b)

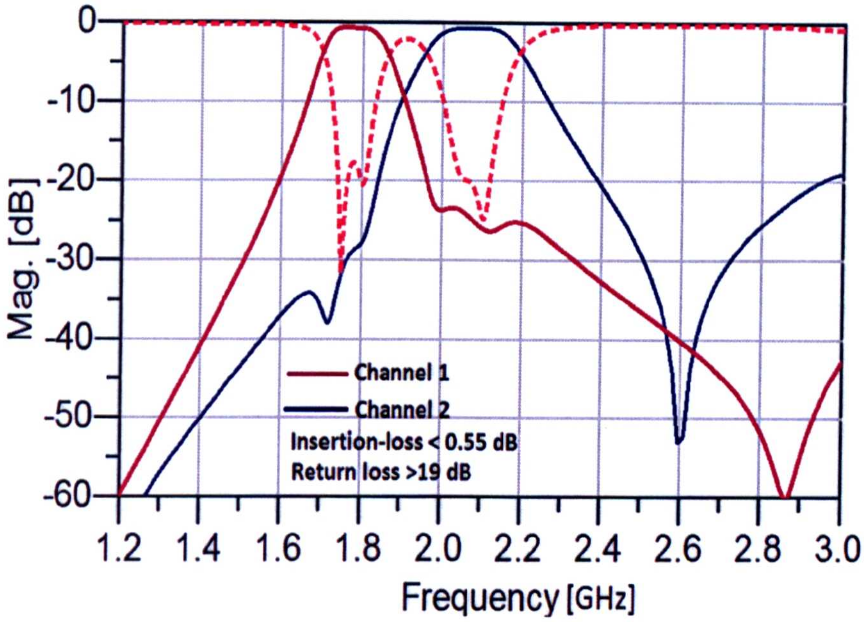

(c)

Fig. 3-7 (a) Microstrip diplexer layout implemented using two 2-pole CRLH-TL filters, (b) impedance matching network, and (c) simulated insertion-loss and return-loss response

According to the simulation analysis, the impedance of L_2 section predominantly controls the insertion-loss (IL) and return-loss (RL) characteristics of the filters. When the value of Z_2 is low, in other words the impedance of section L_2 is low (such as, 50 Ω) then IL of port-2 filter improves significantly. In the analysis the impedance of L_1 and L_3 sections were kept constant at 120 Ω.

The diplexer's simulated response is shown in Fig. 3-7(c). The centre frequency of filter-1 (f_a) is 2.05 GHz and filter-2 (f_b) is 1.79 GHz. For both filters the insertion-loss at the centre frequency is < 0.55 dB and the return-loss is > 18 dB.

For filter-1, the dimensions of *IDC1* and *IDC3* are: *w* = 0.75 mm, *g* = 0.20 mm, g_e = 0.25 mm and *l* = 3.9 mm. The dimensions of *IDC2* are: *w* = 0.5 mm, *g* = 0.35 mm, g_e = 0.25 mm and *l* = 2.4 mm. The length of the stub inductors are 6.9 mm.

For filter-2, the dimensions for *IDC 1* and *IDC 3* are: *w* = 0.5 mm, *g* = 0.2 mm, g_e = 0.25 mm and *l* = 3.5 mm. The dimensions of *IDC2* are: *w* = 0.5 mm, *g* = 0.73 mm, g_e = 0.25 mm and l = 2.4 mm. The length of the stub inductors (l_s) are: 10.8 mm. Z_1, Z_2 and Z_3 represent the characteristic impedance of the three transmission-line sections which have corresponding physical lengths l_1, l_2, and l_3. In Fig. 3-7(b), Z_1 and Z_3 were chosen to be 112.50 Ω and Z_2 was 50 Ω, and the physical lengths L_1, L_2 and L_3 are 6.8 mm, 14.4 mm and 15.8 mm, respectively, to achieve reflection-coefficient better than -10 dB over the filters desired passbands. In addition, the proposed CRLH-TL filter's bandwidth can be controlled by altering the gaps between the inter-digitally coupled transmission-lines of *IDC2* in each filter structure.

Simulation response of the diplexer in Fig. 3-7(c) shows two adjacent bandpass responses of fractional bandwidth 9.72% and 12.39%. No harmonics are observed close to the operating frequency, and the individual filter responses have a steep roll-off and good out-of-band rejection. The fabricated diplexer size is 24.10x34.6 mm^2.

3.2.2 Selectivity Improvement of Diplexer Design

In this section, the multilayer technique is applied in the design of a diplexer to show significant improvement in the selectivity and isolation between the adjacent channels. The design methodology comprises of essentially three steps: initially to design a single layer diplexer that splits signals into two distinct bands. The diplexer construction here consists of two 4-pole CRLH-TL filter structures that are combined through a matching network, as shown in Fig. 3-8(a). The filters were designed to operate at UMTS and GSM1800 bands having centre frequencies of 1.8 GHz and 2.05 GHz, respectively. Details of the design are described in chapter 2, section 2.5. The dimensions of the individual filters are given in Table 3-1.

The diplexer's insertion-loss and return-loss response, shown in Fig. 3-8, is far from the desired performance as the filter's bandwidth is extended so that their passbands overlap. This renders the diplexer unfeasible for practical applications as no distinct guard-band exists in between the channels. In addition, significant loss and rather poor return-loss is observed. To enhance the selectivity and the rejection level between the two channels as well as control the filter's passband in the next step the 4-pole filter structure is duplicated on the other side of the same substrate as described in section 3.1. The only constraint here is the two structures are precisely aligned. The duplicate circuits constituting the diplexer are connected to each other through vias, as shown in Fig. 3-9. Finally the filter circuit is laid onto an identical dielectric substrate with a ground-plane. The input/output ports are located at the top layer. The 50 Ω input/output impedance is tapered into a curved high-impedance line to provide a good impedance match with the CRLH structure and reduce unwanted spurii closer to the selected frequency bands. The dimension of these high impedance lines are: w_7 = 0.2 mm, l_7 = 7 mm and w_g = 0.2 mm and l_g = 4 mm. The length of the matching line l_6 is 97.9 mm and which has an impedance of 50 Ω. The fabricated multilayer filter operates at 1.79 GHz with a fractional bandwidth of 9.47%. Similar technique is employed to design the other filter at 2.05 GHz with fractional bandwidth of 12.22%.

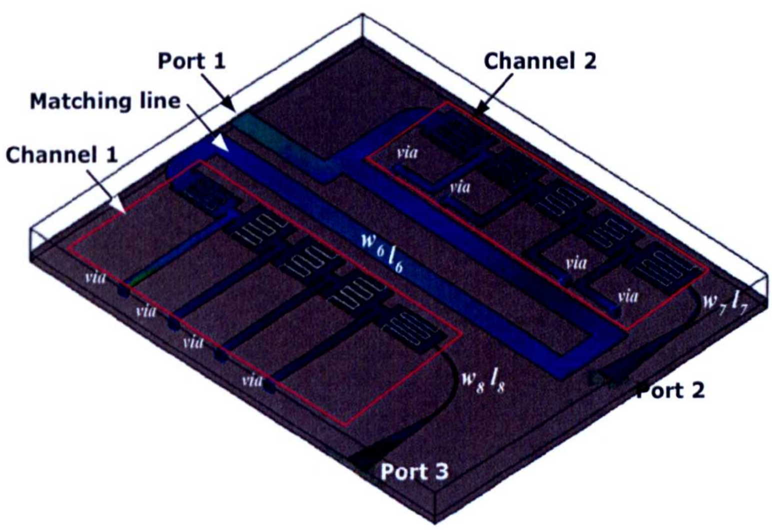

(a)

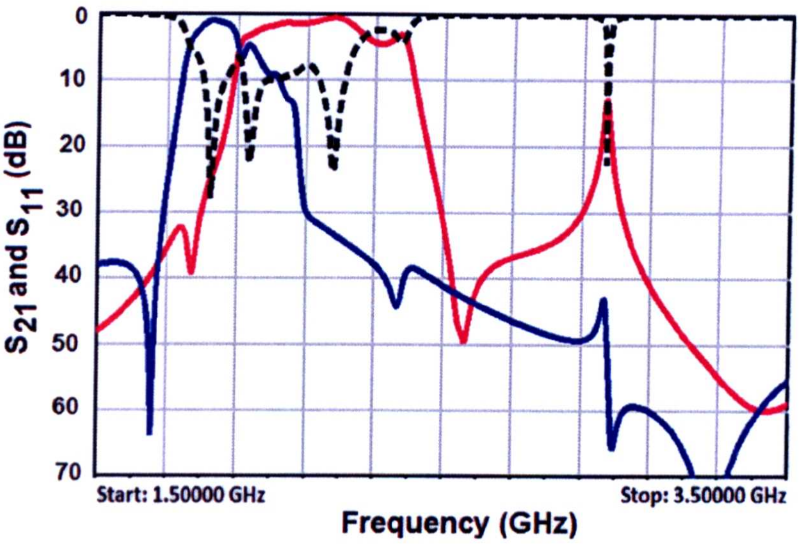

(b)

Fig. 3-8 (a) Diplexer using 4-pole CRLH-TL filters, (b) simulated insertion-loss and return-loss response of the diplexer structure

Channel 1	w (mm)	g (mm)	g_e (mm)	l (mm)	l_s (mm)
IDC1, IDC5	0.40	0.20	0.25	3.5	13.8
IDC2, IDC3, IDC4	0.45	0..43	0.25	2.4	13.8

Channel 2	w (mm)	g (mm)	g_e (mm)	l (mm)	l_s (mm)
IDC1, IDC5	0.55	0.20	0.25	3.5	12.3
IDC2, IDC3, IDC4	0.55	0.20	0.25	2.4	12.3

Table 3-1: Channel 1 and channel 2 filters dimensions

The rejection level and the overall performance of the diplexer were further enhanced by defecting the ground-plane of the lower substrate layer with a dielectric slot. The design constraint is the rectangular dielectric slot must be precisely located underneath the common matching line as illustrated in Fig. 3-9(a). The dimension of the dielectric slots are: a = 6.6 mm, b = 1.5 mm and c = 17.5 mm. It was found that the EM interaction between the dielectric slot and the matching line perturb the LC parameters associated with the microstrip-line to affect the isolation of the channels.

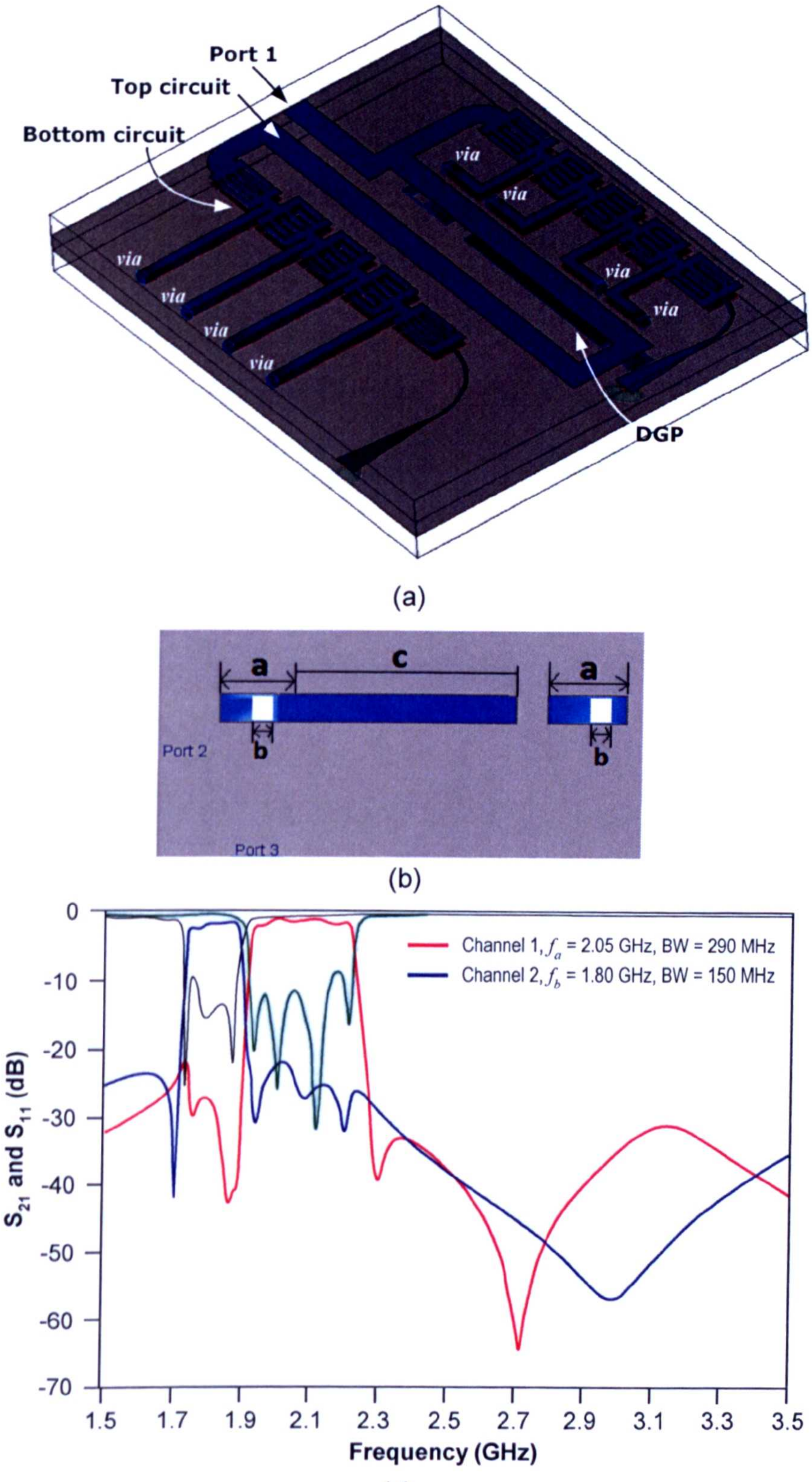

Fig. 3-9 (a) 4-pole CRLH filters forming the diplexer are duplicated on the bottom layer of the same dielectric substrate and linked through vias, (b) defected ground slot, and (c) Simulated transmission and reflection-coefficient response of the proposed diplexer structure.

The measured results in Fig. 3-9(c) show the overlapping response regions between the adjacent bands (GSM 1800 & UMTS 2100) disappears once the novel multilayer technique is invoked. This results in filters with sharp passband skirts and therefore high selectivity, and high rejection level between the adjacent channels, which validates the proposed concept. It is also observed that the filters in the diplexer implemented using this technique create multiple attenuation poles in the passband region of adjacent filter. The gap between the two passband channels is 30 MHz and rejection level between these two channels is 15 dB. The rejection level below and above passband edges for both filters are more than 20 dB. The filter have an insertion-loss of <1.2 dB and high return-loss ≥10 dB. The resulting structure provides an excellent higher order harmonic rejection between 2.3-3.5 GHz. As shown the proposed technique allows the design of diplexers with near contiguous passbands that meet the most demanding technical requirements.

3.3 Triplexer Design Based on CRLH-TL Unit-Cell

Diplexer and triplexer characteristics required for application in multiband wireless communication systems includes: (i) high isolation between channels, (ii) low design complexity in order to avoid unnecessary fabrication cost, and (iii) small size. Design and implementation of typical multiplexers can be found in current literature. An example of a typical triplexer design in [3-25] is based on $\lambda/2$ tap connected stepped-impedance resonators, shown in Fig. 3-10. Here the SIR serves as a through pass at the centre frequency of a bandpass filter or to provide a short circuit at the centre frequency of another bandpass filter. The triplexer's filters have sharp roll-off and the rejection level between the channels is about 25 dB, however its insertion-loss is > 4 dB at the centre frequency of each channel. The triplexer is considered to be large as its dimensions are 87.78×103.12 mm^2.

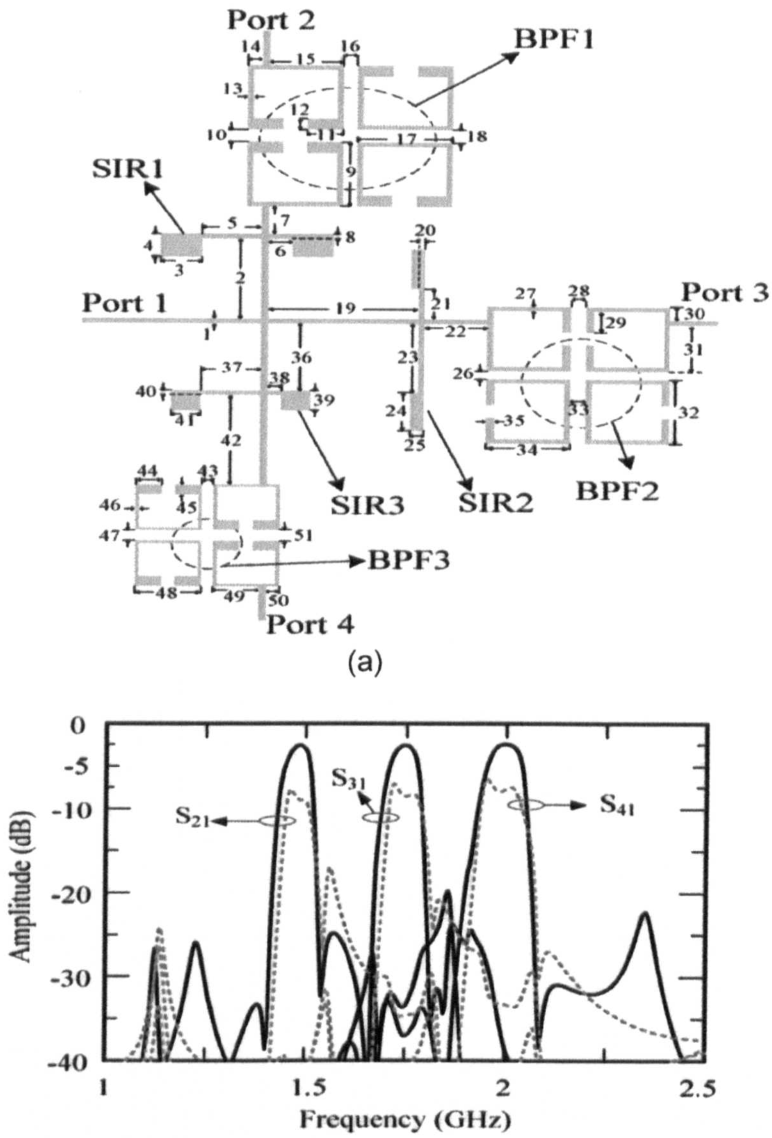

(a)

(b)

Fig. 3-10 (a) Triplexer design using SIR, and (b) simulated and measured transmission and reflection-coefficient characteristics of the triplexer

As in the previous section, the filters constituting the triplexer were designed using CRLH-TL unit-cells and matching networks consist of stepped-impedance lines in order to save space. The proposed triplexer provides a relatively low passband insertion-loss and a good match for practical applications. A simple technique is used to enhance the out-of-band rejection and minimize high order spurii generated by the filters. This was achieved by curving a section of the stepped-impedance microstrip line constituting the matching network. The proposed triplexer topology offers relatively high isolation, good stopband attenuation, low passband insertion-loss, high return-loss and is compact (43.18×27.98 mm^2). This study demonstrates the usefulness of this type of filter for multiband applications, such as WLAN and WiMAX.

3.3.1 Triplexer Design

The proposed triplexer, shown in Fig. 3-11, basically involves the design of individual filters which are combined using a splitter and appropriate matching networks. The matching network is a critical part of the triplexer design as it determines its overall performance. The matching network consists of two tri-section stepped-impedance lines, where one of the sections is curved to minimise reflections at the interface of the filters and therefore to enhance its matching performance. Using this simple technique there is no need for a matching network for the third triplexer channel other than a short high impedance line. The three filters in the triplexer are constructed using CRLH-TL unit-cells.

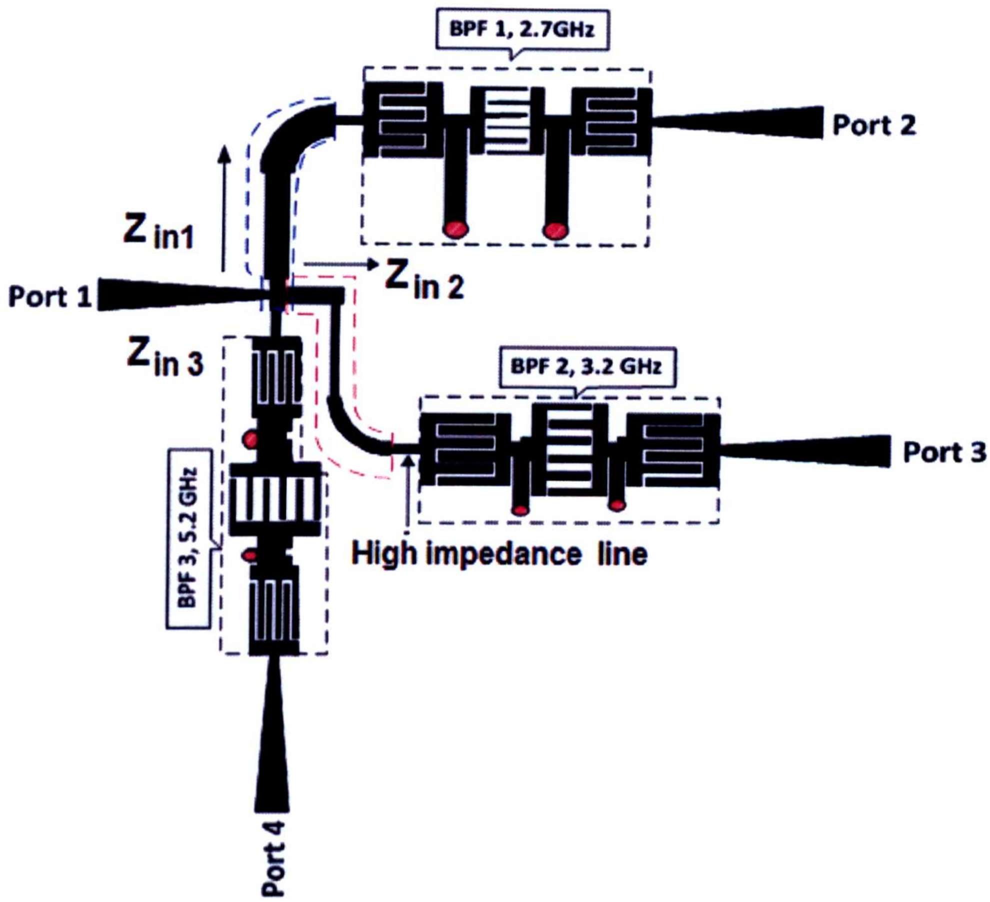

Fig. 3-11 Layout of the triplexer structure using 2-pole CRLH-TL filters

There are two tri-section stepped-impedance lines used for providing a good match to the filters in the triplexer. The first stepped-impedance line is connected to a short high impedance line at the splitter junction. The second stepped-impedance line is preceded with a short low impedance line. This SIL matching technique allows the integration of the filters to create a triplexer without the use of isolators; thus saving cost and space, as no circulator is employed.

The first matching network shown on Fig. 3-12 is connected to the BPF-1 with a centre frequency of 2.7 GHz, and the second matching network is connected to BPF-2 with a centre frequency of 3.2 GHz. From simulation analysis it was found that there is no need for a matching network for BPF-3 with a centre frequency of 5.2 GHz. The triplexer's optimized dimensions where obtain from simulation analysis and given in Table 3-2.

Channel-1	w (mm)	g (mm)	g_e (mm)	l (mm)	l_s (mm)
IDC1, IDC3	0.75	0.20	0.25	3.9	6.9
IDC2	0.50	0.35	0.25	2.4	6.9

Channel-1	w (mm)	g (mm)	g_e (mm)	l (mm)	l_s (mm)
IDC1, IDC3	0.75	0.20	0.25	3.9	5.1
IDC2	0.40	0.65	0.25	2.4	5.1

Channel-1	w (mm)	g (mm)	g_e (mm)	l (mm)	l_s (mm)
IDC1, IDC3	0.40	0.20	0.25	3.60	0.70
IDC2	0.45	0.73	0.25	3.00	0.70

Table 3-2: Triplexer 2-pole CRLH-TL filter dimensions

Photograph of the triplexer and its simulated and measured performance is shown in Fig. 3-12. Salient features of the simulated and measured response are given in Table 3-3. The measured results are in good agreement with the simulation results other than the centre frequency of channel-3. This can be easily corrected by shortening the length of the inductive stub. The discrepancy between the simulated and measured results is mainly due to the fabrication tolerance which can be improved by more carefully fabricating the triplexer design.

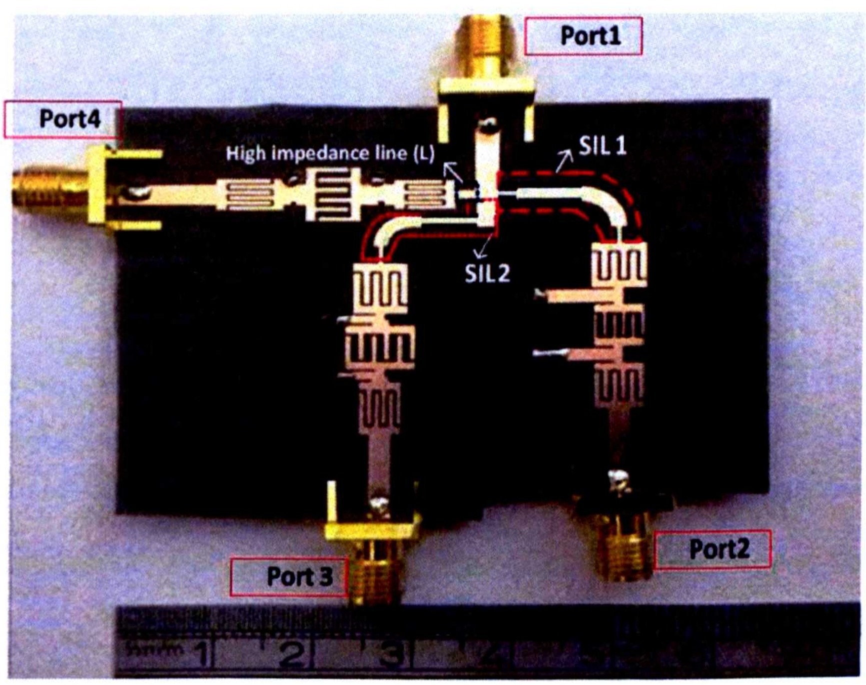

(a)

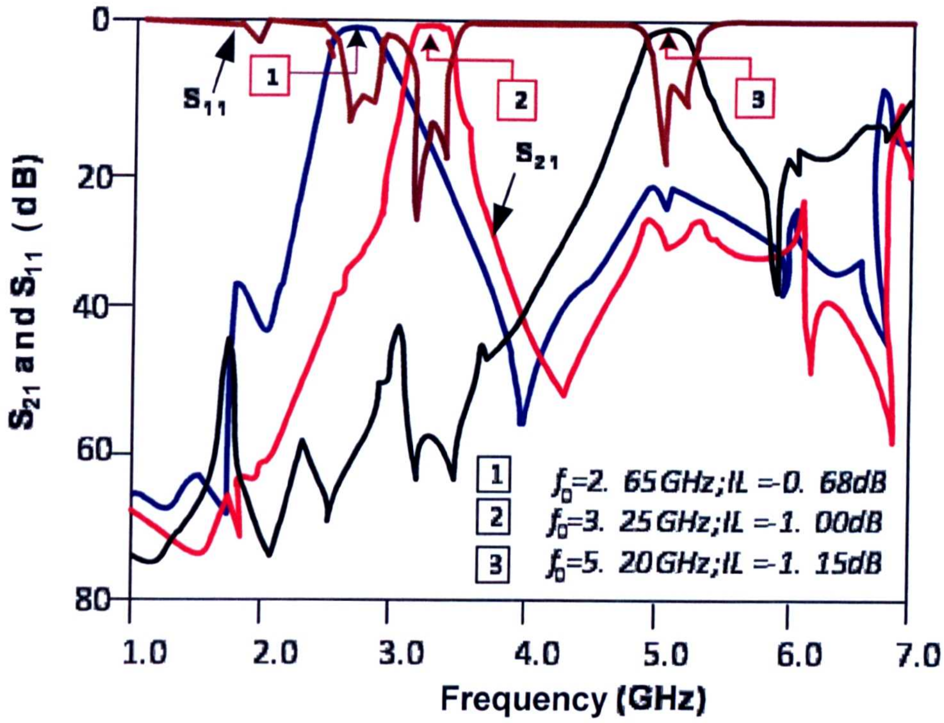

(b)

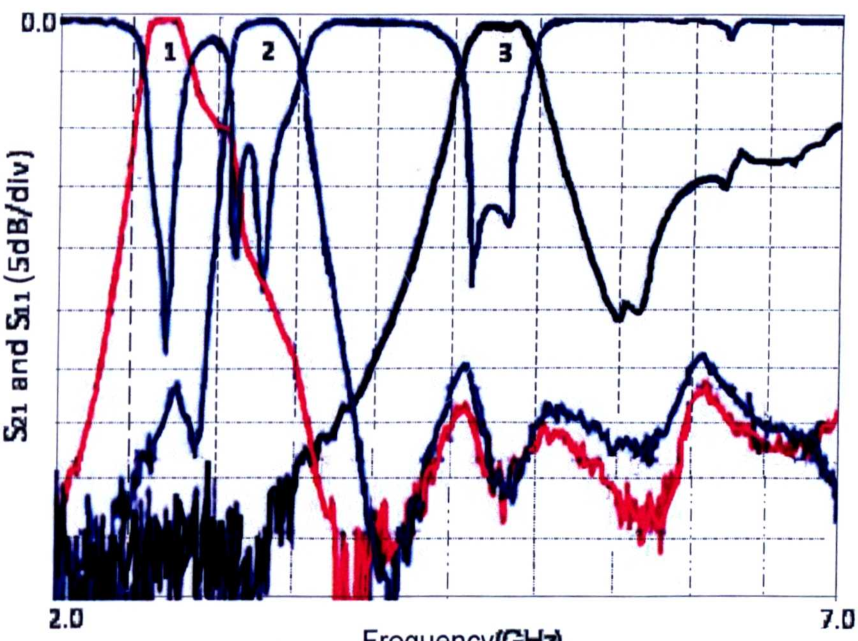

(c)

Fig. 3-12 (a) Photograph of the triplexer fabricated using standard photolithographic technique, (b) simulated response, and (c) measured response

Simulated				
Triplexer	Centre Freq. (GHz)	FBW (%)	IL (dB)	RL (dB)
Channel-1	2.65	14.60	0.68	12.50
Channel-2	3.25	9.50	1.00	13.20
Channel-3	5.20	7.76	1.15	12.50

Measured				
Triplexer	Centre Freq. (GHz)	FBW (%)	IL (dB)	RL (dB)
Channel-1	2.64	11.30	0.52	> 20
Channel-2	3.26	9.20	0.92	> 10
Channel-3	4.75	6.32	1.01	> 15

Table 3-3: Performance of the proposed Triplexer (simulated and measured).

3.4 Conclusion

The size of the CRLH-TL unit-cell doesn't depend on the signal's wavelength hence filters implemented using CRLH-TL unit-cells are substantially smaller than conventional filter designs. In this chapter a novel multilayer technique was proposed for CRLH-TL filters that promotes further size reduction. 3-pole and 4-pole CRLH-TL multilayer filter designs were implemented and practically verified. The technique involves duplicating the filter structure on both sides of the substrate such that they appear superimposed on to each other. The two identical structures are interconnected through vias. Implementation of this technique on CRLH-TL filters shows an interesting phenomenon that causes the filters bandwidth to reduce by approximately 50%. This observation is opposite to implementation of the technique using conventional filters. This can be attributed to the phase reversely in metamaterial structures. The technique also enhances the filter's selectivity.

The implementation of a novel diplexer is described and its feasibility practically demonstrated. The proposed multilayer technique involves duplicating the CRLH-TL filter structure designs on both sides of the dielectric substrate and resting the circuit on top of an identical dielectric substrate. The two circuits are interconnected with vias. This implementation is shown to significantly enhance the selectivity of the individual filters in the diplexer without degrading the filter's overall insertion and return-loss performance. In addition, the isolation between the adjacent channels is enhanced too, thus dispensing the need for an isolator. In fact these features were only possible to achieve with diplexers implemented using waveguide cavity technology. Unlike conventional multilayer techniques the filter's is curtailed. Hence, the proposed technique makes the design more economic and affordable and the design is significantly smaller in size than conventional multilayer filter constructions.

A triplexer design based on CRLH-TL filters is described. The design employs a simple matching network consisting of stepped-impedance lines that is shown to provide good isolation between the three adjacent channels of the triplexer. The three filters are designed at 2.65 GHz, 3.25 GHz and 5.20 GHz. The rejection-level between the second and third filter is more than 30 dB, and the isolation between the first and second channel is 10 dB. The selectivity can be improved by utilizing the multilayer technique described in section 3.1. The triplexer is compact in size (43.18×27.98 mm^2) and triplexer's features make it suitable for multiband and multiservice applications.

3.5 References

[3-1] J.S. Hong and M.J. Lancaster, Microstrip Filters for RF/microwave Application, Wiley, New York: 2001.

[3-2] H. Moon, S. Choi , S. Yun, "A Miniaturized aperture-coupled multilayer hairpin bandpass filter", IEEE MTT-S Int. Microwave Workshop Series on Signal Integrity and High-Speed Interconnects, vol. 8, no.1, pp.45-48, Mar. 2008.

[3-3] J.S. Hong and M.J. Lancaster, "Design of highly selective microstrip bandpass filters with single pair of attenuation poles at finite frequencies," IEEE transaction on MTT, vol.48, issue 7, pp.1098-1107, July 2000.

[3-4] S. Courre`ges, C.A. Donado Morcillo, S. Bhattacharya and J. Papapolymerou, "Reduced-size multilayer X-band filters with stacked resonators on a flexible organic substrate," IET Microwave Antennas Propagation, vol. 4, issue 2, pp. 277–285, 2010.

[3-5] C. Zhu, J. Zhou, and Y. Wan, "Design of microstrip planar triplexer for multimode/multi-band wireless systems," Microwave Journal, Nov. 2010.

[3-6] K.U. Ahmed, B.S. Virdee, "Microwave frequency discriminating devices based on composite right/left-handed transmission-line unit-cell," IET passive component seminar, Issue. 2, pp. 29-37, 2012.

[3-7] T. Yang, P. Chi, T. Itoh, "Compact quarter-wave resonator and its applications to miniaturized diplexer and triplexer," IEEE Transactions on microwave theory and techniques, vol. 59, no. 2, pp.260-269, Feb. 2011.

[3-8] C. Caloz, T. Itoh, Electromagnetic Metamaterials Transmission Line Theory and Microwave Applications, 1st edition, John Wiley & Sons, New Jersey, 2006.

[3-9] J.L. Jimenez-Martin, L.E. Garcia-Munoz, and D. Segovia-Vargas, "Novel Diplexer made with dual-composite right/left-handed Lines (D-CRLH)," COMITE, pp.1-4, 2008.

[3-10] D. Pu-Hua, L. Ming-lu, J. Shyh-Kang, and C. Chun Hsiung, "Design of matching circuits for microstrip triplexers based on stepped-impedance resonators," IEEE Transactions on Microwave Theory and Techniques, vol. 54, pp.4185-4192, 2006.

4. Wideband Filter Based On CRLH-TL Unit-Cell

There is rapidly growing research interest for wideband and ultra-wideband devices for short range and high speed wireless communication systems ever since the Federal Communications Committee (FCC) authorized the unlicensed use of UWB frequency spectrum in 2002 [4-1]. As the dimension of filters is wavelength dependent its size is a limiting factor for miniaturization of such systems. Hence, several methods for designing wideband filters have been reported in [4-1]-[4-6], one of which includes a CRLH wideband filter that uses two linear arrays of metallic vias and short-stub inductors to generate shunt inductors besides the series interdigital capacitors [4-2]. This wideband filter design is complex and exhibits poor selectivity and high passband loss. Another study presents a CRLH-TL wideband filter [4-3] based on complimentary split ring resonators with series gaps between resonators and grounded stubs. In the proposed topology, several stage unit-cells are used which results in a large and complex circuit that is difficult to fabricate. In addition, the circuit losses at the upper band edge increase as the number of split ring resonators increase. Split-ring resonator (SRR) defected ground structure (DGS) has been utilized in [4-4] to design a novel compact wideband filter and the concept is very similar to [4-3]. However, authors employed lumped chip capacitors and open stubs to improve the out-of-band rejection. However, the use of lumped elements makes the design complex. Moreover, wideband filter topology in [4-5] using EBG principle and based on CRLH-TL suffers from poor selectivity and large circuit.

In this chapter, a novel wideband filter structure is developed which comprises of symmetric unit-cell composed of two inter-digital capacitors with four short circuited inductive stubs. This topology generates unwanted higher order spurii which were suppressed by employing open-circuit stubs. In addition, to improve the passband skirt selectivity a T-shape open-circuit stub was inserted between the symmetrical unit-cells. The equivalent lumped element circuit model of the proposed microstrip circuit was developed to characterise its behaviour.

4.1 Wideband Filter Design

This section describes the design of a novel wideband bandpass filter. The filter consists of an inter-digital capacitor whose ends are extended and short-circuited to ground through vias. Fig. 4-1(a) shows two such structures connected in cascade to provide filter passband responses at 4 GHz and 8 GHz. The connection between the feed-line and the capacitors, and between the two capacitors is through a short high impedance line (L_1 and L_5) in order to minimize reflections at the interface of the filter and therefore to enhance its matching performance. The impedance of the transmission-lines L_1, L_3 and L_5 are equal, as well as the short-circuited stubs L_2, L_4, L_6 and L_7 such that $Z_1 = Z_2 = Z_3$ and $Z_4 = Z_5 = Z_6 = Z_7$.

In Fig 4-1(a), the left-handed components include the series inter-digital capacitors with shunt inductive stubs that are short-circuited to ground through vias, and the right-handed contribution is due to the shunt capacitance and series inductance contributed by the inherent parasitic of the inter-digital capacitor and inductive stub. The length of the inter-digital fingers of the capacitors control the centre frequency of the filter, and the gap between the fingers control its bandwidth. Hence, low frequency designs will have a bigger circuit size. Short length of high impedance transmission-lines L_1, L_3 and L_5 which are inserted between the unit-cells and between the feed-lines and unit-cell also affect the filters bandwidth. The simulated transmission response of the wideband filter in Fig. 4-1(b) is for the following circuit dimensions: L_1 and L_5 is 1 mm, and short-circuited stub length L_2, L_4, L_6 and L_7 of 5 mm. The width of the inter-digital fingers are 0.9 mm and the gaps between fingers is 0.2 mm. The size of the finger length for various centre frequencies is given in Table 4-1.

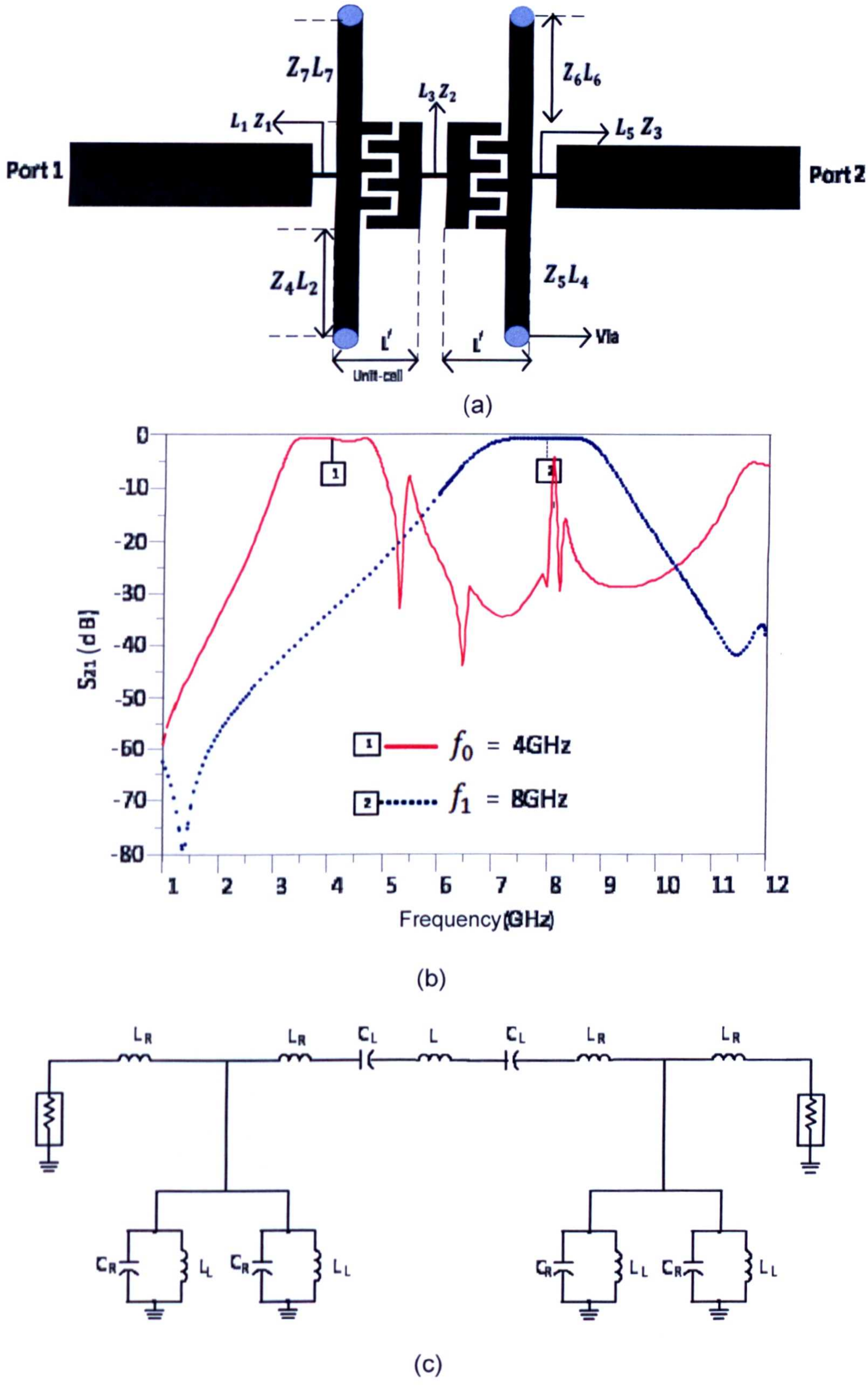

(a)

(b)

(c)

Fig. 4-1 (a) Layout of the wideband bandpass filter, (b) insertion-loss response of the filter, and (c) equivalent electrical circuit of the filter

Centre frequency (GHz)	4	4.5	5	5.5	6	7	8
Finger length (mm)	6.8	5.8	4.5	3.5	3	2	1.8

Table 4-1: Inter-digital capacitor finger length for various filter centre frequencies

The proposed wideband filter was simulated and optimized using ADS^{TM} (MoM) and the prototype was fabricated using standard MIC technique. To demonstrate the practical feasibility of the proposed topology for wideband function it was fabricated on 3M Cu-clad217 substrate from with ε_r = 2.17 and h = 0.794 mm. The filter was designed at centre frequency of 4 GHz. Fig. 4-2 shows a photograph of the filter and its simulated and measured performance. There appears to be good agreement between the simulated and measured results, and validation of the design feasibility.

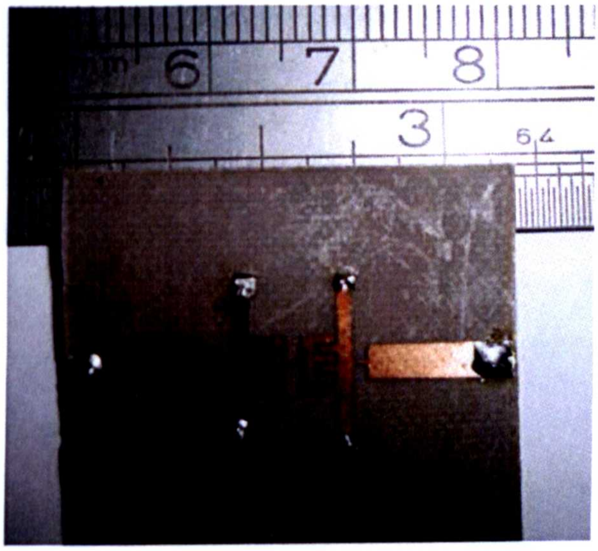

(a)

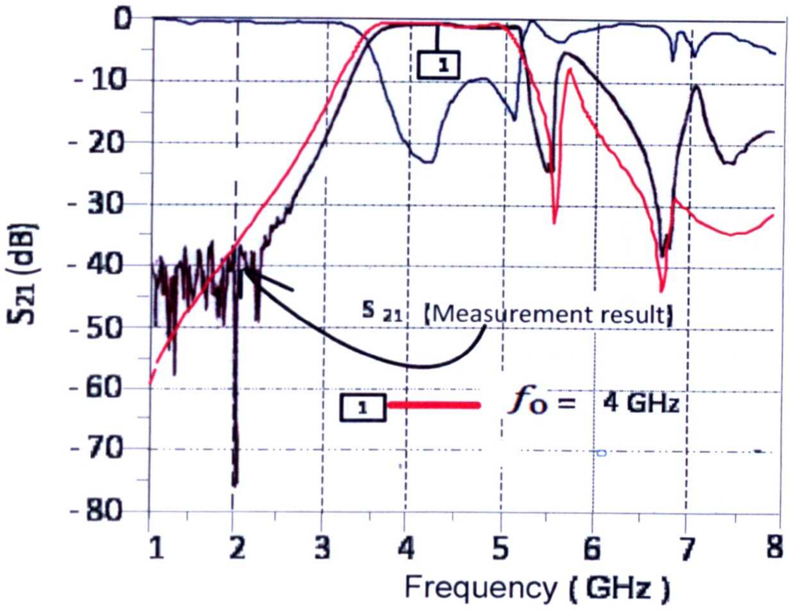

(b)

Fig. 4-2 (a) Photograph of the wideband bandpass filter designed at 4 GHz, and (b) the simulated and measured insertion-loss and return-loss response

4.1.1 Suppression Technique For Higher Order Spurii

At low frequency designs the proposed topology, shown in Fig. 4-2(a), exhibits a good selectivity at the upper passband edge however generates higher order spurii due to mismatch effect resulting from the extended finger lengths. Ref. [4-6]-[4-9] report that an addition of a quarter-wavelength open or short-circuited stub can be used to a introduce transmission zero to enhance selectivity of a filter. This technique is used to suppress spurii in the proposed wideband filter. An open-circuited stub of length L_8 is employed and attached to one of the inter-digital capacitors as shown in Fig. 4-3(a). The impedance of the line is made to match with the width of the capacitors side and its length is made equal to the length of the inter-digital capacitor's finger. Fig. 4-3(b) shows the frequency of the transmission zero is a function of it length. This technique has limitation as it requires multiple open-circuit stubs to generate a series of poles to provide suppression of spurii over a wider bandwidth.

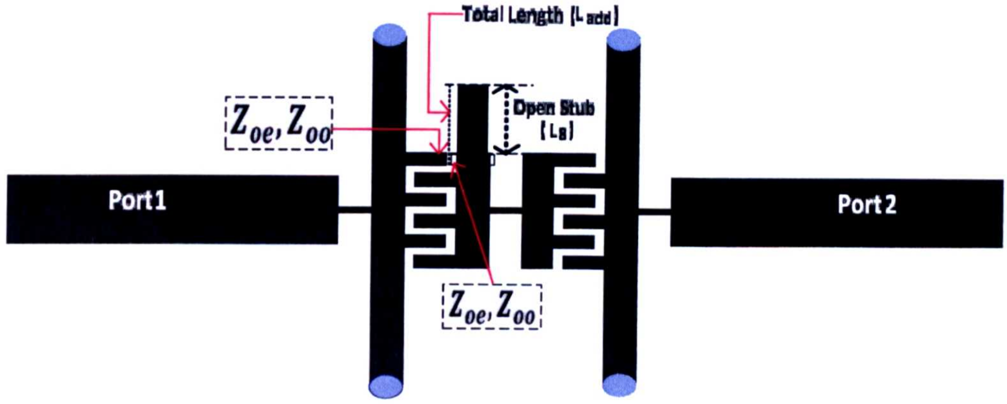

(a)

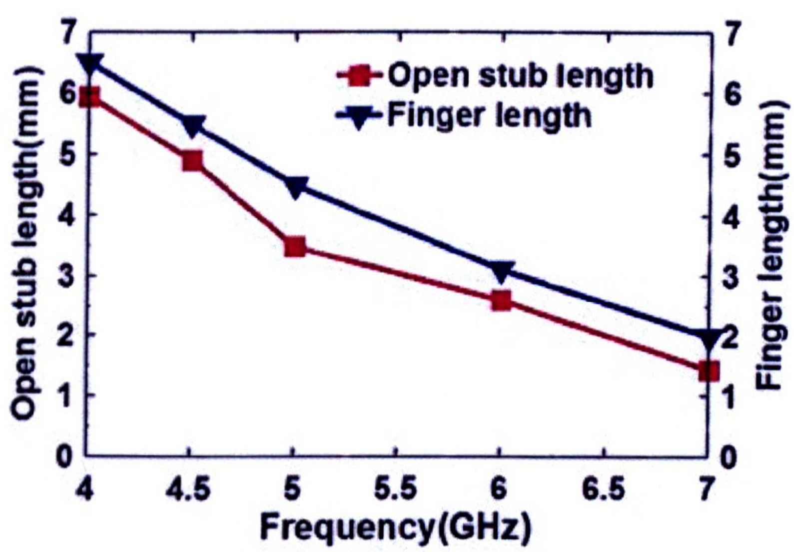

(b)

Fig. 4-3 (a) Layout structure of the proposed wideband filter with open-circuited stub to generate a transmission zero, and (b) Open-circuited stub length as a function of transmission zero frequency, and inter-digital finger length as a function of filter's centre frequency

4.1.2 Improvement of Selectivity Technique

A new technique is proposed here to enhance selectivity and wideband out-of-band rejection. This was achieved by using an inverted *T*-shaped open-circuited stub. The open-circuited stub is designed to generate attenuation poles at upper and lower side of the passband edge to improve the filter's selectivity. This was achieved as shown in Fig. 4-4.

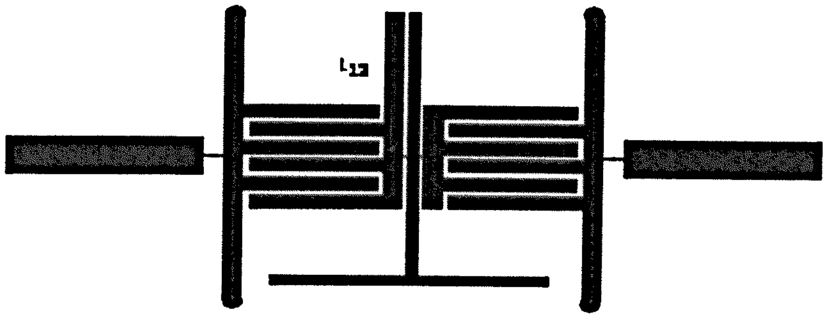

(a)

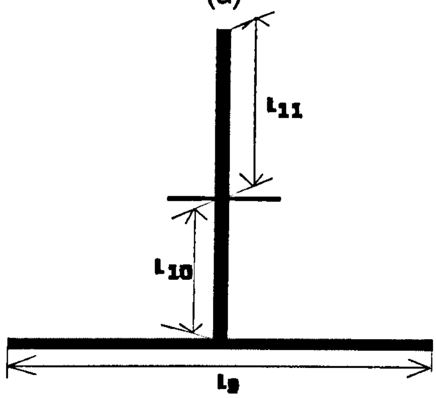

(b)

Fig. 4-4 Inverted T-shaped open-circuited stub incorporated in the wideband filter structure, (a) parameters defining the inverted T-shaped stub

The inverted *T*-stub shown in Fig. 4-4(b) controls location of the two transmission zeros on either side of the filter's passband edge. The inverted T-stub consists of three lines L_9, L_{10} and L_{11}, and their impedance determines the location of the lower and upper transmission zeros. Here the impedance of the lines was selected to create transmission zeros at 3 GHz and 5.30 GHz with respect to the filter's centre frequency at 4 GHz. To achieve higher out-of-band rejection level in excess of 15 dB, the length of the section L_{11} and L_{12} were made equal as shown on Fig. 4-4(a). When length of section L_{11} becomes smaller than the length of section L_{12} then the out-of-band rejection level is found to deteriorate. For example, if the length of section L_{11} is 8 mm which is smaller than L_{12}, the transmission zeros at the lower and upper passband edges become 3.24 GHz and 5.32 GHz, respectively. In addition, the rejection level outside the bands is less than 10 dB. Table 4-2 show the inverted *T*-shaped dimensions and passband performance at various centre frequencies.

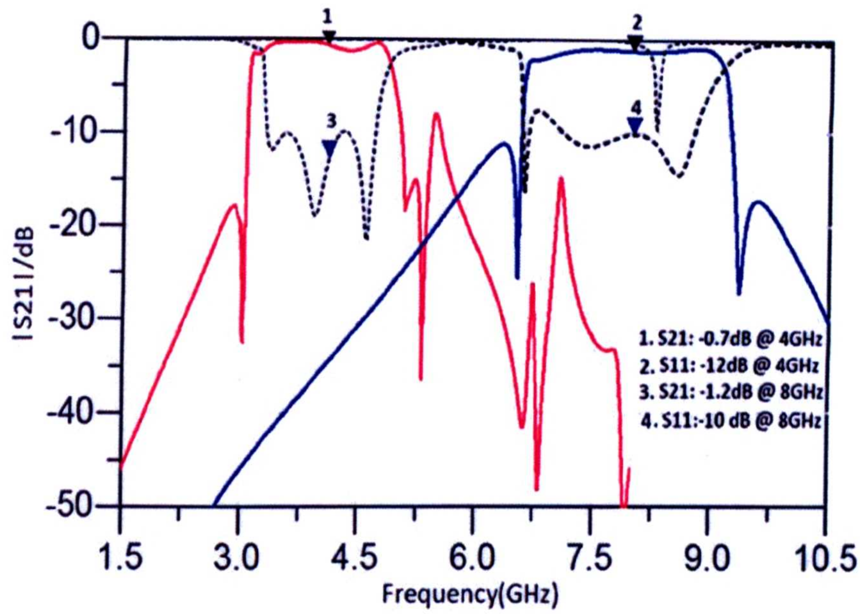

Fig. 4-5 Insertion-loss and return-loss response of the dual wideband filter with centre frequency of 4 GHz and 8 GHz

Centre Frequency (GHz)	4	4.5	5	5.5	6	7	8
L_9 (mm)	14	10	10	8	6	4.3	4.3
L_{10} (mm)	7.5	8	7.5	7	8	6.5	5
L_{11} (mm)	9.2	8	6.5	5.5	8	7.5	6.4
Fractional bandwidth (%)	39	42	42.6	41.6	37.6	27.28	31
Total length (L_{add}) (mm)	6.8	5.8	4.5	3.5	3	2	1.8
Open-circuited stub length (L_{12}) (mm)	5.9	4.9	3.6	2.4	2.2	1.1	1.1
Short-circuited stub width (mm)	1	1	1	1	1	1	1
Return-loss (dB)	15.71	9.8	17.86	10.02	10.43	12.5	9
Insertion-loss (dB)	0.35	0.34	.304	0.76	0.68	0.48	0.78

Table 4-2: Dimensions of the wideband filter structure for different centre frequenices

Analysis show for higher passband centre frequency (>7 GHz) the inter-digital capacitor finger width can be used control the operating frequency. However, at lower centre frequency (<7 GHz), the finger width affects filters bandwidth and can deteriorate the filter's selectivity.

A realistic representation of the unit-cell circuit model with the associate parasitic effects is shown in Fig. 4-1(c). Lumped element of a wideband filter designed at 10 GHz was calculated using:

$$C_R = \frac{2\omega_{UC}}{Z_o\left(\omega_{UC}^2 - \omega_o^2\right)} \tag{4.1}$$

$$L_R = \frac{2\omega_{UC} Z_o}{\omega_{UC}^2 - \omega_o^2} \tag{4.2}$$

$$C_L = \frac{\left(\omega_{UC}/\omega_o\right)^2 - 1}{2\omega_{UC} Z_o} \tag{4.3}$$

$$L_L = \frac{Z_o\left[\left(\omega_{UC}/\omega_o\right)^2 - 1\right]}{2\omega_{UC}} \tag{4.4}$$

These equations were derived in chapter 2, section 2.2. The equivalent circuit of the wideband filter at 10 GHz is shown in Fig. 4-6(a). The simulated and theoretical response of the equivalent circuit, plotted in Fig. 4-6(b), shows excellent agreement. This validates the equivalent circuit model. The return-loss in Fig. 4-6(c) is around 7 dB. The group delay of this filter is inversely proportional to filter bandwidth. Fig. 4-6(d) shows the worst case group delay variation is 0.15 ns within the filter's passband. This is acceptable for practical applications.

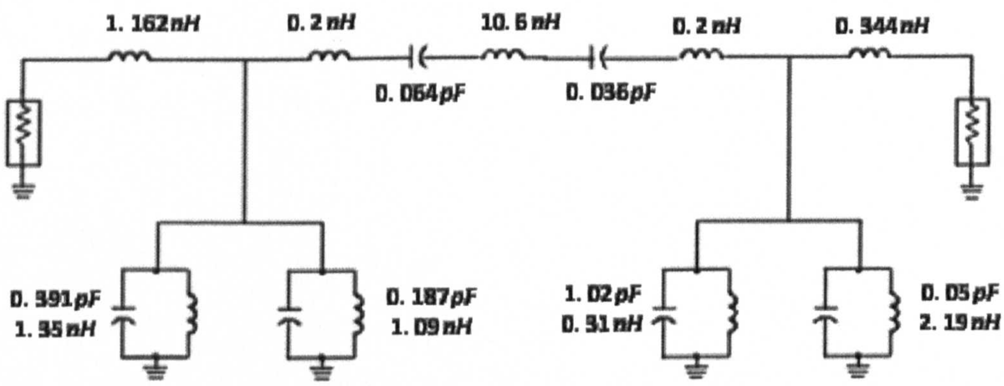

(a)

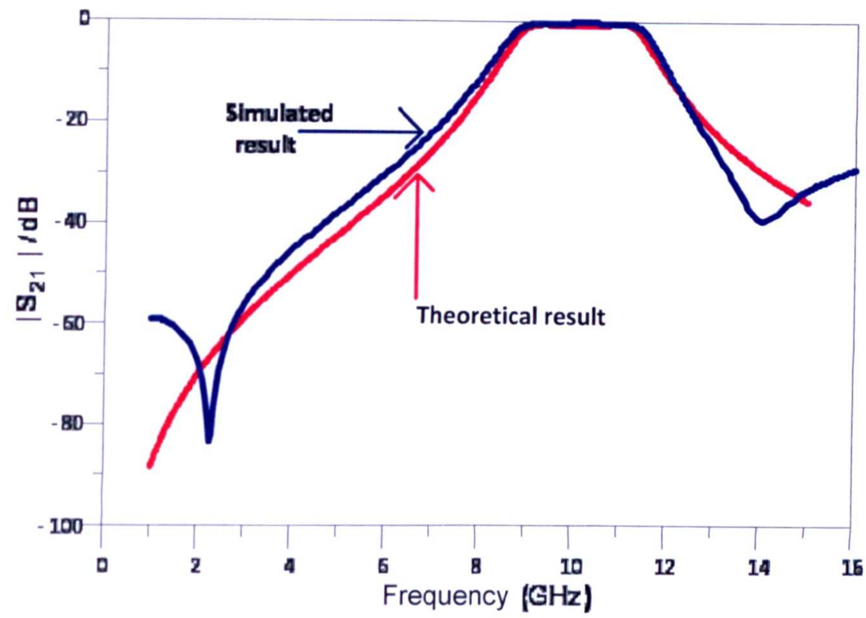

(b)

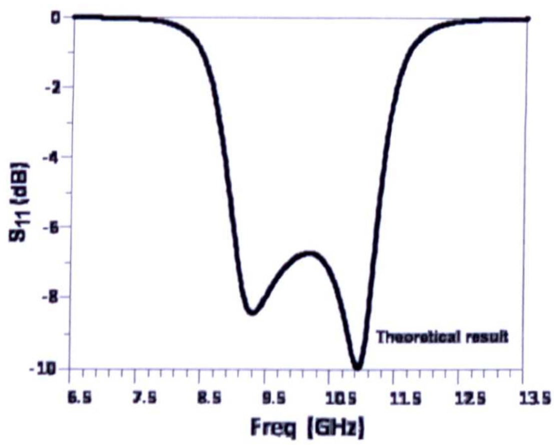

(c)

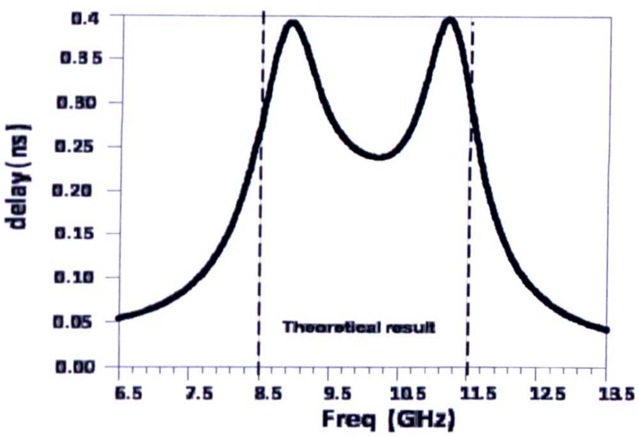

(d)

Fig. 4-6 (a) Lumped equivalent circuit model of the proposed wideband bandpass filter operating at 10 GHz, (b) simulated and theoretical response, (c) return-loss response, and (d) group delay

4.2 Conclusion

The design of novel and highly selective wideband bandpass filter based on CRLH-TL has been implemented and verified practically. Salient parameters of the unit-cell structure were identified that enable the design of wideband filter to a high specification. The wideband filter exhibits good characteristics in terms of low insertion-loss (≤ 0.8 dB), high return-loss (≥ 10 dB), stopband (≥ 15 dB) and compact size (≤ 21x8.5 mm^2). Transmission zeros were generated with the inverted T-shaped open-circuited stub was shown to significantly enhance the filters selective. The planar structure is relatively simple to fabricate and is compatible for integration in microwave systems. In addition, filter is suitable for low cost mass fabrication.

4.3 References

[4-1] G.R. Aiello, and G.D. Rogerson, "Ultra-wideband wireless systems," IEEE Microwave Mag., vol.4, no.2, pp.36–47, June 2003.

[4-2] X.Q. Lin, H.F. Ma, Di Bao, and T.J. Cui, "Design and analysis of super-wide bandpass filters using a novel compact meta-structure," IEEE Transactions on Microwave Theory and Techniques, vol. 55, no. 4, pp.747-753, April. 2007.

[4-3] M. Gil, J. Bonache, J. García-García, J. Martel, "Composite right/left-handed metamaterial transmission lines based on complementary split-rings resonators and their applications to very wideband and compact filter design," IEEE Transactions on Microwave Theory and Techniques, vol. 55, no. 6, pp1296-1304, June 2007.

[4-4] Z. Hou, X. Li, and C. Hao "Design of wideband Filter using split-ring resonator DGS," Progress In Electromagnetics Research Symposium, Hangzhou, China, pp.33-36, March 2008.

[4-5] H.C. Jayatilaka, and D.M. Klymyshyn, "Wideband microstrip bandpass filter based on EBG concept," IEICE Trans. Electron., vol. E90–C, no.12, pp.2212-2217, Dec. 2007.

[4-6] C. Chen, T. Huang, and R. Wu, "Compact microstrip cross-coupled bandpass filters using miniaturized stepped impedance resonators," APMC 2005. Asia-Pacific Conference Proceedings, vol. 1, pp.493-496, Dec. 2005

[4-7] S. Choi, M. Chung, and S. Yun, "Hairpin tuneable bandpass filter with Improved selectivity and tunability," Proceedings of Asia-Pacific Microwave Conference, pp.1-4, 2007.

[4-8] G.Q. Liu and L.S. Wu, "A compact microstrip rat-race coupler with modified lange and t-shaped arms," Progress In Electromagnetics Research, vol. 115, pp.509-523, 2011

[4-9] Y.Z. Zhu, X.J. Zhang, and G.Y. Fan, "General design of compact T-shaped line filter with ultra-wide stopband," Progress In Electromagnetics Research Symposium Proceedings, Moscow, Russia, pp.1555-1558, Aug. 2009.

5.0 ULTRA-WIDEBAND BANDPASS FILTER

Ultra-wideband (UWB) technology has aroused significant interest of researchers since the U.S. Federal Communications Commission (FCC) approved the unlicensed use of UWB (3.1-10.6 GHz) spectrum, shown in Fig. 5-0, for commercial communication purposes [5-1]. This is because UWB systems have several advantages, such as it offers bandwidth of 7.5 GHz that can support a high transmission data rate (up to 500 Mb/s); they have low energy density over a wideband spectrum generated by short pulse excitation, which not only makes the UWB system difficult to interrupt but also minimizes interference from other radio systems; and finally it supports extremely low transmission energy (≤ 1.0 mW), which is favourable for hand held radio systems [5-2]. These features make UWB technology attractive for use in many applications such as rescue radar systems, positioning, geo-location, short range high-speed wireless communications and wireless personal area networks for personal computer and electronic devices.

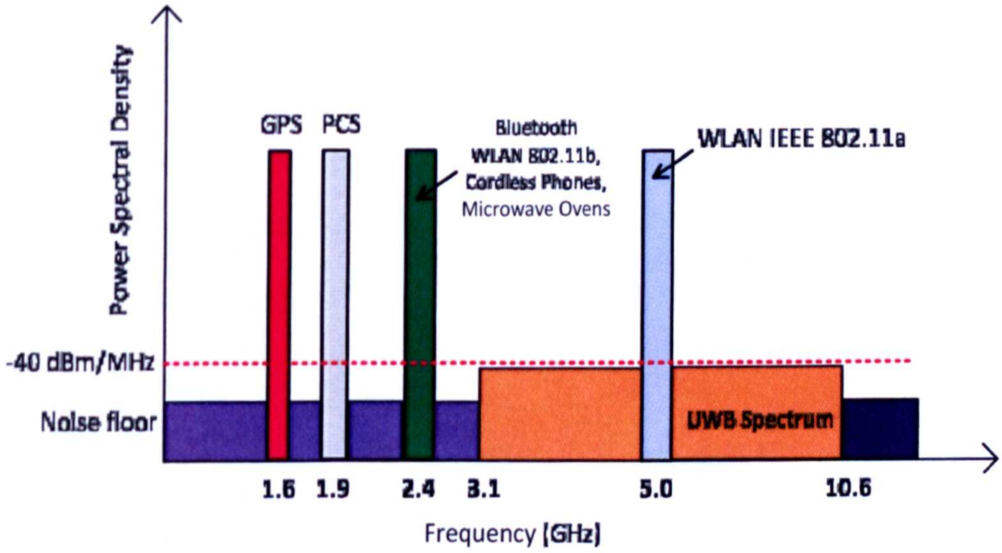

Fig. 5.0 UWB spectrum and existing radio communications systems [5-1]

Dimensions of wireless transceiver components, such as filters are dependent on the wavelength of the signal which can preclude miniaturization of the front-end. Furthermore, characterization, design and fabrication of ultra-wideband filters have been a challenging task compared to narrow-band filter designs. For example high selectivity and low insertion-loss over the UWB frequency range is necessary to minimize distortions of the UWB signal. Moreover, such filters need to possess constant group-delay and therefore linear phase characteristics. To date numerous studies on planar filter technologies have been explored for UWB applications. An example of UWB bandpass filter (BPF) using stub-loaded multi-mode resonator (MMR) is presented in [5-3]. This MMR is formed by loading three open-ended stubs in shunt to a stepped-impedance resonator, as shown in Fig. 5-1, to distribute the resonant modes evenly within the UWB band. A widened upper-stopband is realized by incorporating this MMR with two inter-digital parallel-coupled feed-lines. The insertion-loss obtained is lower than 0.8 dB, return-loss higher than 14.3 dB with a fractional bandwidth of 114%; however its selectivity is rather poor.

F. Martin et al. in [5-4] presented a UWB BPF based on complementary split-ring resonators (CSRR) transmission-line. The filter is formed using three balanced unit-cells, as shown in Fig. 5-2, to create a passband response covering the UWB frequency range. The technique employed includes inter-digital coupled transmission-line balanced unit-cells where the ground-plane is defected with split-ring resonators. This filter topology suffers from poor rejection (< 10 dB) at the edge of upper band along with high insertion-loss across its passband. Moreover, the authors embedded additional CSRRs and complementary spiral resonators (CSRs) to control the upper limit of the transmission band and to introduce extra attenuation poles.

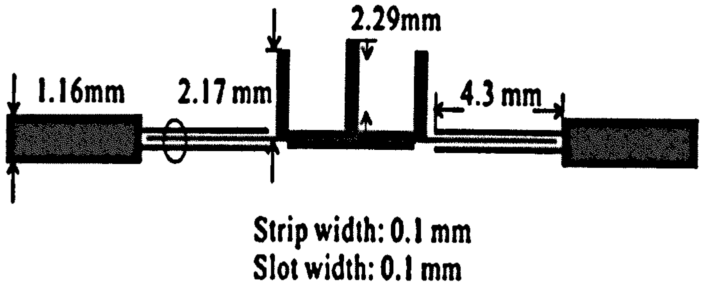

(a)

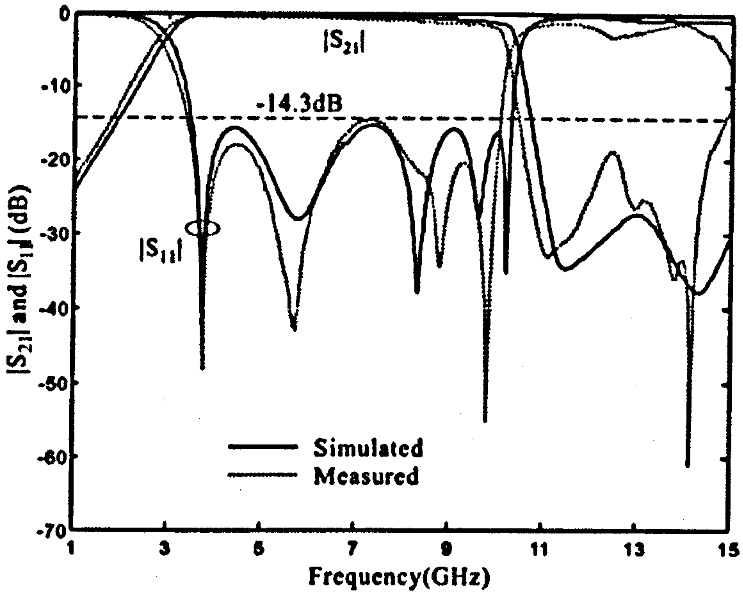

(b)

Fig. 5-1 (a) Layout of UWB filter using MMR [Ref: 5-3], and (b) measured and simulated transmission and reflection-coefficient characteristics of the UWB structure

C. Hsu et al. in [5-5] present an UWB filter design with a 3 dB fractional bandwidth of more than 100%. Here the design involves embedding highpass structure within a lowpass filter. The stepped-impedance LPF is employed to attenuate the upper stopband, and quarter-wave short-circuited stubs are used to realize the lower stopband. Unfortunately, the filter lacks in sharp skirts and the circuit is 30 mm long. UWB BPF with a narrow notched band in the UWB passband is presented in [5-6]. The narrow notched band was introduced by embedding a parasitic coupled line to the filter in order to reject any undesired signals that may interfere with the UWB system. The notched band is easily generated and can be set at any desired frequency by varying the structural parameters of parasitic coupled line. Although the filter is compact (17.8×9.6 mm^2), it suffers from poor skirt selectivity at both passband edges. The discernible issues of the above studies are followings: 1) Size: circuit sizes are comparatively large whereas the filter size must be small enough so that it is compatible to the UWB unit; 2) Fabrication: most designs based on complex geometry which results tight, difficult and expensive fabrication process; and 3) Performance: proposed filters passband selectivity and out of band rejection level is rather poor.

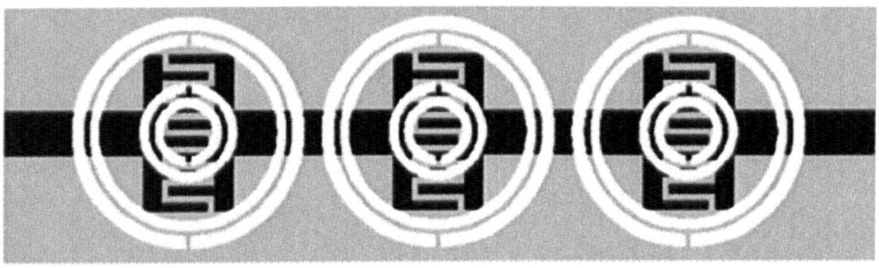

(a)

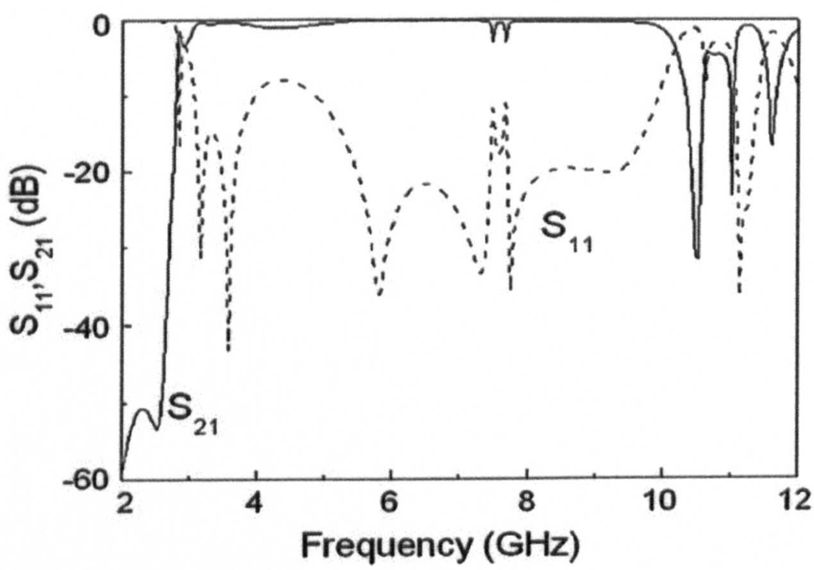

(b)

Fig. 5-2 (a) UWB design layout using DGS and CSRR [Ref: 5-4], and (b) measured and simulated transmission and reflection-coefficient characteristics of the UWB structure

In this chapter, a new UWB bandpass filter structure is proposed which comprises of a symmetric unit-cell composed of inter-digital coupled lines with a short-circuited inductive stub to provide a bandpass filter with high passband selectivity and low passband insertion-loss across the UWB. The capacitively coupled lines are significantly smaller than $\lambda g/4$. The inter-digital capacitor and the short-circuited inductive line accounts for left-handedness (highpass nature) of the structure. The effective inductance of the middle transmission-line section, which is interfaced with the inter-digital lines, and the effective capacitance introduced by the short-circuited inductor represent right-handedness (lowpass nature) characteristics. The filter's middle TL-section forms a multimode resonator that provides bandwidth expansion. To cover the UWB band (3.1-10.6 GHz) the multimode resonator's open-circuit stubs constituting the fingers of the unit-cell are inter-digitally coupled in a particular way with the input or output feed-lines, as shown in Fig. 5-3, to realize the required filter response and desired out-of-band rejection. Enhancement to the filter's selectivity was achieved by making the unit-cell asymmetric by directing coupling the input feed-line to the short-circuited stub using an *L*-shaped structure. The authors also propose a technique to control the lower attenuation pole determining the filter's lower band edge. The UWB filter prototype exhibits a fractional bandwidth of more than 100% and its insertion-loss less than 0.5 dB and return-loss is better than 10 dB. Finally, a simple and effective technique is demonstrated to create controllable narrow-band rejection notches within the UWB filter's passband to reject any coexisting radio signals including WLAN operating at 5.8 GHz (5725-5825 MHz), and thus to avoid interference. Several structures for UWB BPF with notched bands have been previously proposed [5-7]-[5-9]. Although these topologies offer a relatively wide notched band, however they suffer from poor selectivity and design methodology can be complex. To overcome these disadvantages a unique method is introduced in this paper that is effective and relatively simple to implement.

In this section presents a novel propose a new UWB bandpass filter structure that comprises of a symmetric unit-cell composed of inter-digital coupled lines with a short-circuited inductive stub to provide a filter with high passband selectivity and low passband insertion-loss across the UWB. The capacitively coupled lines are much smaller than $\lambda_g/4$. The inter-digital capacitor and the short-circuited inductance accounts for left-handedness (highpass nature) of the structure. The effective inductance of the middle transmission-line section, which is interfaced with the inter-digital lines, and the effective capacitance introduced by the short-circuited inductor represent right-handedness (lowpass nature) characteristics. The filter's middle TL-section forms a multi-mode resonator that provides bandwidth expansion. To cover the UWB band (3.1-10.6 GHz) the multi-mode resonator's open-circuit stubs constituting the fingers of the unit-cell are inter-digitally coupled in a particular way with the input or output feed-lines, as shown in Fig. 5-3, in order to realize the required filter response and desired out-of-band rejection. Enhancement to the filter's selectivity was achieved by making the unit-cell asymmetric by directly coupling the input feed-line to the short-circuited stub using an *L*-shaped structure. A technique is proposed to control the lower attenuation pole that determines the filter's lower band edge. The UWB filter prototype exhibits a fractional bandwidth of more than 100%, and its insertion-loss is less than 0.5 dB and return-loss is better than 10 dB. Finally, a simple and effective technique is demonstrated to create controllable narrow-band rejection notches within the UWB filter's passband to reject any coexisting radio signals including WLAN operating at 5.8 GHz (5725-5825 MHz); thus avoiding unnecessary interference.

5.1 Filter Design and Synthesis

The proposed microstrip ultra-wideband bandpass filter topology is shown in Fig. 5-3(a). This is based on the composite right/left handed unit-cell structure comprising of series inter-digital capacitor and shunt inductive line of length $\lambda g/4$ that accounts for left-hand property (high-pass function). The effective inductance of the middle microstrip TL-section and effective capacitive component of the shunt inductive line represent right-hand property (lowpass function). The middle transmission-line structure in Fig. 5-3 comprises of high-low-high step-impedance sections that behaves like a multimode resonator that affords the filter its UWB property. The following analysis gives insight on the behaviour of the step-impedance section. To simplify the analysis the structure includes just one high impedance TL-section disposed on either side of the low impedance section, as shown in Fig. 5-4. In the analysis the influence of the step discontinuity and the associated fringe capacitance are ignored. The characteristic impedance of the high and low step impedance sections are defined by Z_1 and Z_2, which have corresponding electrical lengths θ_1 and θ_2, as shown in Fig. 5-4. The two high impedance sections are used to couple with the input and output feed-lines.

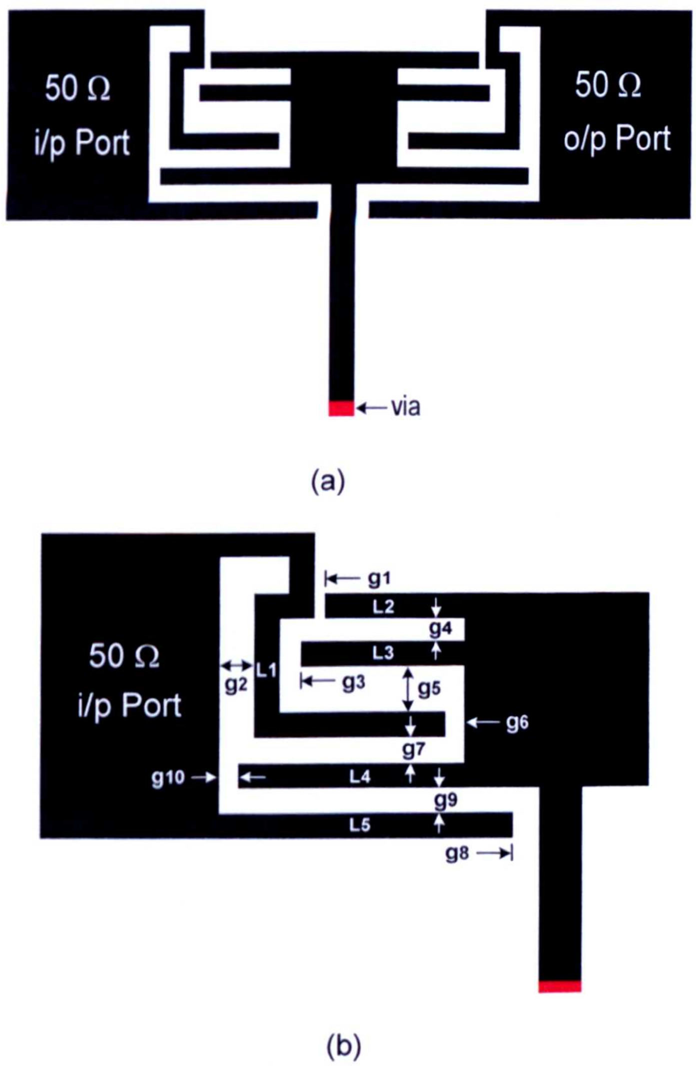

Fig. 5-3 (a) Configuration of the proposed UWB filter, and (b) parameters of the unit-cell.

In the analysis, two scenarios are examined, when the symmetry plane *p-p'* is short-circuited and when it's not, in order to model the extreme cases of the multi-mode resonator's characteristics.

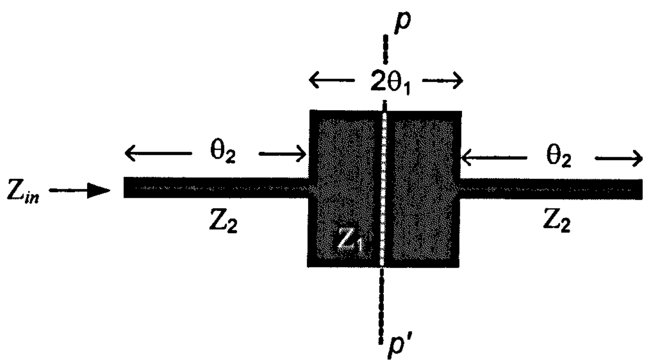

Fig. 5-4 Simplified multimode structure

Scenario 1: When symmetry plane is short-circuited the input admittance is given by:

$$Y_i = jY_2\left\{\frac{k - \tan\theta_2 \tan\theta_1}{\tan\theta_1 + k\tan\theta_2}\right\} \tag{5.1}$$

Where the impedance ratio of the high and low lines are defined by $k = Z_2/Z_1$. At resonance the input admittance is equated to zero. Hence, when $\theta_1 = \theta_2$ the structure resonates at a frequency given by:

$$f_1 = \frac{c}{2\pi l}\tan^{-1}\sqrt{k} \tag{5.2}$$

When $\theta_1 = 2\theta_2$ the structure resonates at:

$$f_1 = \frac{c}{2\pi l}\tan^{-1}\sqrt{\frac{k}{2+k}} \tag{5.3}$$

Scenario 2: When symmetry plane not short-circuited the input admittance is given by:

$$Y_i = jY_2\left\{\frac{2(k\tan\theta_1 + \tan\theta_2)(k - \tan\theta_1\tan\theta_2)}{k(1-\tan^2\theta_1)(1-\tan^2\theta_2) - 2(1+k^2)\tan\theta_1\tan\theta_2}\right\} \tag{5.4}$$

The resonance condition is defined when $Y_i = 0$, hence when $\theta_1 = \theta_2$, the resulting four resonance frequencies are at:

$$f_1 = \frac{c}{2\pi l}\tan^{-1}\sqrt{k} \tag{5.5}$$

$$f_2 = \frac{c}{4l} \tag{5.6}$$

$$f_3 = \frac{c}{2\pi l}\left(\pi - \tan^{-1}\sqrt{k}\right) \tag{5.7}$$

$$f_4 = \frac{c}{2l} \tag{5.8}$$

The relationship of resonant mode frequencies relative to the fundamental mode as a function of impedance ratio k is depicted in Fig. 5-5. The graph shows that decreasing value of $k < 1$, the resonant mode frequencies deviate away from the fundamental mode. This feature is useful to enhance stop-band rejection in narrow-band filters. However, for $k > 1$, the second and third resonant mode frequencies become closer together, which is a feature necessary for realizing ultra-wideband filters.

When $\theta_1 = \theta_2/2$, the resulting resonance frequencies at defined by:

$$f_1 = \frac{c}{2\pi l}\tan^{-1}\sqrt{\frac{k}{2+k}} \tag{5.9}$$

$$f_3 = \frac{c}{2\pi l}\tan^{-1}\sqrt{\frac{k+2}{k}} \tag{5.10}$$

$$f_2 = \frac{c}{4l} \tag{5.11}$$

$$f_4 = \frac{c}{2l} \tag{5.12}$$

For this condition the graph in Fig. 5-5(b) shows how the impedance ratio of the step-impedance line in the quad-mode resonance structure can be controlled to realize an UWB bandpass filter. The simulated frequency response of the proposed structure, depicted in Fig. 5-6, confirms the multiple resonances generated within the structure provide UWB bandpass filter performance.

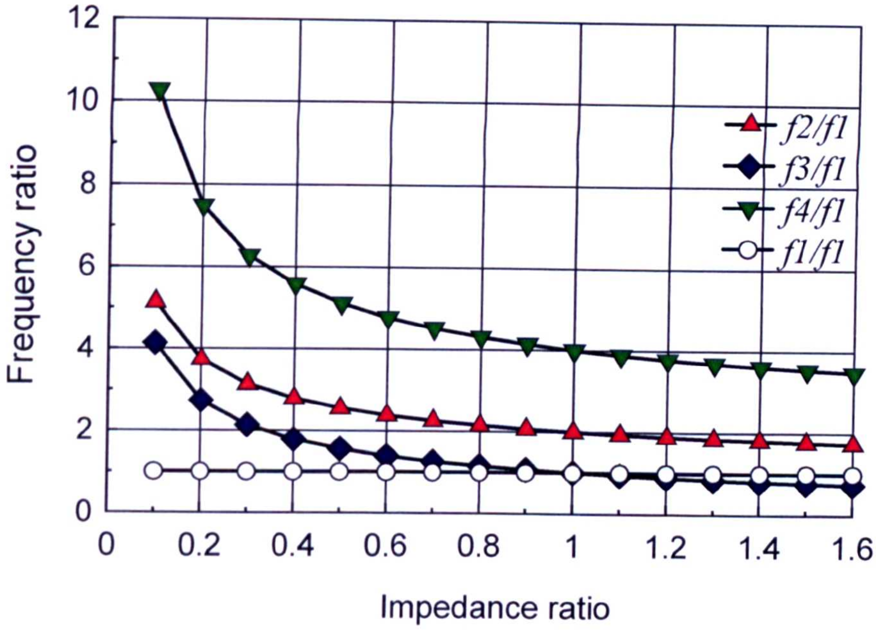

(a)

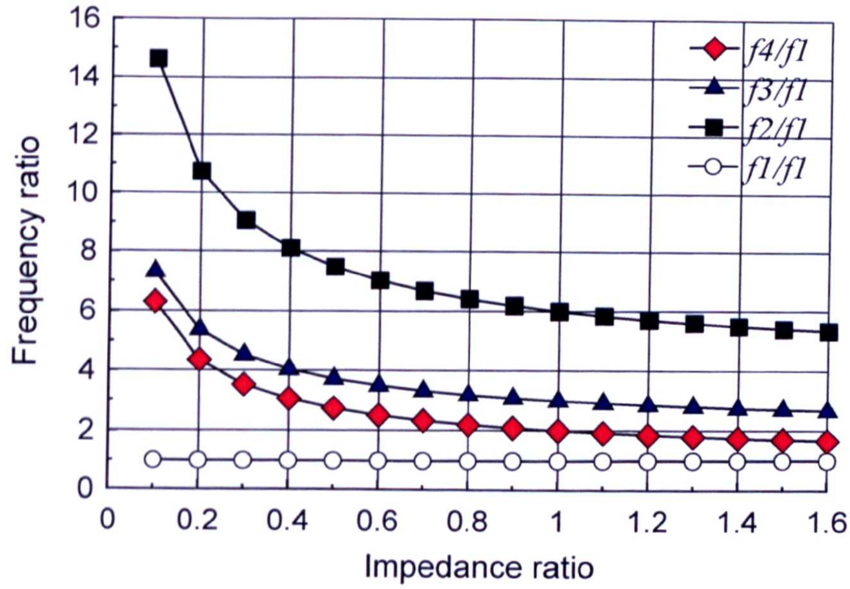

(b)

Fig. 5-5 Relationship between the impedance ratio and normalized resonance frequency.

The open-circuit stubs constituting the inter-digital capacitor's coupling arms have identical impedance of magnitude 146.86 Ω corresponding to a width of 0.2 mm. The electromagnetic analysis shows that these coupling stubs behave as a parallel *LC* tank. The length of stub L_4 affects the filter's passband response. When L_4 is reduced the response shifts to higher frequencies without significantly undermining the filter's 3 dB bandwidth. The length of stubs L_2 and L_3 contribute in generating higher resonance modes and affects the filter's bandwidth too. When length of L_2 and L_3 are reduced the upper cut-off frequency of the filter increases resulting in increased bandwidth. The length of the coupling stub L_1 and its coupling arrangement was designed to determine the upper attenuation pole's frequency. The length of the short-circuited shunted stub affects the lower cut-off frequency of the passband response, in particular it shifts it towards higher frequencies which results in an effective bandwidth reduction. The optimized dimensions of the proposed UWB BPF are given in Table 5-1. The dimension of the multi-mode section is 4.4×1.5 mm^2, and length of the shunted line is 2.8 mm. The simulated frequency response of the proposed filter, shown in Fig. 5-6, exhibits a wide out-of-band rejection level which is greater than 12.5 dB for frequencies beyond 11.4 GHz. The filter exhibits an average insertion-loss < 0.5 dB across the UWB passband between 3.1-10.6 GHz. The coupling gaps g_2 and g_3 are determined in such a way as to avoid attenuation poles at unwanted frequencies within passband. The simulation shows the filter exhibits an average insertion-loss $|S_{21}|$ less than 0.5 dB and return-loss $|S_{11}|$ greater than 15 dB across the UWB passband between 3.1-10.6 GHz. Later in this chapter, a technique is described to improve the filter's selectivity for practical applications.

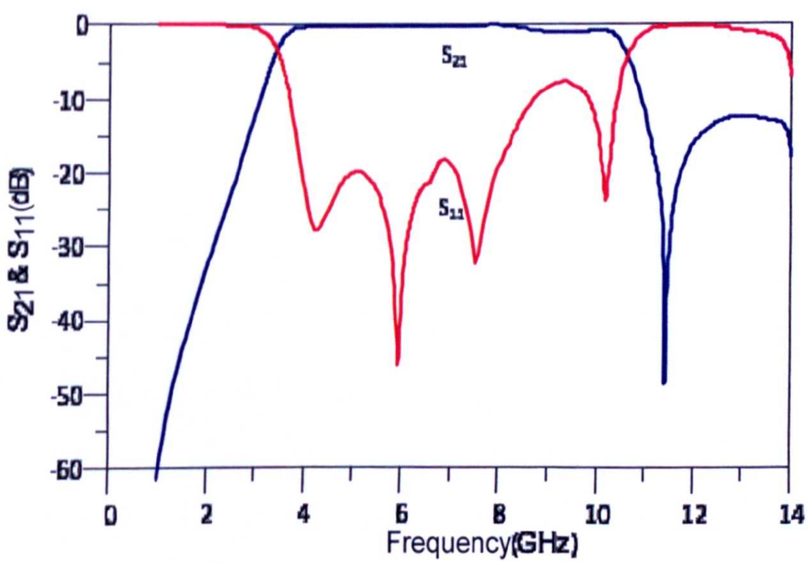

Fig. 5-6 Simulated transmission and reflection-coefficient characteristics of the proposed UWB bandpass structure

g_1	g_2	g_3	g_4	g_5	g_6	g_7	g_8	g_9	g_{10}
0.3	0.9	0.9	0.2	0.3	0.4	0.2	0.5	0.2	0.8

L_1	L_2	L_3	L_4	L_5
8.4	3.9	4.0	5.2	7.2

Table 5-1: Dimensions (mm) of the CRLH UWB filter parameters defined in Fig. 5-3

5.1.1 Selectivity Improvement of UWB Filter

An effective method to sharpen the passband skirts of the filter is to introduce transmission zeros in the stopband region immediately adjacent to the passband response. The implementation of source/load coupling arrangement to the multimode resonator section used here supports the approach described below to create attenuation poles on either sides of the filter's passband to satisfy FCC's UWB outdoor specifications. The selectivity of the lower passband edge is enhanced by the step-impedance line loading between the input feed-line and the short-circuited $\lambda g/4$ stub line, as shown in Fig. 5-7. This results in the creation of steep skirt selectivity at the edge of the lower passband. In fact the combination of coupling stub L_1 and the stepped-impedance appendage determines the location and magnitude of attenuation pole. The coupling gap g_1 and g_3 enhance the rejection level for frequencies above and below the filter's upper and lower band edge. It was also observed that the gaps increase the frequency of the lower attenuation pole when the gap is increased.

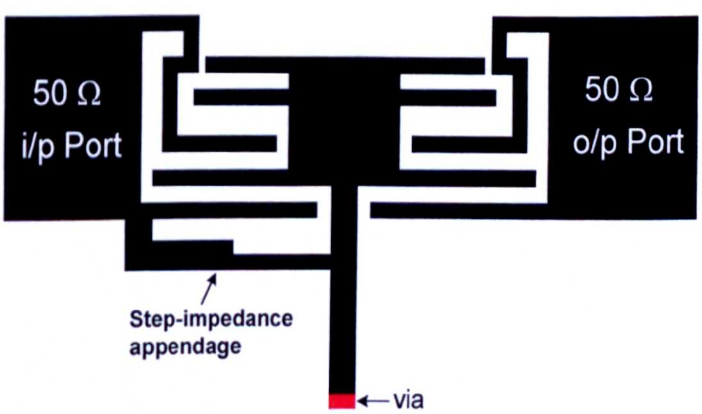

Fig.5-7 Layout of the proposed UWB filter

The characteristic impedance of the two sections constituting the step-impedance line are Z_1 and Z_2 with corresponding electrical lengths of θ_1 and θ_2 respectively, as shown in Fig. 5-8.

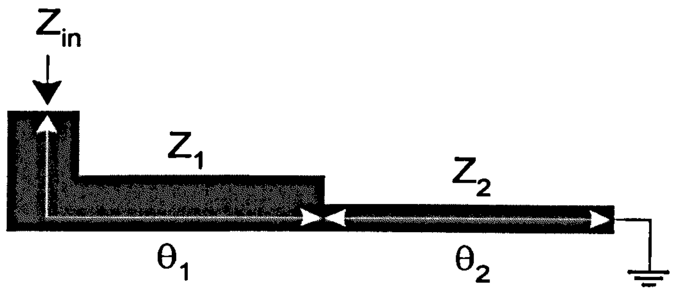

Fig 5-8 Step-impedance line appendage.

The optimized values of the two sections are: Z_1 = 131.62 Ω and Z_2 = 146.86 Ω. The corresponding electrical length of θ_1 and θ_2 are 22.46° and 17.32°, respectively. Therefore, $\theta_{total}=\theta_1 + \theta_2=$ 39.78°, which is smaller than $\lambda_g/4$. This line controls the selectivity of the lower passband and the frequency of the lower transmission zero. A transmission zero at 3 GHz requires the length of the step-impedance line θ_{total} to be 8.6 mm.

5.1.2 Fabrication And Measurement

The proposed filter was simulated and optimized using ADS™ (MoM) and the prototype filter was fabricated using standard MIC technique. To demonstrate the practical feasibility of the proposed topology for UWB function it was designed and fabricated on 3M Cu-clad217 substrate from Arlon with ε_r = 2.17 and h = 0.794 mm. The filter's design was initially simulated and optimized using electromagnetic solver ADS™ (MoM). Fig. 5-10(a) shows the simulated and measured S-parameter performance of the fabricated CRLH filter depicted in Fig. 5-9. The filter's transmission and reflection coefficient performance was characterized using a network analyzer.

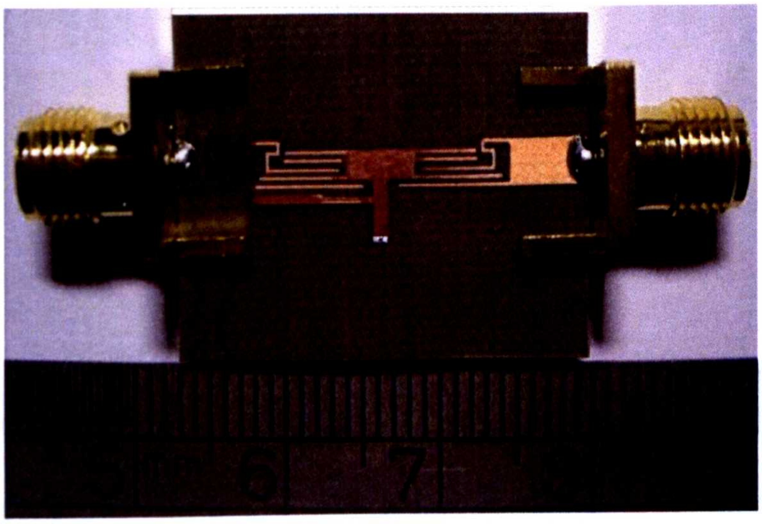

Fig. 5-9 Photograph of the proposed UWB filter

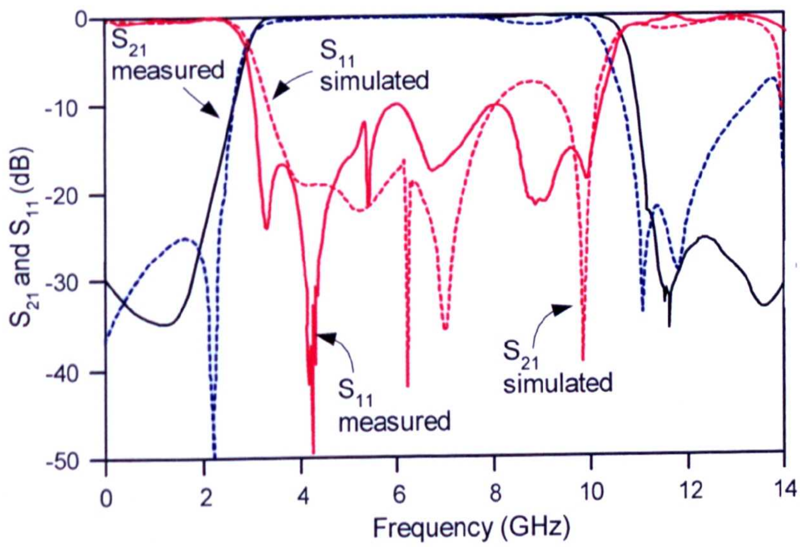

(a)

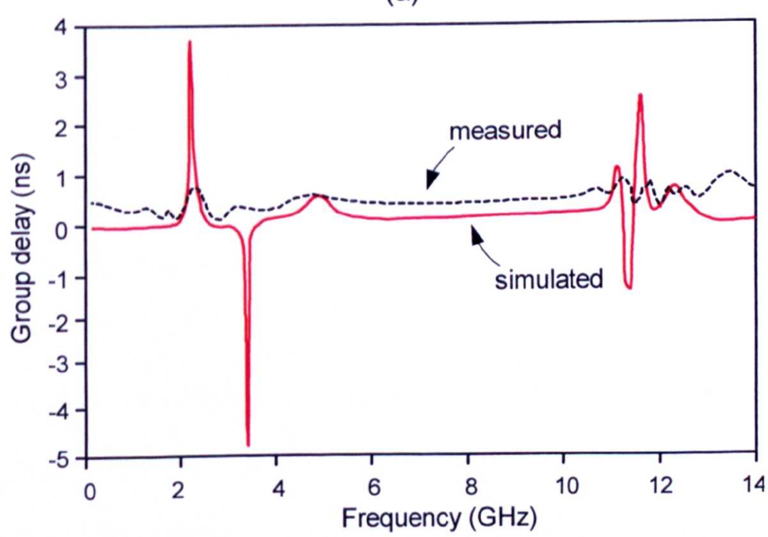

(b)

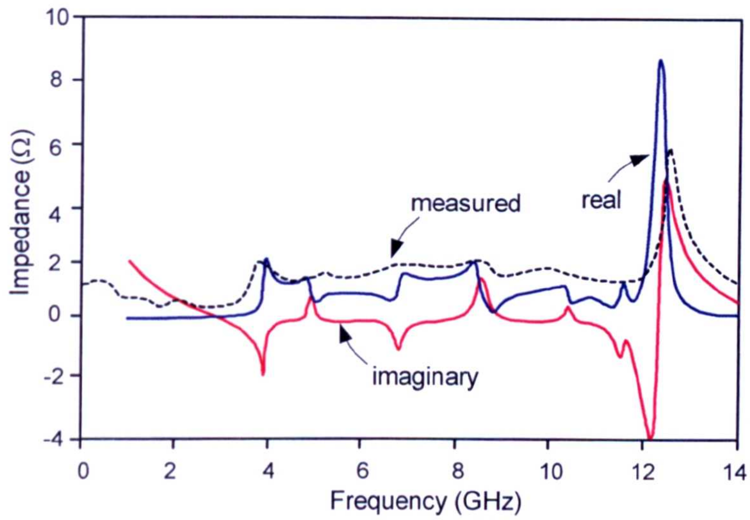

(c)

Fig. 5-10 (a) Simulated and measured performance of the filter, (b) group delay, and (c) impedance

The measured result depicted in Fig. 5-10(a) confirms the validity of the proposed structure. The discrepancy between the simulation and measurement results are attributed to fabrication tolerance. The measured 3 dB passband, which is between 2.9 to 10.75 GHz, provides a fractional bandwidth of 115%. The measured results show the worst case passband insertion-loss is 0.5 dB; return-loss over the passband is better than 10 dB. The filter is compact in size with a length of 16.4 mm. The group-delay time over the passband is constant as shown in Fig. 5-10(b). The measured group-delay within the 3-11 GHz passband varies between 0.1 and 0.5 ns. Large variation of group-delay can be observed near the filter's passband edges, which is caused by the steep transition in the rejection level. The filter's real impedance measured across its passband varies between approximately 0.3 and Ω, as shown in Fig. 5-10(c).

Table 5-2, shows the proposed structure exhibits relatively low passband insertion-loss, a better group-delay and is smaller in size than MMR structures in [5-14] & [5-15] that employ a substrate with similar dielectric constant. Furthermore, the proposed structure has a better loss and size when compared to structures fabricated with a higher dielectric constant substrate [5-3][5-4][5-13][5-16]-[5-23]. The measured result depicted in Fig. 5-10(a) confirms the validity of the proposed structure. The discrepancy between the simulation and measurement results are attributed to fabrication tolerance. The measured 3 dB passband, which is between 2.9 to 10.75 GHz, provides a fractional bandwidth of 115%.

Ref	S_{21} (dB)	S_{11} (dB)	FBW (%)	Group Delay (ns)	Size (mm^2)	Geometry	Relative permittivity of substrate
[5-3]	0.8	14.3	114	0.64	13.8 x 2.5	MMR	10.8
[5-4]	0.8	8.0	90	Not shown	14 x 5	DGS	10.2
[5-12]	0.5	15	104	0.75	25.8 x 4	MMR	9.80
[5-13]	1.7	10	111	0.65	31.2 x 12.6	MMR	2.65
[5-14]	1.2	<15	112	0.60	16.4 x 15.65	MMR	2.55
[5-15]	1.6	13	110	0.12	30 x 6	MMR	9.60
[5-16]	2.0	10	110	0.70	28 x 15	MMR	6.15
[5-17]	>2.5	>15	106	0.54	26.2 x 11.9	DGS	4.30
[5-18]	>1	<14	120	0.20	20 x 30	BC	4.50
[5-19]	0.83	>15	114	0.53	15.6 x 12.3	MMR & slotline	10.2
[5-20]	0.45	15	103	0.60	17.8 x 9.6	MMR	3.38
[5-21]	>1	11	110	0.72	25 x 30	BC	10.2
[5-22]	<1	10	116	<0.3	13.6 x 4.8	MMR	10.8
This work	0.5	11	110	0.50	16.8 x 4.8	MMR	2.17

Table 5-2 Comparison of the proposed filter with best reported UWB bandpass filters

5.1.3 Transmission Zero Control

The impedance of coupling stub L_1 in Fig. 5-3 controls the frequency of the lower transmission zero and also affects the transmission loss of UWB filter, as shown in Fig. 5-11(a). The impedance of stepped line section θ_1 in Fig. 5-8 controls the magnitude of the attenuation pole at the lower passband edge. Simulation results confirms that when the normalized impedance (Z_1/Z_o) values are 2.62 and 2.92 then the transmission zero locates at 3.16 GHz and 3.28 GHz, respectively, as depicted in Fig. 5-11(b). The experiment results demonstrates that it is possible to control the lower transmission zeros by changing the normalized impedance value of the step-impedance line section θ_1, as depicted in Fig. 5-11(a). This technique is effective and simple to realize, thus avoiding unnecessary fabrications complexity too.

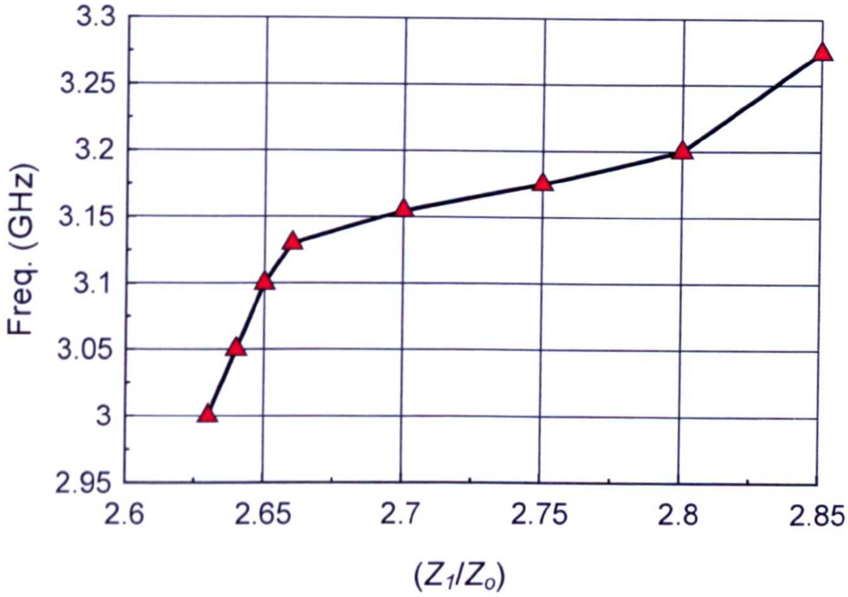

(a)

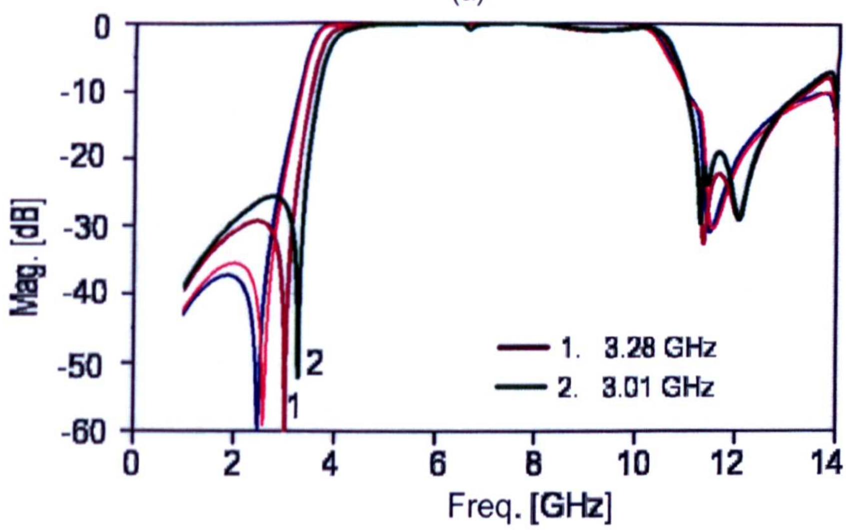

(b)

Fig. 5-11 (a) The affect on the lower transmission zero as a function of normalized impedance (Z_1/Z_o) of step-impedance line section L_1, and (b) Insertion-loss response of UWB filter showing the location of transmission zeros.

5.2 UWB Filter With Notched Passband

To meet the UWB specifications the filter characteristics need to exhibit high passband selectivity as well as a notch band to filter out coexisting signals like IEEE 802.11, which may cause unwanted interference with the UWB communication system.

To overcome this electromagnetic interference, various notch function techniques have been studied [5-10][5-11]. However, the existing notched-band techniques suffer from poor selectivity. In [5-12], a filter with multiple notched-bands is designed which is based on multilayer structures that would require complex fabrication technology and is not easily compatible with the existing microwave-integrated circuits. However, in this section we propose a simple technique to design a controllable notched-band UWB filter for practical applications. It is shown here that by modifying the proposed filter in Fig. 5-3 we can create a rejection notch band within the UWB passband that is controllable. To design the UWB bandpass filter with high rejection notch band and good overall performance the transmission-line L_5 on the output section is extended, as shown in Fig. 5-12(a). Notched band depends on the total length (L_5+L_6) of the asymmetric unit-cell. L_6 is bent backwards to prevent excessive coupling and to provide a sharp notch.

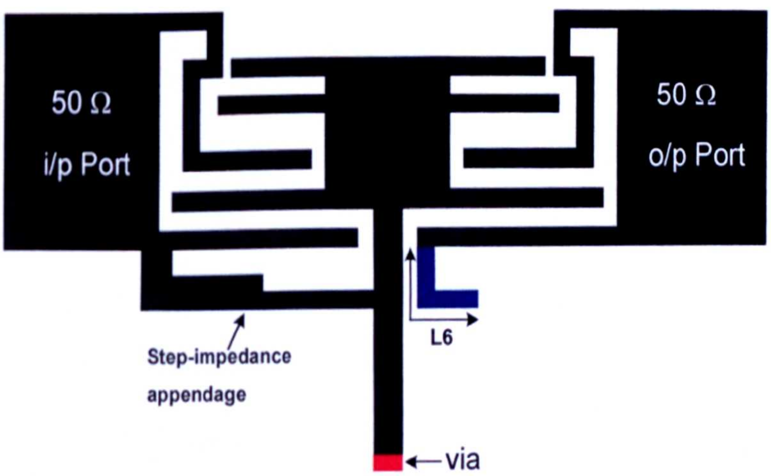

(a)

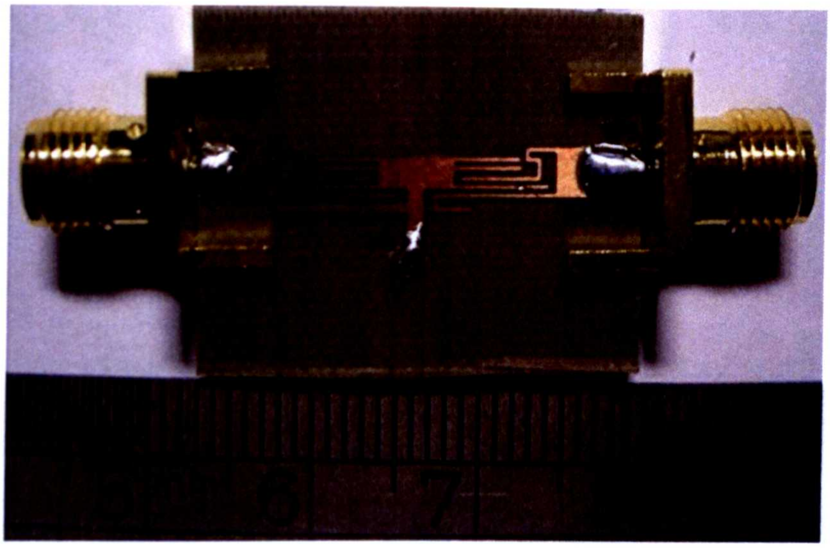

(b)

Fig. 5-12 UWB bandpass filter structure for passband with notched-bands, (a) physical layout, and (b) fabricated filter

The length of the coupling stub L_6 determines the notch frequency. The dimension of L_6= 4.2 mm corresponding to an electrical length of 37° creates a notch at frequency 5.7 GHz; L_6 = 2.7 mm corresponding to 25.62° creates a notch at 6.15 GHz; and L_6 = 0.7 mm or θ_5 = 7° produces a notch at 6.50 GHz, as shown in Fig. 5-13. However, to create notched-band at 5.7 GHz it was necessary to reduce the length L_3 to 5.2 mm. Fig. 5-13(a) shows considerable tuning can be achieved, in the example shown it's over 5.7-6.5 GHz. Although the highest notch frequency is limited by the length of stub L_6 its tuning range encompasses the WLAN interfering signal (5.725-5.825 GHz) in the UWB spectrum. However, to create notched-band at 5.7 GHz it was necessary to reduce the length L_4 to 5.2 mm in order to maintain the filter's optimum insertion-loss performance. The width of L_6 of the coupling stub is 0.2 mm. The relationship between the notch frequency and L_6 is given by:

$$\text{Notch frequency (GHz)} = 0.235\, L_6 + 6.73$$

This equation is valid for the specific example described here. The measured response in Fig. 5-13(b) shows the out-of-band rejection is 18 dB between ~11-16 GHz. With further optimization this can be improved.

The current density distribution across the structure of the proposed UWB filter is shown in Fig. 5-14. The input signal energy at the notch frequency is coupled between the feed-line and inter-digital capacitor through coupling stubs L_1, L_4 and L_5 at the input and predominantly L_1 and L_4 at the output to create a notched-band within the filter's passband response. Other coupling stubs remain non-resonating at this frequency.

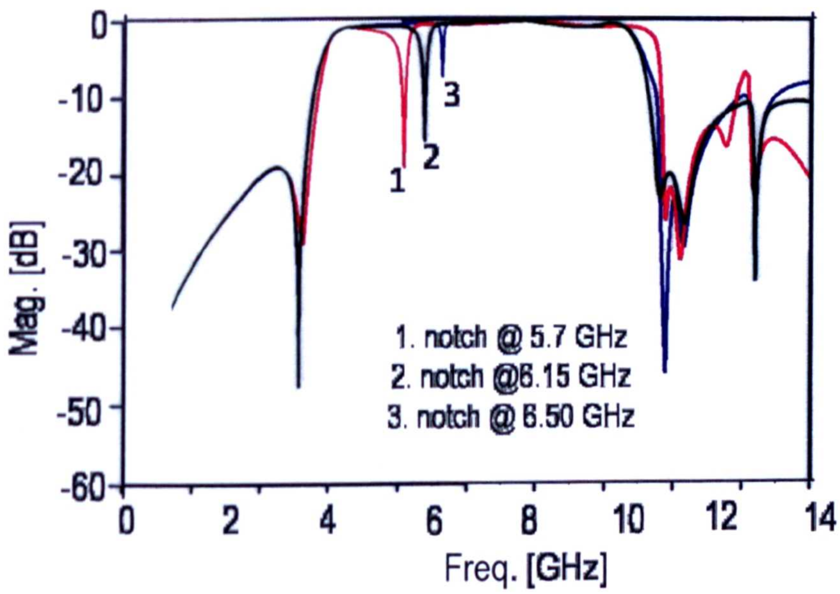

(a)

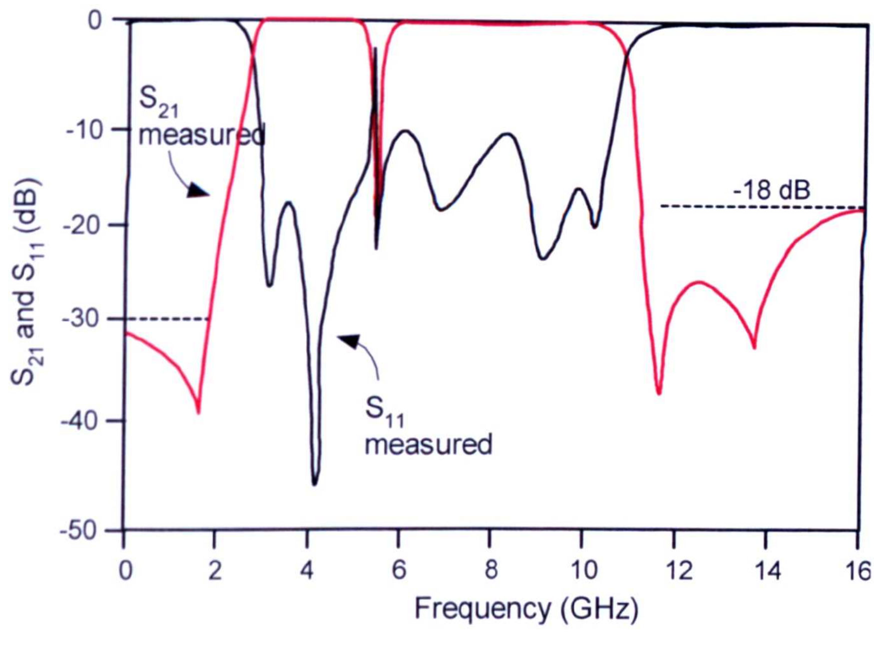

(b)

Fig. 5-13 UWB filter with notched-band, (a) simulated insertion-loss, and (b) measured simulated insertion-loss and return-loss response

Fig. 5-14 Current density distribution across the UWB filter structure at notched band frequencies of: $f = 5.7$, 6.15, and 6.50 GHz

5.3 Conclusion

The feasibility of a highly selective UWB microstrip filter that exhibits low-loss and is compact has been practically demonstrated. The proposed multi-coupled line structure is incorporated within the multi-mode resonator to provide wide transmission band and enhance out-of-band performance. The technique presented allows the control of the filters transmission zeros to provide steep passband edge selectivity. The filter exhibits excellent characteristics: passband insertion-loss < 0.5 dB and return-loss > 10 dB; a flat group delay (0.5±0.2 ns); and stopband property ($|S_{21}|$ <= 30 dB between 0.0-2.7 GHz and $|S_{21}|$ <= 25 dB over the upper stopband region. The design methodology of the proposed UWB filter is simple and easy to fabricate. Also shown is a technique to introduce notched-band within the passband of the filter to provide interference immunity from the narrowband services, such as WiMAX and WLANs coexisting with the UWB. The technique allows easy control of the centre frequency of the notch band and does not require increase of the filter's overall dimensions or adding complex defected ground structure. The final size of the filter is 16.4×4.8 mm^2, which is suitable for modern ultra-wideband wireless communication systems.

5.4 References

[5-1] Federal Communications Commission (FCC), Revision of part 15 of the commission's rules regarding ultra-wideband transmission systems, First Report and Order, FCC 02-48, 2002.

[5-2] Z.C. Hao, and J.S. Hong, "Ultrawideband filter technology," IEEE Microwave Magazine, , pp. 56-68, Jun. 2010.

[5-3] R. Li and L. Zhu, "Compact UWB bandpass filter using stub-loaded multiple-mode resonator," IEEE Microwave Wireless Compon. Lett., vol. 16, no. 8, pp.440–442, Aug. 2006

[5-4] M. Gil, J. Bonache, F. Martín, "Metamaterial filters: A review," Invited paper, Metamaterials 2, pp.186–197, August 2008

[5-5] C.-L. Hsu, F.-C. Hsu, and J.-T. Kuo, "Microstrip bandpass filters for ultra-wideband (UWB) wireless communications," IEEE MTT-S Int'l. Dig., pp.675-67, June 2005.

[5-6] S. Piran, J. Nourini, C. Ghobadi, "Band-notched UWB bpf design using parasitic coupled line," IEEE Microw. and Wireless Compon. Lett., IEEE, 20(8), pp.444-446, Aug. 2010.

[5-7] G.-M. Yang, R. Jin, C. Vittoria, V.G. Harris, and N.X. Sun, "Small ultra-wideband (UWB) bandpass filter with notched band," IEEE Microwave Wireless Compon. Lett., vol. 18, no. 3, pp.176–178, Mar. 2008.

[5-8] M.H. Weng, C.T. Liang, H.W. Wu, and S.R. Vargas, "An ultrawideband bandpass filter with an embedded open-circuited stub structure to improve in-band performance," IEEE Microwave and Wireless Components Letters, vol.19, no.3, pp.146-148, Mar. 2009.

[5-9] R. Ghatak, P. Sarkar, R.K. Mishra, D.R. Poddar, "A Compact UWB bandpass filter with embedded SIR as band notch structure," IEEE Microwave and Wireless Components Letters, vol.21, no.5, pp.261-263, May. 2011.

[5-10] H. Shaman, J.S. Hong, "Asymmetric parallel-coupled lines for notch implementation in UWB filter," IEEE Microw. Wirel. Compon. Lett., vol.17. no.7, pp.516-518, 2007.

[5-11] H. Shaman, J.S. Hong, "Ultra-wideband (UWB) bandpass filter with embedded band notch structures," IEEE Microw. Wirel. Compon. Lett., vol.17, no.3, pp.193-195, 2007.

[5-12] Z.C. Hao, J.S. Hong, "Ultra-wideband (UWB) bandpass filter with multiple notch-bands on multilayer liquid crystal polymer substrate," IEEE Microw. Antennas Propag., vol.5, no.5, pp.749-756, 2009.

[5-13] Z. Ma, W. He, C.P. Chen, Y. Kobayashi, and T. Anada, "A novel compact ultra-wideband bandpass filter using microstrip stub-loaded dual-mode resonator doublets," IEEE MTT-S Int Microwave Symp Dig., WE3A-02, pp.435–438, 2008.

[5-14] M.J. Gao, L.S. Wu, J.F. Mao, "Compact notched ultra-wideband (UWB) bandpass filterwith improved out-of-band performance using quasi electromagnetic bandgap structure," Progress In Electromagnetics Research, vol. 125, pp.137-150, 2012.

[5-15] X.-K. Tian, Q.-X. Chu, "A compact UWB bandpass filter with improved out-of-band performance using modified coupling structure," Progress In Electromagnetics Research Letters, vol.22, pp. 191-197, 2011.

[5-16] J.Z. Chen, G.-C. Wu, and C.-H. Liang, "A novel compact ultra-wideband bandpass filter (BPF) with simultaneous narrow notched band and out-of-band performance improvement," Progress in Electromagnetics Research Letters, vol.24, pp.35-42, 2011.

[5-17] M. Mokhtaari, J. Bornemann, S. Amari, "A modified design approach for compact ultra-wideband microstrip filters," International Journal of RF and Microwave Computer-Aided Engineering, vol.20, no.1, pp.66-75, Jan. 2010.

[5-18] B. Xia, L.-S. Wu, J.F. Mao, "An ultra-wideband (UWB) balanced bandpass filter based on defected ground structure," *Progress in* Electromagnetics *Research C, vol. 25, pp.* 133-144, 2012.

[5-19] A.M. Abbosh, "Ultrawideband balanced bandpass filter," IEEE Microwave and Wireless Components Letters, vol.21, no.9, pp.480-482, Sept. 2011.

[5-20] C.H. Lee, C.I. G. Hsu, and C.J. Chen, "Band-notched balanced UWB BPF with stepped-impedance slotline multi-mode resonator," IEEE Microwave and Wireless Components Letters, vol. 22, no. 4, pp.182-184, Sept. 2012.

[5-21] S. Pirani, J. Nournia, and C. Ghobadi, "Band-notched UWB BPF design using parasitic coupled line," IEEE Microw. Wireless Compon. Lett., vol.20, no.8, pp. 444–446, Aug. 2010.

[5-22] A.M. Abbosh, "Planar bandpass filters for ultra-wideband applications", IEEE Transactions on Microwave Theory and Techniques, vol.55, no.10, pp.2262-2269, Oct. 2007.

[5-23] B. Yao, Y. Zhou, Q. Cao, Y. Chen, "Compact UWB bandpass filter with improved upper-stopband performance," IEEE Microw. Wireless Compon Lett., vol.19, no.1, pp.27–29, Jan. 2009

6.0 Conclusion And Future Work

Electromagnetic metamaterials have been an object of a great interest especially in the last few years, since the publication of the first left-handed synthesized metamaterial in 2000. However, very little work has been done thus far on metamaterial filters. Metamaterials are new artificial materials with unusual electromagnetic properties that are not found occurring in natural materials. The electrical permittivity (ε), which responds to an electrical field, and the magnetic permeability (μ), which responds to a magnetic field, are the main determinants of a material's response to electromagnetic wave. The main aim of this research was to development of enhanced planar RF/microwave bandpass filters based on metamaterial unit-cells for application in future wireless communications. In particular, the investigation addressed some of the key challenges surrounding RF/microwave bandpass filters such as compactness, selectivity, harmonic suppression, low transmission-loss and prefabrication tuning.

It is always difficult to develop miniaturized filters using conventional design technique as the dimensions of the conventional filters are fixed to the wavelength of the signal. This is a critical design issue that not only limit the size reduction but also limit the system bandwidth. To circumvent these problems this thesis presents CRLH-TL based filters whose dimensions are not fixed to the signal's wavelength due to their special electromagnetic characteristics. Results of the investigation show the optimized metamaterial filter prototypes offer significant device miniaturization and bandwidth expansion without detrimental impact on its overall transmission performance. This dissertation includes novel compact metamaterial filter configurations for narrowband and wideband filter applications. The experimental results demonstrate the filters *exhibit low insertion*-loss and high return-loss. The overall size of the each filter is substantially reduced by 60-70% compare to conventional filters designed at the same *operating frequency* and using identical dielectric substrate. This clearly demonstrates the feasibility of the left-handed metamaterial concept at microwave frequencies. An equivalent electrical model for the configurations was developed in order to gather deeper insight into the relationship between the physical and electrical parameters. A theoretical model developed enables the calculation of the lumped elements representing the metamaterial unit-cell. In addition, an electromagnetic parameters retrieval technique was used to prove the unique electromagnetic properties of the CRLH-transmission-line unit-cells. The original metamaterial microstrip frequency discriminating devices developed in this work were verified through simulation and practical experimental work.

It is obvious that the ever increasing demand from wireless systems also results in new challenges with the limited radio frequency spectrum and a complex space-time varying wireless environment. To aid design of metamaterial filter at a precise frequency a prefabrication technique was developed that enables fine tuning of the filter's centre frequency. This was achieved by defecting the ground-plane of the metamaterial unit-cell with a dielectric slot, which is located immediately below the unit-cell. It is shown the technique enables substantial tuning of the unit-cell's resonant frequency as a function of the slot position, which is in the order of 26.5%. Microstrip bandpass filters were developed based on the proposed metamaterial unit-cell structure. The defected ground-plane slot provides the necessary tuning mechanism that relaxes the tradeoffs constrains for filter realisation using distributed transmission-line technology, especially for designs requiring stringent specifications.

Today, the rapidly expanding competition for spectrum use for wireless communication systems and the practice of spectrum auctions have increasingly necessitated the efficient usage of the limited frequency spectrum. In addition, with increasing subscriber numbers the interference between different systems is likely to increase. To avoid inter-modulation in the RF/microwave front ends, highly selective preselect filters are required for an efficient exploitation of the spectrum. Hence the aim of this research was to investigate and develop a novel microwave metamaterial structure that enables fabrication of highly selective compact narrowband microwave filters. A novel multilayer filter technique based on the composite right/left-handed transmission-line has been proposed. It was shown this technique significantly enhances the filters' passband selectivity. This type of multilayer structure offers the design engineer great flexibility to design highly selective filters with the desired bandwidth at a prescribed operating frequency. It was confirmed that the proposed multilayer technique reduces the filters length by approximately 86% compared to a conventional coupled-line filter with identical specifications and implemented on a single layer. This technique was exploited to design a miniature diplexer at GSM1800 and UMTS2100 bands. It was confirmed the closely spaced adjacent diplexer channels have excellent isolation and good transmission performance for practical applications.

A novel wideband filter based on CRLH-TL metamaterial was developed which is suitable for wireless applications. The wideband filter offers high selectivity, low transmission-loss and miniaturization compare to the conventional wideband filters. The planar geometry of the proposed structure is relatively simple and compact making it compatible for integration in microwave systems. In addition, filter is suitable for low cost mass fabrication.

Ultra-wideband (UWB) technology has aroused significant interest of researchers since the U.S. Federal Communications Commission (FCC) approved the unlicensed use of UWB (3.1-10.6 GHz) for commercial applications. A new UWB bandpass filter was developed that comprises of a symmetric unit-cell composed of inter-digital coupled lines with a short-circuited inductive stub to provide a filter with high passband selectivity and low passband insertion-loss across the entire UWB. The proposed multi-coupled line structure is incorporated within the multi-mode resonator to provide wide transmission band and enhance out-of-band performance. The filter has been designed to also provide a notch band function within the ultra-wideband spectrum to suppress coexisting signals within like IEEE 802.11 that can cause unwanted interference with the UWB communication system. The UWB filter has dimensions of 16.4×4.8 mm^2, which is the smallest size published to date for the such a device fabricated on a low dielectric constant substrate use.

In this research work the filters developed, which are based on composite right/left-handed unit-cells, exhibit superior performance in terms of low passband insertion-loss, sharp passband skirts and high out-of-band selectivity. In addition, the filters are physically smaller in size and relatively cheap to fabricate compared to existing planar filters. The commercial advantage of these filters is very significant in terms of reduction in power consumption by wireless systems that employ it, as well as increase in channel capacity of the system. The low power consumption means improvement in system reliability and life.

6.1 Contribution To The Thesis

The contribution of the research is recaptured in the following summary:

1. It was demonstrated the feasibility of composite right/left-handed unit-cells for narrowband filter applications. The devices realised are compact in size with good insertion-loss and return-loss characteristics that make them suitable for various RF and microwave applications. The filters were analyzed and characterized using an electromagnetic parameter retrieval technique to show the existence of the special electromagnetic properties (i.e. negative index) inherent in the proposed unit-cell structure. Electrical equivalent circuit for the unit-cell was established in order to fully comprehend the relationship between distributed and electrical parameters. Equations were derived that enable the lumped elements of the filter to be determined for a given filter specification. It was shown unlike for conventional resonators the metamaterial unit-cell's dimensions are independent of wavelength which makes miniaturization of filters possible. In fact, size reduction of around 70% is achieved compared to conventional parallel coupled-line filters designed with the same specifications.

2. A novel prefabrication tuning technique was developed and implemented by defecting the ground-plane of the metamaterial structure with a rectangular dielectric slot orientated

orthogonal to the shunt inductive line of the CRLH-TL unit-cell. It was shown the technique provided substantial tuning of the unit-cell's resonant frequency, in the order of 26.5%, as a function of the slot position. This technique relaxes the tradeoffs constrains for filter realisation using distributed transmission-line technology using metamaterial unit-cells, especially for designs requiring stringent specifications.

3. Multiplexers design based on the CRLH-TL unit-cells was proposed and implemented. *Diplexer and triplexer* structures developed offer good isolation and rejection level between the channels. A novel multilayer technique is proposed *that is shown to* significantly enhance the selectivity and stop bandwidth of the diplexer/triplexer channels; thus avoiding both in-band and out-of-band interference. This technique also allows the reconfiguration of the filter's bandwidth.

4. A design procedure of wideband bandpass filter based on the CRLH-TL unit-cell was proposed and verified. The resulting filter design exhibits enhanced selectivity. The filter is easy to fabricate.

5. A highly selective UWB microstrip filter was developed that exhibits low-loss and is compact in size. The UWB device consists of a multimode resonator with multi-coupled line structure to provide a very wide transmission band and enhanced out-of-band rejection. The technique presented allows the control of the filters transmission zero to provide steep passband edge selectivity. The filter exhibits excellent characteristics: passband insertion-loss < 0.5 dB and return-loss > 10 dB; a flat group-delay (0.5±0.2 ns); and stopband property ($|S_{21}|$ <= 30 dB between 0.0-2.7 GHz and $|S_{21}|$ <= 25 dB over the upper stopband region. The design methodology of the proposed UWB filter is simple and easy to fabricate. Also shown is a technique to introduce notched-band within the passband of the filter to provide interference immunity from the narrowband services such as WiMAX and WLANs coexisting with the UWB. The technique allows easy control of the notch band centre

frequency and doesn't require increasing the filter overall dimension or adding complex defected ground structure. The final size of the filter is 16.4×4.8 mm^2, which is suitable for modern ultra-wideband wireless communication systems.

6.2 Future Work

This dissertation presented novel highly compact CRLH-TL filters for application in RF and microwave systems. Although the filters exhibit a good transmission and reflection coefficient response and significant size reduction, it lacks sharp passband skirts. Sharp passband skirts are necessary to achieve a good rejection-level between two adjacent channels in order to avoid unnecessary interference between channels.

The dissertation includes a triplexer design that is suitable for multiband microwave applications. Although many aspects of the design were investigated within the allotted time the rejection-level between the first two channels requires further improvement to about 30 dB. It should be interesting apply the proposed multilayer technique to achieve a higher better rejection level.

The wideband filter design provided in chapter 4 exhibits sharp passband edge and the low passband insertion-loss. However, the out-of-band rejection level is less than 25 dB, which makes it unsuitable for some wireless systems. Further work is required to improve the out-of-band rejection.